Activity Report
2000-2001

Association
EURATOM / IPP.CR

INSTITUTE OF PLASMA PHYSICS
ACADEMY OF SCIENCES OF THE CZECH REPUBLIC

TABLE OF CONTENTS

PREFACE

This report presents the main results achieved during the first two years of the existence of the Association EURATOM/IPP.CR which undertakes research and development within the European fusion energy research programme. The long term aim of this research is the realisation of fusion as a practically unlimited energy source with a minimum environmental impact. The Association participates in the joint European effort in this field by carrying out relevant plasma physics and technology R&D, including participation in JET and other European devices and design activities related to the proposed experimental reactor ITER.

The Association was founded on December 22, 1999 through a contract between the European Atomic Energy Community (EURATOM) represented by the European Commission and the Institute of Plasma Physics, Academy of Sciences of the Czech Republic (IPP). Several other institutions in Prague have been included in the Research Unit to contribute to the programme of physics and technology research:

- Faculty of Mathematics and Physics, Charles University in Prague (FMP)
- Institute of Physical Chemistry, Academy of Sciences of the Czech Republic (IPCH)
- Faculty of Nuclear Science and Physical Engineering, Czech Technical University (FNSPE)
- Nuclear Physics Institute, Academy of Sciences of the Czech Republic (NPI)
- Nuclear Research Institute, Rez, Plc (NRI)

The overall manpower involved in the Association's fusion research at the end of 2001 was 59, of which 48 were professionals (those with a University degree). The total effort expended is about 38 personyear/year of which roughly 75% is devoted to physics tasks and the remaining 25% to underlying technology and technology tasks. The overall annual budget is about 0.8 M€ out of which the Commission contribution is about 0.22 M€.

Over the first years, the activities in physics were based on the continuation of existing plasma physics research in the Czech Republic both in experiment and theory. Fusion-relevant plasma physics is experimentally studied on the small tokamak CASTOR which has been operated at the IPP Prague since 1977. The research is focused on the study of phenomena at the plasma edge, such as biasing, impurity radiation, and the measurement of the structure of edge turbulence by arrays of electric probes. In addition, new advanced probes are being developed as edge plasma diagnostics. A part of the Association's activities was devoted to studies of wave-plasma interaction, in particular in the range of lower hybrid frequencies. Some selected atomic processes relevant to fusion plasmas, such as recombination and the interaction of ions with surfaces, were studied in test-bed experiments.

There has been a great effort to establish collaborations in experiment and theory with other Associations and to strengthen the Association's participation in the collective exploitation of the JET facilities under EFDA. In particular, close bi-lateral collaborations were established already in 2000 with the Associations CEA, the Belgium state, the Suisse Confederation, UKAEA and ŐAW.

In the technology area, the programmes of several facilities, already operational in the Czech Republic, were partially redirected toward fusion research. The cyclotron at the NPI was exploited to measure the cross sections of nuclear reactions relevant to the IFMIF project. The fission reactor at the NRI was used to start activation studies of ITER-relevant materials. The water-stabilised plasma torch at the IPP was used to manufacture coatings of first wall elements.

Jan Stöckel
Head of Research Unit
Association EURATOM/IPP.CR

I RESEARCH UNIT

1 Association EURATOM/IPP.CR

Composition of the Research Unit

IPP **Institute of Plasma Physics, Academy of Sciences of the CR**
Address: Za Slovankou 3,
182 21 Praha 8, Czech Republic
Tel: +420 286 890 450
Fax: +420 286 586 389
Contact Person: Jan Stöckel
e-mail: stockel@ipp.cas.cz

IPCH **Institute of Physical Chemistry, Academy of Sciences of CR**
Address: Dolejškova 3,
182 23 Praha 8, Czech Republic
Tel: +420 266 053 514 (3485-laboratoř)
Fax: +420 286 582 307
Contact person: Zdeněk Herman
zdenek.herman@jh-inst.cas.cz

NPI **Institute of Nuclear Physics, Academy of Sciences of the CR**
Address: 250 68 Řež, Czech Republic
Tel: +420 266 172 105 (3506)
Fax: +420 220 941 130
Contact person: Pavel Bém
e-mail: bem@ujf.cas.cz

FMP **Faculty of Mathematics and Physics, Charles University**
Address: V Holešovičkách 2,
182 00 Praha 8, Czech Republic
Tel: +420 221 912 305
Fax: +420 221 912 332
Contact person: Milan Tichý
tichy@mbox.troja.mff.cuni.cz

FNSPE **Faculty of Nuclear Science and Physical Engineering, Czech Technical University**
Address: Břehová 7,
115 19 Praha 1, Czech Republic
Tel: +420 224 358 296
Fax: +420 222 320 862
Contact person: Vojta Svoboda
svoboda@br.fjfi.cvut.cz

NRI **Nuclear Research Institute Ltd., Rez**
Address: 250 68 Řež, Czech Republic
Tel: +420 266 172 453
Fax: +420 266 172 045
Contact person: Milan Zmítko
e-mail: zmi@ujv.cz

Steering Committee

EURATOM

Umberto Finzi
Hardo Bruhns
Johannes P.M. Spoor

IPP.CR

Ivan Wilhelm (Charles University)
Petr Křenek (Ministry of Education, Youth and Sports)
Pavel Chráska (Institute of Plasma Physics)

Head of Research Unit

Jan Stöckel

Secretary of the SC

Pavol Pavlo

2 Manpower and Budget

Manpower Analysis of the Association EURATOM/IPP.CR 2000-2001

2000	Institution	Professional Person	Professional PY	Non-Prof Person	Non-Prof PY	Total Person	Total PY	%
Physics	IPP	26	19,4	4	4	30	23,4	
	IPCH	4	2	0	0	4	2	
	FNSPE	2	1	0	0	2	1	
	FMP	3	1,5	0	0	3	1,5	
	Total	**35**	**23,9**	**4**	**4**	**39**	**27,9**	**83,28**
Technology	NPI	8	4,1	2	1,5	10	5,6	
	NRI	0	0	0	0	0	0	
	Total	**8**	**4,1**	**2**	**1,5**	**10**	**5,6**	**16,72**
TOTAL		43	28	6	5,5	49	33,5	

2001	Institution	Professional Person	Professional PY	Non-Prof Person	Non-Prof PY	Total Person	Total PY	%
Physics	IPP	24	17,8	6	4,5	30	22,3	
	IPCH	6	3,1	0	0	6	3,1	
	FNSPE	1	0,5	0	0	1	0,5	
	FMP	5	2,5	0	0	5	2,5	
	Total	**36**	**23,9**	**6**	**4,5**	**42**	**28,4**	**75,53**
Technology	NPI	9	4,4	2	1,5	11	5,9	
	NRI	3	1,3	3	2	6	3,3	
	Total	**12**	**5,7**	**5**	**3,5**	**17**	**9,2**	**24,47**
TOTAL		48	29,6	11	8	59	37,6	

Expenditures 2000 - 2001

	2000	2001
Physics	420 466	558 253
Underlying Technologies	39 290	75 392
JET Notifications		
Sub-total	**459 756**	**633 645**
Technology tasks Art 5.1a	15 029	86 780
Priority Actions		
Collaborative Actions	0	0
Technology tasks Art 5.1b	0	0
EFDA Article 6.3 Contracts	0	0
EFDA Article 9 - secondment to Culham	0	0
EFDA Article 9 - secondment to Garching	0	0
Sub-total	**15 029**	**86 780**
Mobility Actions	**41 552**	**35 242**
TOTAL	516 337	755 667

3 International Collaboration

Survey of Collaboration with Other Associations

2000-2001

The Association EURATOM/IPP.CR has established a close collaboration with other Associations. At the moment, the main strategic goals are formulated as follows:

A. Participation of IPP.CR in the experimental and theoretical program of larger fusion experiments
B. Exploitation of the CASTOR tokamak for testing of novel diagnostics
C. Joint research of CASTOR plasmas
D. Fabrication and testing of in-vessel components

A. ***Collaboration with the six large experiments.***

- **TORE Supra**: measurements in the proximity of the LH grill - in particular, development of rf probes mounted on the grill to measure random fields (F. Zacek). Theoretical studies of generation of fast electrons in TS (V. Petržílka)
- **TEXTOR-94**: Measurements of magnetic fields with the array of Hall sensors (I. Duran).
- **TCV**: Measurement of USXR radiation of light impurities on TCV by means of four channel monochromator (V. Piffl).
- **MAST**: Modeling of propagation of Electron Bernstein Waves in MAST (J. Preinhealter).
- **JET**: Participation in fluctuation measurements (M. Hron).
- **W7 AS**: Participation in measurements of edge fluctuations by means of arrays of Langmuir probes (M. Hron).

B. ***Retarding Field Analyzer***

- **Retarding Field Analyzer** developed at CEA Cadarache was tested on the CASTOR tokamak.
- Fabrication and testing of in-vessel components.

C. ***Joint experiments on CASTOR:***

• Fluctuation measurements with 2D matrix of Langmuir probes	RFX, Tore Supra, Alfven Lab, Ghent University
• Flow measurements with oriented Langmuir probes	Tore Supra, CEA
• Fast Electron Generation	Tore Supra, CEA

D. ***Material production and testing:***

- Manufacturing and testing of plasma sprayed samples (B_4C layer) in FZ Juellich (J. Matějíček)
- Examination of in-vessel components (divertor plates from Tore Supra) damaged by suprathermal particles (V. Petržílka).
- Joint experiments on ion surface interaction with University of Innsbruck (Z. Herman)
- Neutronics for IFMIF - Joint EFDA Task with FZ Karlsruhe (P. Bem)

Collaboration and Participation at JET
2001

Task Force E

Martin HRON has joined the C4 campaign on JET in frame of the task force E (Physics and technology of heat and particle removal, divertor, shallow and deep fuelling, K. Erents and C. Hidalgo), concentrated on the scaling properties of the turbulent transport in the JET plasma boundary region. This programme was carried out in collaboration with G. Matthews, M.A. Pedrosa, and C. Silva. The properties of the SOL and the edge plasma were observed in D and He discharges.

He plasma

The influence of X point height on L-H threshold was measured in 1.25 MA / 1.3 T shots where no indication of any change in L-H threshold was found. Nevertheless, generally the power threshold was significantly higher in the He plasma compared to D discharges. For comparison of He and D plasmas behavior were used data obtained during previous experimental campaigns, namely # 50760-1, 50765, 50573, and 50420 performed in deuterium under equivalent experimental conditions as current helium shots.

Further, scaling experiments in EDGE and SOL region were performed. Power and density dependence, P_{NBI} = 2 – 5.4 MW and n = (9-15)x10^{19} m^{-3}, was measured in # 53981-4 with B = 2.4 T and I_{pl} = 2.4 MA. A slight increase in ExB transport in the SOL near LCFS was observed with increasing heating power.

D plasma

B_T ramp down (from 2 T to 1 T) and n_e scan experiments for several plasma current values were performed, magnetic field and density were varied during a single discharge.

The link between the edge plasma profiles, the ExB shear and the magnetic configuration was studied. The influence of q (q_{95} = 2.2-3.3) in the frequency resolved fluctuation-driven radial particle flux was investigated.

Representatives of the Association EURATOM/IPP.CR in European Committees
2000-2001

Consultative Committee for the EURATOM Specific Programme on Nuclear Energy Research - Fusion

Pavel Chráska	Institute of Plasma Physics, Academy of Sciences of the Czech Republic
Karel Jungwirth	Institute of Physics, Academy of Sciences of the Czech Republic

Fusion Physics Committee

Jan Stockel	Institute of Plasma Physics, Academy of Sciences of the Czech Republic
Milan Tichý	Faculty of Mathematics and Physics, Charles University, Prague

EFDA Steering Committee

Jan Dobeš	Institute of Nuclear Physics, Academy of Sciences of the Czech Republic

EFDA JET Steering Committee

František Žáček	Institute of Plasma Physics, Academy of Sciences of the Czech Republic

II PHYSICS

1 Edge Plasma and Magnetic Confinement Physics

Study of Electrostatic and Magnetic Fluctuations in the Edge Plasma with Polarization

ITEM: II.1.a)

J. Stöckel, K. Jakubka, L. Kryška, M. Hron, I. Ďuran, J. Horáček, F. Žáček

Institute of Plasma Physics, Prague

1. Plasma polarization of the separatrix on the CASTOR tokamak

Cooperation:

K. Dyabilin, High Energy Density Centrum, Moscow, Russia

E. Martines, Conzorzio RFX, Padova, Italy

S. Nanobashvili, Institute of Physics, Georgian Academy of Sciences, Tbilisi, Georgia

G. Van Oost, Department of Applied Physics, Ghent University, Belgium

M. Tendler, Alfven Laboratory, RIT, Stockholm, Sweden

1.1 Introduction

The impact of the sheared electric field on the global particle confinement and on the structure of edge fluctuations was investigated on the small tokamak CASTOR (R=0.4 m, a= 0.085 m). The biasing electrode is immersed into the plasma from the top of the torus and its radial position can be changed on a shot to shot basis. Here, confinement properties are contrasted for the two positions of the electrode with respect to the separatrix (Last Closed Flux Surface), as shown schematically in **Fig. 1**.

- "Standard" configuration of biasing experiments: Electrode is located deep in the edge plasma, i.e. in the region with closed magnetic field lines. Consequently, the sheared radial electric field is amplified between the electrode and the separatrix. This arrangement was demonstrated to be efficient to study properties of polarized plasmas, however, it can be hardly accepted in practice in large-scale or reactor-size experiments, since the electrode would not survive high thermal loads.

- Biasing of separatrix: Alternatively, the biased electrode is inserted only into the scrape-off layer (SOL). In this case, the thermal load should be certainly significantly smaller than in the previous case and such scheme can be employed as non-intrusive one.

Note that the second one can be materialized only if the scrape-off layer is broader then the radial extent of the biasing electrode. It is arranged on CASTOR by a downward shift of the plasma column. The minor radius of the plasma is reduced with respect to the limiter radius and, as a consequence, an "additional"

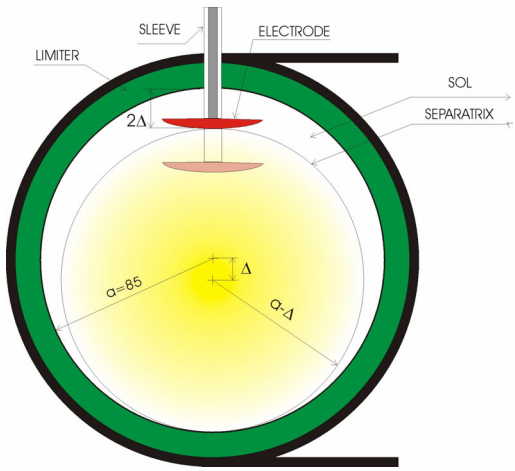

Figure 1 *Poloidal cross section of the CASTOR tokamak, where positioning of the biasing electrode at a "standard" and at "separatrix biasing" arrangements is shown.*

scrape-off layer appears at the top of the torus. It is clearly seen that et separatrix biasing the mushroom electrode is hidden in SOL and its top is just touching the separatrix.

1.2 Global Particle Confinement

The confinement properties at both the biasing schemes are compared for similar discharge conditions in **Fig. 2**. The electrode is positively biased by the pulsed voltage, U_b =+200 V.

As seen in Fig. 2, the current of about 35-40 A is drawn by the electrode during the biasing period. The line average density increases noticeably with biasing in both cases. However, the evolution of the H_α spectral line intensity $I_{H\alpha}$ exhibits different shapes. For the standard configuration, the intensity drops immediately with biasing, which evidently implies a reduction of recycling and results in improvement of the global particle confinement. On the other hand, at the separatrix biasing, the H_α emission slightly increases during the initial phase of the biasing period. Nevertheless, the global particle confinement time τ_p increases substantially (by ~80% at standard biasing and by ~50% at the separatrix biasing), as seen in the bottom panel of Fig. 2.

1.3 Radial Electric Field

All these observations are interpreted as formation of a transport barrier. Its radial position is deduced from the radial electric field profile $E_r(r)$, measured by the rake probe with floating tips. The radial profiles of $E_r(r)$ for both the cases discussed are shown in **Fig. 3**. The transport barrier is localized in the region of highest shear.

It is evident from the figure that the radial electric field is sheared in both the cases. However, at separatrix biasing, the ExB shear rate $\omega_{ExB} \sim dE_r/dr/B_T$ is larger then for the "standard" scheme although the particle confinement improvement is higher in the latter case. The value of $\omega_{ExB} \sim 10^6 s^{-1}$ evidently prevails the typical growth rate of unstable modes ($\gamma \sim 10^5$ s^{-1}). Fluctuation measurements have shown a strong impact on the poloidal correlation of turbulent eddies [1] in this case.

References

[1] J. Stöckel et al: In Proc. of 26th EPS Conf. on Contr. Fusion and Plasma Physics, 1999, p.1589.

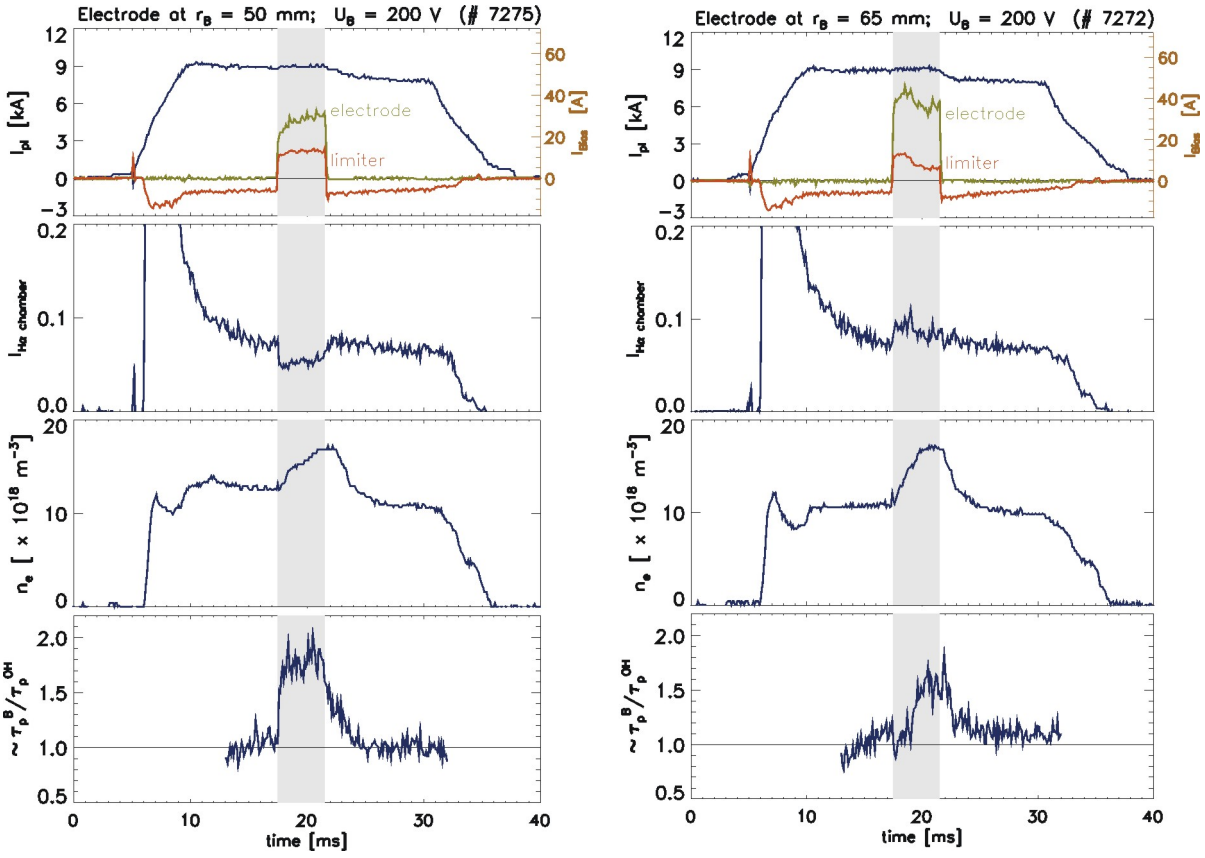

Figure 2 *Evolution of polarized discharges at "standard" and "separatrix biasing" arrangement at almost identical discharge conditions (I_p = 9kA, B_T= 1T and n_e = 1 - 1.2×10^{19}m^{-3}). Panels from top to bottom: Electrode current and the return current to the poloidal limiter together with the evolution of plasma current; the line averaged density over the central vertical chord (in 10^{18}m^{-3}); the intensity of H_α spectral line (in [a.u.]); and the relative improvement of the global particle confinement time, calculated using the expression $\tau_p^B/\tau_p^0 = (n_e^B I^0_{H\alpha})/(n_e^0 I^B_{H\alpha})$ (the superscripts "B" and "0" denote the values in biasing and ohmical heating phases).*

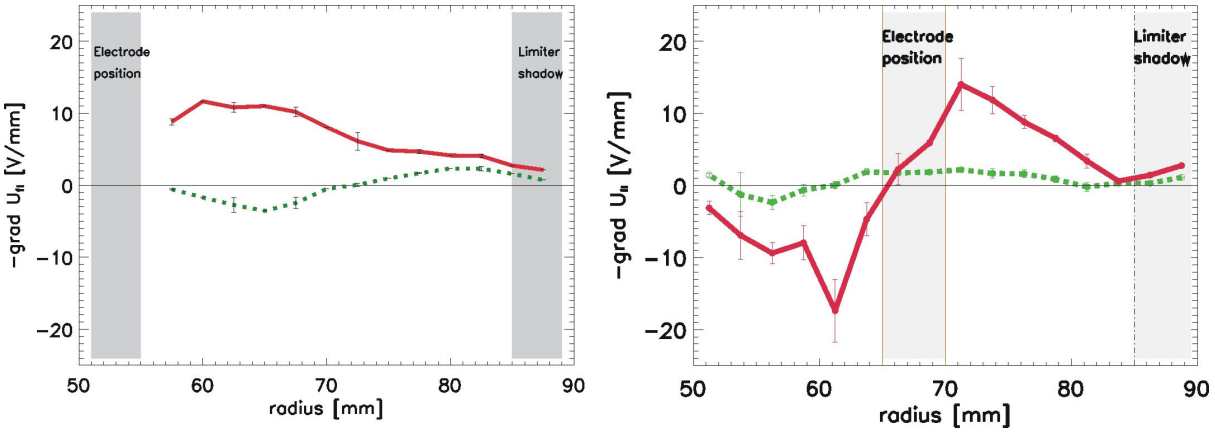

Figure 3 *Radial electric field profile at "standard" (left) and "separatrix biasing" (right) arrangements.*

2. Direct measurements of *E*×*B* flow and its impact on edge turbulence in the CASTOR tokamak

Cooperation:

G. Van Oost, Department of Applied Physics, Ghent University, Belgium

J. Gunn, Association EURATOM-CEA sur la Fusion Contrôlée, DRFC, CEA Cadarache, France

Experimental evidence of the correlation between edge sheared ExB flow and reduction of electrostatic turbulence has recently been found in the CASTOR tokamak (R=0.4 m, a=0.085 m, B_T=1T) in so called "separatrix biasing" regimes [1]. The biasing electrode is placed at the separatrix in a configuration, which has demonstrated strongly sheared electric fields and consequent improvement of the global particle confinement. A set of movable electrostatic probes (rake, Langmuir, Gundestrup) is used [2] to provide simultaneous measurements of poloidal and toroidal flows, electron temperature, density, and radial electric field at the same poloidal location and with high temporal resolution.

The relation between the ExB and ion flow velocities was systematically investigated in biased discharges. To that end, the "Ideal Gundestrup Probe" (IGP) was located at two distinct radial positions in front of and behind the biasing electrode, in the region of highest radial electric field (r=70 mm and r=85 mm), deduced from the radial profile of the floating potential measured by the means of the rake probe, see **Fig. 4.**

It is seen from the figure that the gradient of the floating potential is enhanced with biasing (U_b= +100 V) at both sides of the electrode, i.e. in the SOL as well as inside the separatrix. The radial electric field is calculated following the expression

$$E_r = -(\nabla U_{fl} + \alpha \nabla T_e)$$

where the factor α is rather uncertain in magnetized plasmas [3] and ranging from 1.3 to 3.

As seen from the left panel of Fig. 4, the actual radial profile of the electron temperature must be taken into account because of rather large local gradients of the electron temperature observed within the separatrix (∇T_e ~ -2 V/mm), but also in the SOL (-1V/mm). Note the similar shape of Te(r)-profiles in ohmic as well as at separatrix biasing regimes.

Series of discharges at different biasing voltage have

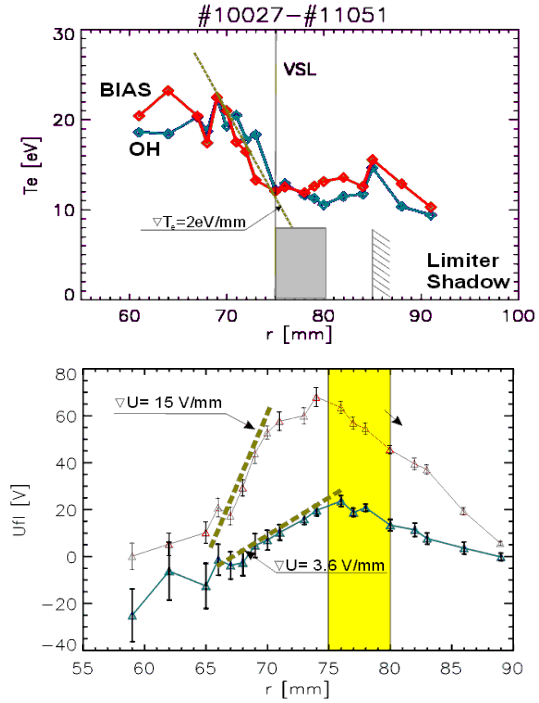

Figure 4 *Radial profile of electron temperature (top) and floating potential (bottom) in ohmic and biased phase of discharges measured by the single Langmuir probe located at the top of the IGP. Position of the separatrix is at r=75 mm, which corresponds to the location of the top of the biasing electrode. The radial extent of the biasing electrode is marked by the yellow box.*

been performed. The resulting dependency of the perpendicular Mach number on the radial electric field is shown in **Fig. 5**.

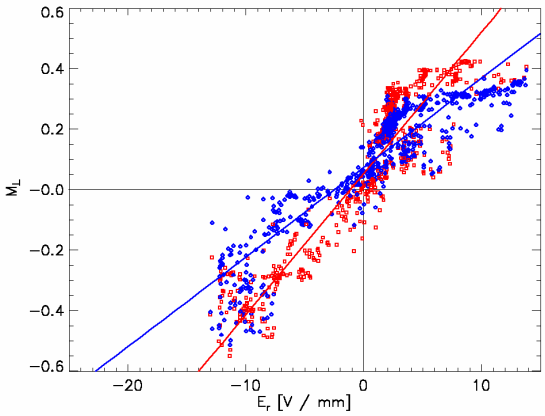

Figure 5 *Perpendicular Mach number versus the radial electric field. The red points correspond to Mach numbers deduced from the KD model [4], while the blue marks are calculated using the VG model [5].*
$E_r < 0$ - IGP is within sepratrix
$E_r > 0$ - IGP is in the SOL

It is evident from the figure that the perpendicular Mach number is proportional to the magnitude of the radial electric field. The slope of the curves is determined by the ion sound velocity, which is either $c_s = v_{ExB}/M_\perp \sim 21.5$ km/s (KD-fit) or 32 km/s (VG-fit).

It is interesting to compare this experimental value with the expression

$$c_s = \sqrt{\frac{k(ZT_e + \gamma T_i)}{m_i}} \cong 9.8.10^3 \sqrt{ZT_e + \gamma T_i}$$

c_s[m/s], T_e[eV],

which gives for the experimentally measured electron temperature 16 eV a significantly higher value,~ 40 km/s, even in the case of T_i=0, Z=1. This may indicate that the actual value of the electron temperature is less than that measured from I-V characteristics of the single Langmuir probe. This may appear, for example, if the edge plasma is non-maxwellian, and contains a few percent of suprathermal electrons. It is clear that this observation needs further analysis.

References

[1] G. Van Oost et al.: ITC-11, TOKI 2000, *J. Plasma Fusion Research Series* **4** (2001) 29-35.
[2] J. Stöckel et al.: In Proc. of 28th EPS Conf. on Controlled Fusion and Plasma Physics, Funchal, Madeira, Portugal, 2001, poster P1.057.
[3] R. Schrittwieser et al.: ibid., poster P1.106.
[4] K. Dyabilin et al: In Proc. of 27th EPS Conf. on Controlled Fusion and Plasma Physics, Budapest, 2000, p. 1653.
[5] H. Van Goubergen et al.: *Plasma Phys. Contr. Fusion* **41** (1999) L17.

Measurement of Light Impurities at the Plasma Edge

ITEM: II.1.b)

V. Piffl, J. Badalec, V. Weinzettl
Institute of Plasma Physics, Prague

Cooperation: H. Weisen, CRPP EPFL Lausanne

I. Introduction

The manifold influence of the impurities on plasma parameters has been often demonstrated in current plasma experiments. The radiation losses - the primary effect of an impurity presence in a plasma - occur already at the impurity concentration level near or higher than one percent of the electron plasma density. At this concentration the impurity ions increase the effective ion charge of the plasma (Z_{eff} up to 1.5), which is mostly consistent with measured Carbon content, insofar that Carbon seems to be the main impurity under most operating conditions in now days high temperature plasma experiments. We expect that the experimental methods of plasma spectroscopy and the modelling of plasma emission could play an important role in the development of a confinement system for controlled fusion in the near future.

The scanning of line emission spectra in an ultra-soft x-ray (XUV) wavelength range, 1-10 nm, allows to get a basic information on impurities be contained in a plasma. The absolute measurement of the line power intensity for an estimation of the impurity concentration, as well as the spatial (and temporal) resolved investigation of the line intensity radial profile for an evaluation of the impurity transport parameters, is an important task now.

II. Power line density radial profile and transport effects

In order to calculate the spectral shape and the line intensities from a low-Z impurity contaminated plasma for comparison with an observed spectrum, it is necessary to first estimate the populations of the impurity ionisation stages and then calculate the spectrum and line intensities from each ionisation stage. In addition to collisional excitation and photo-recombination into the ground state (coronal equilibrium) transport effects must be taken into account at least for the conditions prevailing near the periphery of the magnetically confined plasmas where light impurities are partially ionised. The ionisation and radiation code uses measured electron temperature and density profiles and calculates power intensity profiles of selected main lines of each charge state of the impurity ion species under consideration.

The effect of transport is demonstrated in **Fig. 1** and **Fig. 2** for a simulated plasma of a cylindrical shape

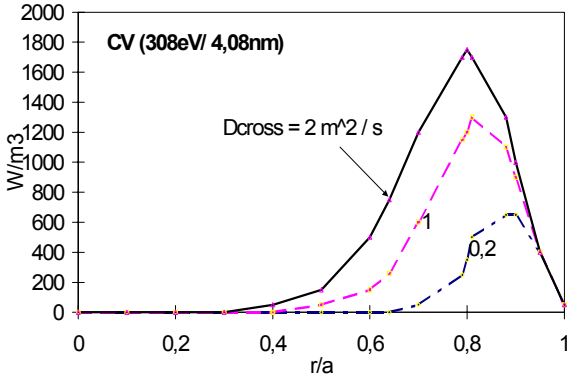

Figure 1 *Computed CV line emission density profile for different $D_\perp$ =0.2; 1; 2m^2s^{-1}.*

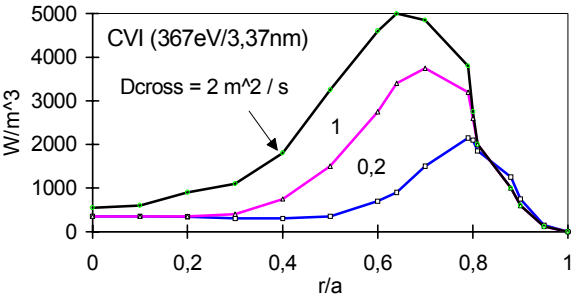

Figure 2 *Computed CVI line emission density profile for different $D_\perp$ =0.2; 1; 2 m^2s^{-1}.*

using the STRAHL code**.** The computed emission density profile of the CV and CVI lines for three selected values of the diffusion coefficient $D_\perp$= (0.2, 1.0, and 2.0) m^2s^{-1} are shown, for small plasma radius a = 0.2 m (for TCV tokamak). With increasing $D_\perp$ the line maximum is closer towards the central part of the plasma, where the temperature and density are higher. This displacement represents a couple of cm in radial direction if $D_\perp$ changes from 0.2m^2s^{-1} to 2m^2s^{-1}. Evidently the radial profile of the line emission density is sensitive to changes of the diffusion coefficient $D_\perp$.

We can see: the transport effects lead to some deviations of the line emission density profiles from those calculated using pure coronal equilibrium ($D_\perp \rightarrow 0$). They lead also to the changes in the line intensity radial profile, **Fig. 3**, and line intensity ratios of He- and H-like ionisation stages measured using line-integrating spectrometers at different radial positions, Z(r/a). Simulations for Carbon indicate that He- to H-like line intensity ratios are sensitive to $D_\perp$ for $D_\perp$<1m^2/s especially at outer diameter of a plasma column, see **Fig. 4**. This opens the possibility of using an imaging spectrometer of high spatial resolution for ion transport study in magnetically confined plasmas.

Experimentally observed ratios of the line intensity from the He-like lines (such as CV at 308eV) to the H-like lines (such as CVI at 367eV) in TCV tokamak plasma discharge are several times larger than expected from coronal equilibrium without transport. In order to

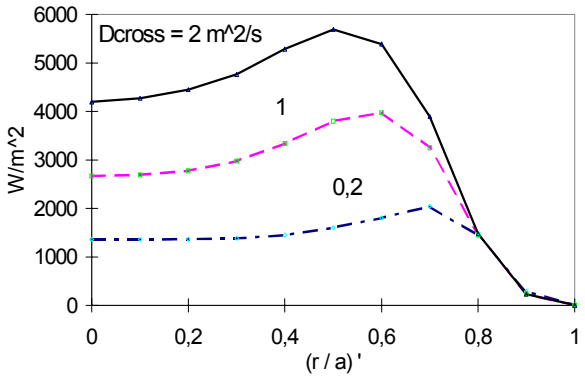

Figure 3 *Computed CVI line intensity radial profile for different $D_\perp$= 0.2; 1; 2 m^2s^{-1}.*

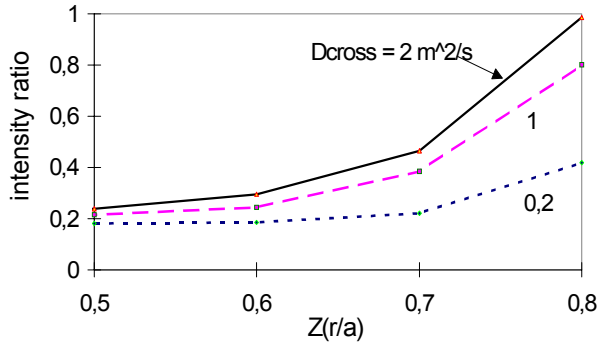

Figure 4 *Computed CV/CVI line intensity ratio for Dcross=0.2; 1; 2 m^2/s^{-1} as dependence on view-chord position, Z(r/a).*

reproduce the observed line intensity ratios of He- to H-like lines it is necessary to assume a diffusion coefficient $D_\perp$>0.5m^2/s [1].

III. Radial profiles of H- and He-like Oxygen and Carbon lines on the TCV tokamak

The scientific co-operation between the Institute of Plasma Physics, Association EURATOM/IPP.CR, Prague and CRPP, Association EURATOM/Confederation Suisse EPFL, Lausanne is performed in the frame of the **„Framework agreement for scientific collaboration“**, which has been signed in August - September 2000. The Institutes decided to undertake the specific joint research project on **„USX-ray spectroscopy and transport effects on light impurity ionisation in TCV“** , lead by V. Piffl (IPP) and H. Weissen (CRPP) for 2000 and 2001 years.

The experimental work was executed in two step:

1. Line ratio measurements, during the August - September 2000
2. Radial profile measurements in March-April 2001

a) MLM based USX spectrometer

The multi-layer mirror (MLM) based USX spectrometer was continually operating on TCV from the summer of 1996. The last alignment was performed in January 1997. The first check of the spectrometer elements setup, in August 2000, has shown unchange-

able parameters in Boron, Carbon and Oxygen channels. Only the amplifier in the nitrogen channel had to be changed due to the low amplification. The instrument shock resistivity and main parameters stability have been demonstrated during the almost 15 000 shots performed in relative harsh experimental conditions (high intensity external magnetic field, hard x-ray background emission). The MLM based instruments may open up the new diagnostic possibilities for the next generation of large fusion research devices.

b) Refurbishing of the USX spectrometer for line ratio measurements

Almost three weeks have been spent to refurbish the USX spectrometer by multi-layer mirrors for simultaneous intensity line measurements of the resonance lines of H- and He-like stages of Carbon and Oxygen. A new arrangement of the filters and detection part was necessary. The reason was the low level of the detected signal of the He-like lines, especially of OVII, due to the low concentration of Oxygen in a plasma. The new set of filters and application of the „open“ channeltron in OVII channel have partially solved this problem. The spectrum scanning near to the chosen lines by new installed mirrors has been performed as first and compared to the previous one (from 1996).

c) Spectral lines monitoring

The monitoring of the relevant spectral lines at the standard operation during the series of specific experiments by the USX spectrometer was performed.

The output signal of the channeltron detector represents the series (chain) of the rectangular pulses. The pulses are counted by a counter with one millisecond time resolution. If the count rate is small, 5 counts/ms, the decrease of the time resolution (changing in software) by factor ten leads to the appropriate decrease of the statistical error of the line intensity signal and to the signal separation from the low intensive noise background.

d) Line intensity ratio measurements

Determination of the line intensity ratios of the He-like and H-like Carbon and Oxygen lines was undertaken in the different TCV discharge conditions. The first computer programmes for signals processing and for the preliminary line intensity ratio evaluation were prepared. The investigation of the line intensity ratios of the He- like and H-like Carbon and Oxygen lines in the different TCV discharge conditions began during the second half of the September. The signals of the He- like and H-like Carbon of a more than one hundred shots in the four different discharge regimes (reduced IOH breakdown, X2 ECCD, high kappa with ECH, pump out) were stored in TCV database for a later evaluation.

IV. Light impurity emission measurements in the CASTOR tokamak

The radiation of the light impurities (Carbon and Oxygen) has been measured in the VUV and USX ranges in the CASTOR tokamak (R=0.4 m, a=0.085 m, T_e~200 eV).

a) Experimental setup

The two-channel multilayer-mirror-based USX spectrometer [2,3]**,** constructed in IPP Prague, allows the absolute spectrum measurements in the ranges of 1.4-2.4 nm and 3.1-4.5 nm with the space resolution about 10 mm on plasma and time resolution 100 μs. This spectrometer can be mechanically tilted by ±10°, so that both the time and space resolved spectral lines of the He- and H-like Carbon (C V 4.03 nm, C VI 3.37 nm) and Oxygen (O VII 2.16 nm, O VIII 1.86 nm) are measured. Additionally, the time behavior of the lower ionization states can be monitored in a visible and VUV range by a photomultiplier with interference filters (C III, 464.7 nm).

b) Radial profiles of Oxygen and Carbon lines on the CASTOR tokamak

The temporal evolution of the spectrum in the Carbon and Oxygen lines range was measured during the standard OH regimes for low (I_p~10 kA) and high (I_p~16 kA) plasma current. The spatial profile of the selected most intensive lines C V 4.03 nm, **Fig. 5**, and O VII 2.16 nm **Fig. 6**, was composed from a set of chordal measurements done shot-by-shot.

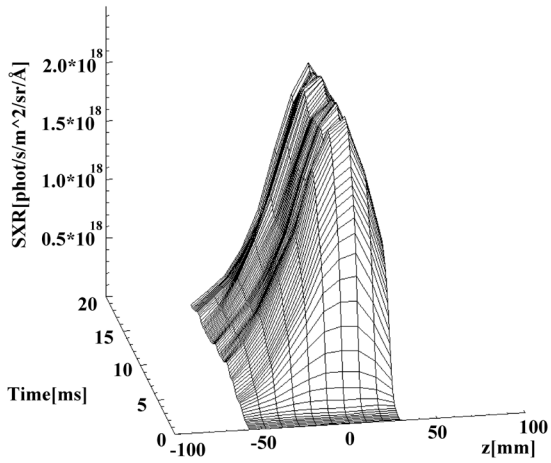

Figure 5 *Non-abelized line intensity radial profile of CV 4.03 nm line measured by XUV monochromator.*

We have found, the regimes with a strong poloidal rotation of plasma, inducted by biasing, are influenced by the high impurity content during the high-current discharges. In this case, the spectral measurements in shot-by-shot series are practically impossible. We hope, the new-built XUV high-throughput monochromator, which is in test processing, make possible the spectral study of the regimes with a strong poloidal rotation of plasma in the low-current discharge.

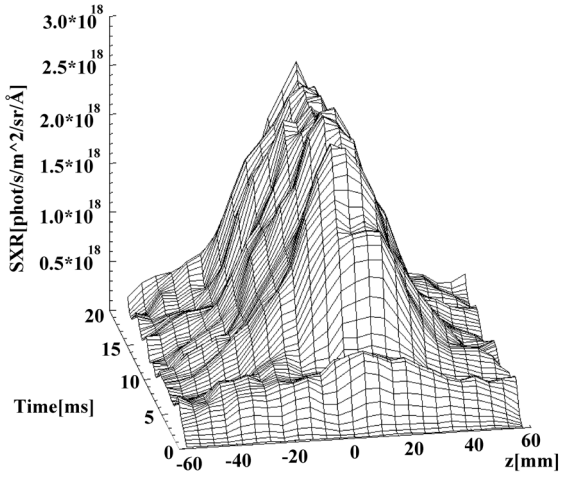

Figure 6 *Non-abelized line intensity radial profile of O VII 2.16 nm line measured by XUV monochromator*

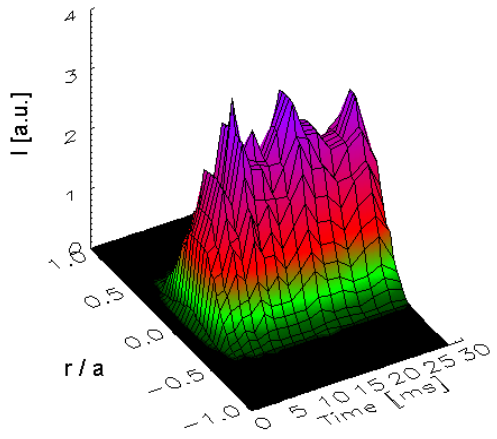

Figure 7 *Line intensity radial profile of C V 4.03 nm line computed by EVIMP*

We have found that the regimes with a strong poloidal rotation of plasma, inducted by biasing, are influenced by the high impurity content during the high-current discharges. In this case, the spectral measurements in shot-by-shot series are practically impossible. We hope, the new-built XUV high-throughput mono-chromator, which is in test processing, make possible the spectral study of the regimes with a strong poloidal rotation of plasma in the low-current discharge.

c) Impurity emission model

The time dependent coronal model with transport phenomena can be used to compute the light impurity distribution. A new version of the STRAHL fortran code was written, in co-operation with Garching, by adapting it for the small-size tokamak, such as the CASTOR tokamak. Moreover, the new EVIMP (EVolution of IMPurities) IDL code was developed especially for a small radius, high temperature tokamak plasmas. The EVIMP allows to include a real plasma parameters behavior, such as $n_e(r,t)$, $T_e(r,t)$, etc. An example of computed data by EVIMP is shown in **Fig. 7**.

Both the codes are ready to compare experimental and computed data. The fisrt data comparison suggests the value of diffusion coefficient near $D_\perp \sim 2 m^2 s^{-1}$.

References

[1] H. Weisen, V. Piffl, A. Weller and TCV Team: Measurement and modelling of the light impurity behaviour in TCV tokamak. *Proc. 23rd EPS Conf.*, 24-28 June 1996, Kiev; LRP 550/96, CRPP-EPFL Lausanne,1996, p.29.

[2] V. Piffl, J. Badalec, A.V. Golubev, S.V. Bobashev: Absolute measurement of light impurities line radiation using MLM-based spectrometer on CASTOR tokamak, IPPCZ-340, IPP Prague, 1994.

[3] V. Weinzettl, J. Badalec, V. Piffl: Space and time resolved XUV spectroscopy of CV and OVII lines. *27th EPS Conf. Contr. Fusion and Plasma Physics*, Budapest, Hungary 2000, P 4.112, p.555.

[4] V. Piffl, J. Badalec, V. Weinzettl, A. Burdakov: Intensity radial profile study of CV (308eV) line at tokamak CASTOR, *28th EPS CFPP,* Funchal, Madeira, Portugal, 2001, *ECA* 25A, pp.1233-1236.

Modelling of Edge Plasma

ITEM: II.1.c)

1. Modelling of electrostatic turbulence at the edge of the CASTOR tokamak

R. Klíma, I. Ďuran, J. Horáček, M. Hron, P. Pavlo, J. Stöckel, F. Žáček

Cooperation:

K. Dyabilin, Institute of High Energy Density, Moscow, Russian Federation

Electrostatic drift wave turbulence of the CASTOR tokamak edge plasma was simulated by using a set of equations similar to those of Hasegawa – Wakatani[1)]. Sheared poloidal plasma rotation was taken into account by means of a fluid model of the plasma polarization.

Modelling was performed for the experimental conditions of the CASTOR tokamak with the aspect ratio R/a = 40cm / 8.5cm, B_t = 1 T, I_p = 10÷15 kA. Typical

[1)] A.Hasegawa, M.Wakatani: Phys.Rev.Lett. **50** (1985) 682; M. Wakatani, A. Hasegawa, Phys. Fluids **27** (1984) 611.

central ion and electron temperatures are 50÷70 eV and 150÷200 eV, respectively, line average density 10^{19} m^{-3}. In the simulations, the region of the edge contained plasma and of the limiter shadow was considered (6 cm < r < 10 cm). The simulations yield the temporal evolution and spatial distribution of the electric potential and plasma density fluctuations. Their power spectra, the radial profiles of rms values of fluctuating quantities, and the spatial correlation lengths have been derived. Finally, the fluctuation-induced particle flux was computed. [1]. The results are compared with the experimental data obtained on the CASTOR tokamak using the 2-D matrix of Langmuir probes [2].

Theoretical Model - Basic Equations

Normalized equations for the particle density perturbation n, the potential fluctuation ϕ and vorticity w are generalized for the whole poloidal range:

$$\frac{\partial n}{\partial t}+(\nabla\phi\times\nabla n)_{\parallel}=\frac{\partial n_0}{\partial x}\frac{\partial\phi}{\partial y}-V_\theta\frac{\partial n}{\partial y}+\sigma_2 n_0\left(\frac{\phi}{T_e}-\frac{n}{n_0}\right)+D\nabla_\perp^2 n$$

$$\frac{\partial w}{\partial t}+(\nabla\phi\times\nabla w)_{\parallel}=-G_b\left(\frac{\cos\theta}{n_0}\frac{\partial n}{\partial y}+\frac{\sin\theta}{n_0}\frac{\partial n}{\partial x}+\frac{n}{n_0}\left(\frac{1}{T}\frac{\partial T}{\partial x}\right)\sin\theta\right)+$$
$$+\sigma_1\left(\frac{\phi}{T_e}-\frac{n}{n_0}\right)-V_\theta\frac{\partial w}{\partial y}+\frac{\partial^2 V_\theta}{\partial x^2}\frac{\partial\phi}{\partial y}+\mu\nabla_\perp^2 w,$$

$$w=(\nabla\times\mathbf{v})_{\parallel}\approx\nabla_\perp^2\phi$$

where $\sigma_1=\dfrac{\omega_{ci}^2 v_{T_e}^2}{\nu_{ei}L_{\parallel}^2}\tau_0$, $\sigma_2=\dfrac{v_{T_e}^2}{\nu_{ei}L_{\parallel}^2}\tau_0$,

$G_b=\dfrac{c_s^2}{x_0 R}\tau_0^2$, $T=T_e+T_i$

According to the CASTOR geometry and typical plasma parameters, we use the following normalization: $x, y \to x/x_o$, y/x_o, $t \to t/\tau_o$, $\phi \to e\phi/T_o$, $T_e \to T_e/T_o$, $\tau_o = x_o^2/(T_o/eB)$, where x_o = 5 mm, T_o = 25 eV. For the magnetic field B = 1 T, the characteristic time τ_o = 1 μs. Boundary conditions for all variables are zero for both $r = r_{min}$ and $r = r_{max}$, and periodic in the poloidal direction. The parallel scale length $L_{\parallel}$ in the scrape-off-layer is obviously given by the circumference of the torus; in the confinement region ($r < a$), $L_{\parallel} = 2\pi Rq$ was assumed. The safety factor $q(r)$ is calculated from the ohmic current profile for Spitzer resistivity and given $T_e(r)$.

Poloidal plasma flow velocity is obtained by solving the equation for the poloidal ion force balance [3].

The system of equations is solved on a rectangular grid of 100 × 1256 points corresponding to the radial and poloidal directions. The grid is uniform in both directions. The radial coordinates extend from r = 0.06m up to r = 0.1m and the poloidal angle is $0 < \theta < 2\pi$.

Results

The snap-shots of the density and potential structures in the regime of saturated turbulence are shown in **Fig. 1**. It is seen that they are of a similar character, which is obviously because of their strong coupling. Such saturated level of turbulence is observed hundreds of microseconds (for the CASTOR case) after beginning the computation. In accordance with the unfavorable curvature of the magnetic field lines, the turbulent structures appear at first in the low field side region of the torus, $-\pi/2 < \theta < \pi/2$. Then, they are redistributed poloidally, reaching a dynamic equilibrium. However, the poloidal asymmetry remains not only in the "in-out" direction, but it develops also in the "top-bottom" direction.

Local radial particle flux induced by the density and potential fluctuations can be estimated as

$$nv_r=(n_0(x)+\tilde{n})\frac{(B\times\nabla\tilde{\phi})_r}{B^2}.$$

The simulations show that the strong outward local flux is concentrated at the low field side and tends to zero at the high field side of the torus. The flux

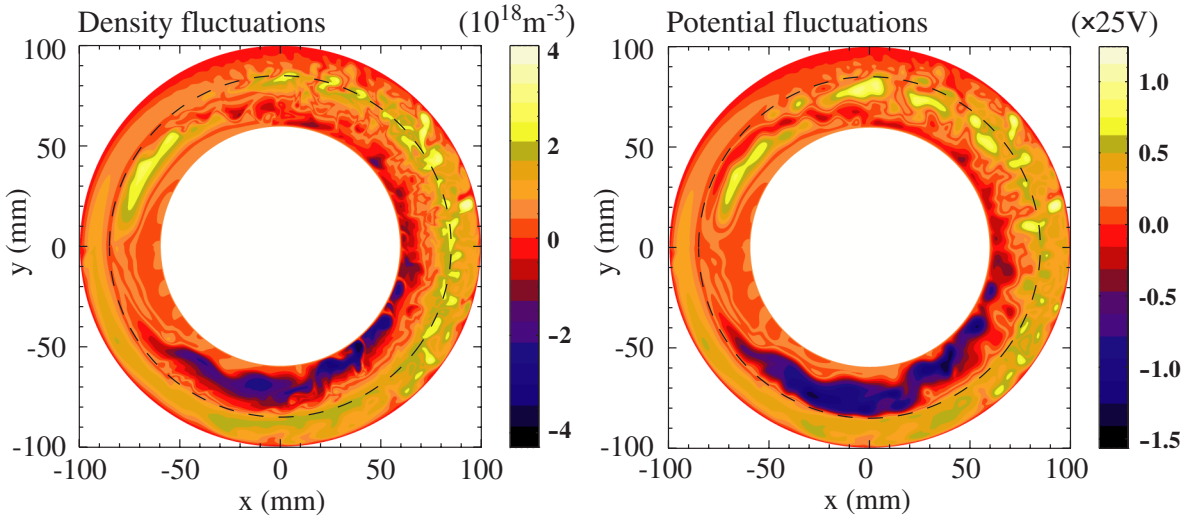

Figure 1 *Snap-shots of turbulent structures. Left: plasma density, the scales are in 10^{18}m^{-3}. Right: plasma potential normalised to 25V.*

appears to be negative (inward) at some poloidal angles, however, the poloidal average is always positive. Temporal behaviour of the poloidally averaged particle flux is shown in **Fig. 2a**, for two different radial positions. Characteristic time of fluctuations is in the range of tens microseconds. Radial profile of the flux, averaged over time and poloidal angle is shown in **Fig. 2b**. In the vicinity of the separatrix, the flux decreases nearly three times as compared with that in the confinement region. It should be noted that the global particle confinement time on the CASTOR tokamak is 1÷2 ms. This implies the global particle flux across the separatrix in the range of (2÷4) × 10^{20}m^{-2} s^{-1}. As seen from Fig.2b, the numerical simulation yields values close to that numbers.

The spectral analysis of fluctuation data, computed at the separatrix (r = 85 mm), are presented in **Fig. 3a**. Three frequency bands, with the power spectrum density decaying as $f^{-\alpha}$ are apparent, the corresponding exponents being $\alpha \approx 0$, 0.83, or 4.2. Apart from the very low power spectra densities, the above mentioned exponents are close to the experimentally measured, cf. **Fig. 3b.**

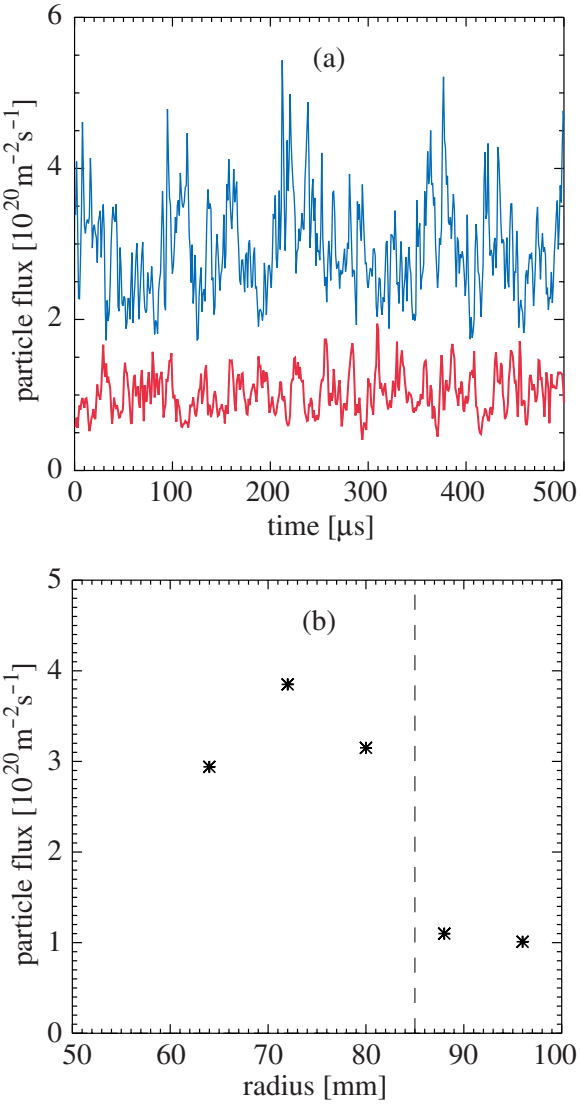

Figure 2 *(a) Temporal evolution of the poloidally averaged particle flux. Radial positions r = 64mm (upper trace) and r = 96mm (lower trace). (b) Radial profile of the poloidally averaged particle flux.*

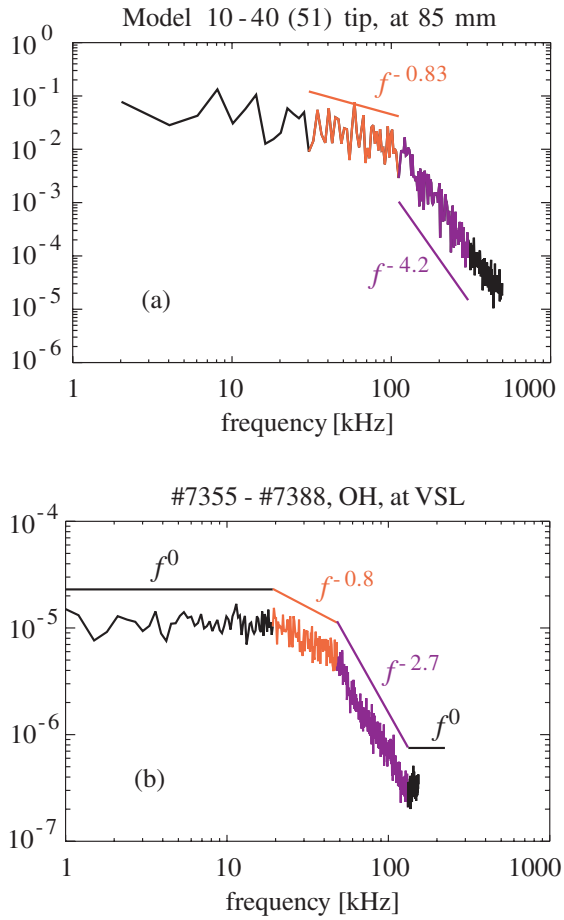

Figure 3 *(a) Power spectra of potential fluctuations from simulation. Top of the torus, radial position r = 85 mm (separatrix). (b) Power spectrum of potential fluctuations measured at the top of the torus by a probe positioned at the separatrix (r = 85mm).*

Detailed pictures of the potential structures at the top of the torus obtained in the simulations are given in **Fig. 4 a-d**. The individual panels represent the situation in four consequent moments. It is seen that the characteristic poloidal and radial dimensions of potential structures are about (5÷10) mm. The poloidal and radial correlation lengths, derived from the spatial-temporal correlation analysis of the computed data are of the same range. This is in agreement with the picture obtained in experiments performed on the CASTOR tokamak using the 2-D matrix of Langmuir probes [2], see **Fig. 5** (the size is in scale with Fig. 4). The matrix is positioned at the top of the torus.

Conclusions

Various experimentally studied regimes including externally polarized (biased) plasma have been simulated. The effect of the sheared poloidal plasma flow on the turbulent structures and on the resulting particle flux observed in experiments has been reproduced.

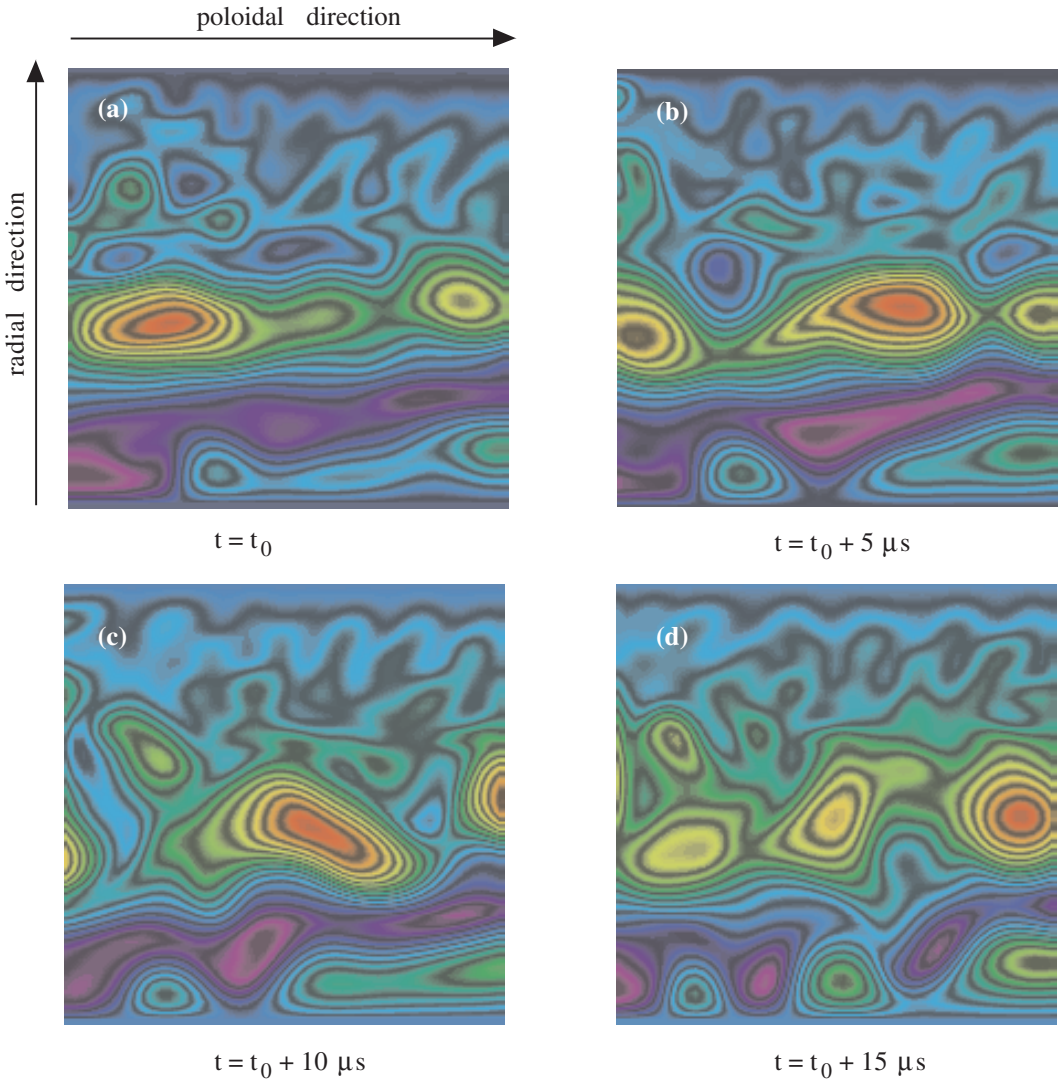

Figure 4 *Snap-shots of potential structures at the top of the torus. Each panel depicts the area of 40 mm × 40 mm.*

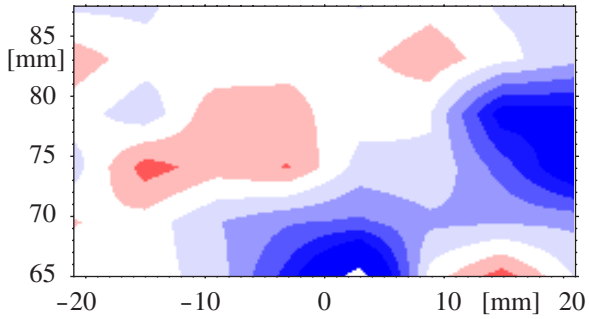

Figure 5 *Potential structures measured by using 2-D matrix of Langmuir probes (size in scale with Fig. 4).*

References

[1] K. Dyabilin, R. Klíma, I. Ďuran, J. Horáček, M. Hron, P. Pavlo, J. Stockel, F. Žáček: Modelling of the effect fo the sheared poloidal flow on the electrostatic turbulence on the CASTOR tokamak. *Czechoslovak Journal of Physics* **51** [10] (2001) 1107-1117.

[2] J. Stöckel, M. Hron, I. Ďuran, K. Dyabilin, J. Horáček, K. Jakubka, L. Kryška, E. Martines, S. Nanobashvili, G. Van Oost, M. Tendler, F. Žáček: Plasma polarization of the separatrix on the CASTOR tokamak. *27th EPS Conf. Contr. Fusion Plasma Phys.*, Budapest 2000, ECA Vol.**24B**, p. 1032.

[3] K. Dyabilin, I. Ďuran, M. Hron, J. Horáček, R. Klíma, P. Pavlo, J. Stockel, F. Žáček: Modelling of electrostatic turbulence at the edge of the CASTOR tokamak. *Research Report* IPPCZ-366, IPP Prague, Dec. 2000.

[4] K. Dyabilin, et al.: Modelling of electrostatic turbulence. In: *28th EPS Conf. on Controlled Fusion and Plasma Physics,* Funchal, Madeira, Portugal, June 18-22, 2001, pp. 1669-1672.

2 Diagnostics Development

Soft X-ray (SXR) Spectroscopy of Light Impurities

Item II.2/a

V. Piffl, V. Weinzettl

Institute of Plasma Physics, Prague

During recent years, the technology of curved multilayer mirrors for ultra-soft x-ray focusing optics had some applications that have further increased the diagnostic potential of the MLM-based spectroscopy:

- separation and detection of the spectral lines of the low-Z plasma impurities (B, C, N, O),

- imaging of the weakly plasma emanation regions in chosen line

The programme of the XUV spectroscopy group at CASTOR involves:

- measurements of the Carbon line C^{4+}(4.03 nm) emission with a time resolution 10 μsec in a regime of "one-chord detection"**,**
- the time and spatial evaluation of the radial distribution of the C^{4+} line emission in plasma column cross-section of 80 mm diameter with space resolution better than 1 mm during the one tokamak discharge in an "imaging regime".
- modelling of light impurities emission in tokamak CASTOR by use of the ionisation and radiation code with respect of the particles transport phenomena.

In the frame of our current research programme, we have fabricated the prototype of a high-throughput XUV monochromator based on spherical multilayer mirror, see **Fig. 1**. The completed apparatus is testing on CASTOR tokamak in the regime of the Carbon C^{4+} (4.03 nm) line imaging.

XUV monochromator design

Relatively high reflectivity and small difference in the meridional and sagittal focal length for near normal incidence angle makes the MLM spherical mirror to be both the dispersive and imaging element of the presented XUV monochromator[1,2].

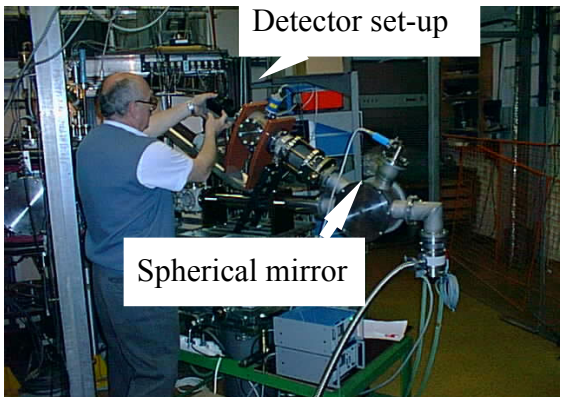

Figure 1 *XUV imaging monochromator*

The **spherical multilayer Fe/C mirror** with the diameter 50 mm, the curvature of 1000 mm and the number of periods 100 is tailored for detection of the spectral line of Carbon C^{4+}(4.03nm). The mirror reflection R=1.24% and spectral resolution $\lambda/\delta\lambda$ = 81 is calculated at 4.027nm wavelength and at appropriate Bragg angle 74.2 deg. The reliability of calculated data for chosen wave range of 4.027 nm is confirmed by good coincidence (of the order 3%) of both: experimental and calculated data for several emission characteristic lines of different elements. The experimental data shown in the Table 1 are slightly corrected for an angular divergence of the probing beam is taken into account. The homogeneity of the Fe/C layers-period at a diameter of 40 mm is 1%. The major mirror characteristics are consulted with the manufactory: The Budker Institute of Nuclear Physics, Novosibirsk, Russia.

According to our previous measurements, the brightness of the Carbon C^{4+} (4.03nm) line is about 5.2×10^{17} photon/m^2.sec.ster in CASTOR. Due to the increase of the effective surface of the spherical mirror by in the comparison to the previous used flat mirror configuration, the expected number of detected photons (and consequently number of generated photon-electrons) could be approximately two orders higher. Really, the input (S1) and output (S2) aperture are about of 1000 mm^2 and are placed at the distance L =

[1] L.K. Huang, S.P. Regan, M. Finkenthal, H.W. Moos: Laboratory test of a LSM-based narrow bandpass and high throughput camera for Tokamak plasma imaging between 100 and 200 Å, Review of Scientific Instruments, 63 (10), October 1992, 5171-5173

[2] S.V. Bobashev, D.M. Simanovskii, Yu.Ya. Platonov, P. Roewekamp, G. Decker, W.Kies: Spectral selective plasma imaging in the wavelength range 2.4-4.5 nm at SPEED 2 device, Plasma Sources, Sciences&Technology, 5(3), (1996), 578-581

Table 1: The characteristics of the spherical multilayer Fe/C mirror

Wavelength	Experimental data			Calculated data		
Å	Θ_{max}, ded.	Refl., %	$\lambda/\delta\lambda$	Θ_{max}, ded.	Refl., %	$\lambda/\delta\lambda$
8.34	11.5	4.7	95	11.52	4.60	83.4
9.89	13.8	3.6	94	13.75	3.70	94
13.33	18.6	1.7	90	18.58	1.76	81
14.56	20.3	1.3	79	20.35	1.35	80
17.59	24.7	5.2	73			
40.27				74.2	1.24	81

1500 mm; so the "étendue": $S1.S2/L^2 = 10^{-1}$ is two to three orders higher than the "étendue" of our flat MLM spectrometers[3] .

Because the expected count-rate is higher than 10^6 impuls.sec^{-1} in a regime of one-chord detection we use a two-step microchannel plate (MCP) detector. The effective dead time of the whole MCP is about 6.10^{-8} sec. Therefore, in the case of homogenous photons flux up to 10^7 - 10^8 photon/100 mm^2 on the whole active detector area, and supposing the individual microchannels work independently, the gain remains constant during the irradiation.

The imaging properties of the spherical mirror monochromator system have been analysed in geometrical optics approximation using a ray-tracing procedure. The calculated space resolution in meridional plane is better than 0.1 mm (!), while the experimentally observed space resolution is about 1 mm. This value was evaluated in visible light on an optical stand.

The high throughput XUV monochromator represents an additional huge volume connected to the tokamak vacuum system through the large surface slot. The intensive differential pumping is needed to avoid an undesirable influence on the tokamak discharge regime.

Experimental proof of the XUV monochromator

As a first experimental test of the complete monochromator system, we have proved to image the plasma radial profile in visible integral spectra during the total period of a plasma discharge in simple reflection mirror mode. The image of plasma has been created at a ground-glass and successfully recorded by CCD camera. Unfortunately, the back-ground lightness due to the mirror surface effect strong affects the quality of the picture. As the monochromator system could be tilted, the plasma has been imagined at different view angle and the finish result has been created by processing of different picture exposition. So the apparatus background lightness has been almost eliminated during the acquisition image process. The very preliminary results indicate the maximum of the visible light emission near to the plasma column axis, as we expected.

The first effort to detect the radial distribution of the Carbon C^{4+}(4.03 nm) line emission was realised by microchannel plate detector, screened by 0.24 μm thick Ag filter of 20 mm effective diameter and equipped by the four anode collectors of 2mm width and 0.5 mm spacemen between the collectors. The multi-collector detect the MCP current at different radii and covers almost of the 30 mm spacing in the plasma column. The four collector signals are recorded during the one plasma shot. The different plasma profile sectors could be imagined onto the multi-collector by tilting of the monochromator.

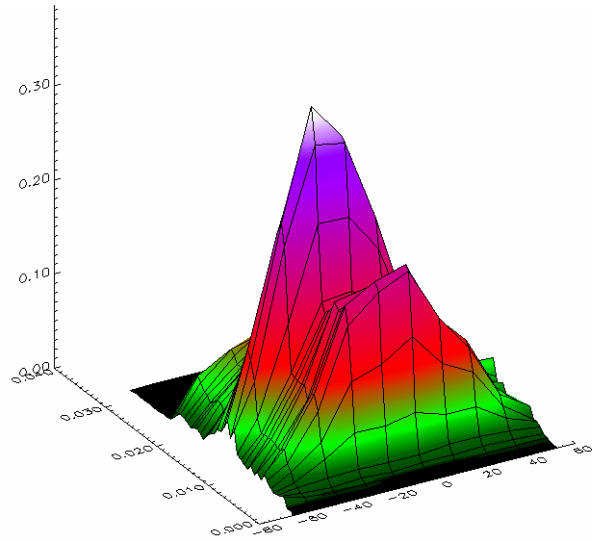

Figure 2a *Time evolution of the radial profile of* C^{4+} *signal.*

An example of C^{4+} (4.03 nm) row signal, which is detected at different radii, is plotted in **Fig. 2a.** Some profile changes and displacement of the position of signal maximum during the period of biasing application (V= +200 V, at r=75 mm) is evidently observed. A systematic test of the XUV monochromator apparatus set-up using a single spherical multilayer mirror to form a large plasma volume image in Carbon C^{4+}(4.03 nm) line onto a MCP converter array will continue.

[3] V. Piffl, J. Badalec, A.V. Golubev, S.V. Bobashev: Absolute measurement of light impurities line radiation using MLM-based spectrometer on CASTOR tokamak, IPPCZ-340, IPP Prague, 1994

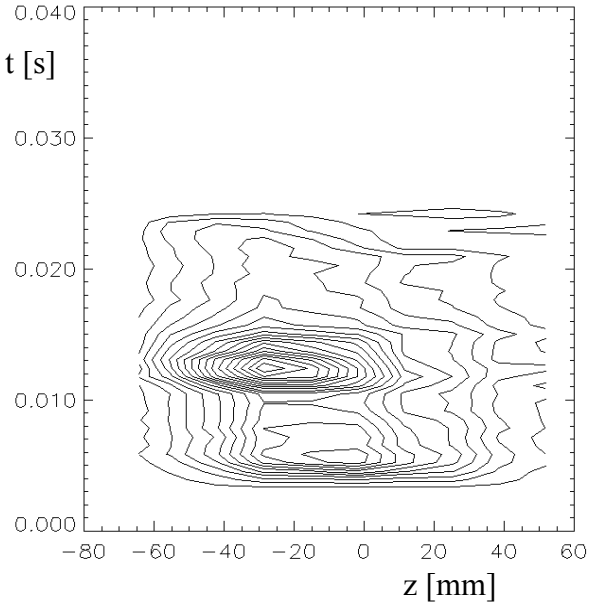

Figure 2b *Contour plot of the radial profile of* C^{4+} *signal (see Fig. 2a).*

Acknowledgements

We wish to thank Mr. A.Baumruk for technical design of the monochromator. This work was supported by the Grant: AVK 104 36 01/99.

References

[1] V. Weinzettl, J. Badalec, V. Piffl: Space and time resolved XUV spectroscopy of CV and OVII lines. *27th EPS Conf. on Contr. Fus. and Plasma Physics*, Budapest, Hungary 2000, Abstracts of Invited and Contributed Papers, P 4.112, p.555.

[2] V. Piffl, J. Badalec, V. Weinzettl, K. Koláček: Imaging XUV monochromator on base of spherical multilazer mirror. *Proc. 13th Int. Conf. on High-Power Particle Beams*, BEAMS 2000, Nagaoka, Japan, June 25-30, 2000, p.81.

[3] V. Piffl, H. Weisen: Ultra-soft X-ray spectroscopy using multilayer mirror. *Transactions of Fusion Technology. An International Journal of the American Nuclear Society* **39** [1] 155-158 (2001).

Development of an Advanced Probe for Edge Tokamak Plasma

Item II.2/b

J. Stöckel, I. Ďuran, M. Hron, J. Adámek, J. Horáček, K. Jakubka, L. Kryška, F. Žáček,

Institute of Plasma Physics, Prague

R. Hrach, M. Vicher, M. Tichý

Charles University in Prague, FMP

Cooperation:

J. Gunn, Association EURATOM-CEA sur la Fusion Contrôlée, DRFC, CEA Cadarache, France

G. Van Oost, Department of Applied Physics, Ghent University, Ghent, Belgium

R. Schrittwieser, EURATOM/OAW, Innsbruck Uni, Austria

Optimization of Gundestrup probe for ion flow measurements in magnetized plasmas

Gundestrup probes are used to measure ion flows in magnetized plasmas. The standard design consists of six to twelve conducting pins mounted around an insulating housing in order to obtain a significant variation of the angle between the magnetic field and the probe surface. According to fluid and kinetic modeling, the current density collected by each pin is largely determined by the Bohm-Chodura boundary condition [1]. Despite the rigour of the physics formulation, the precision of flow measurements by Gundestrup probes has so far been limited to large parallel and perpendicular Mach numbers ($|M_{||}|, |M_{\perp}| > 0.1$). This is because slight angular misalignments and finite gap width between the pins and the housing cause non-negligible uncertainty of the individual effective collecting areas.

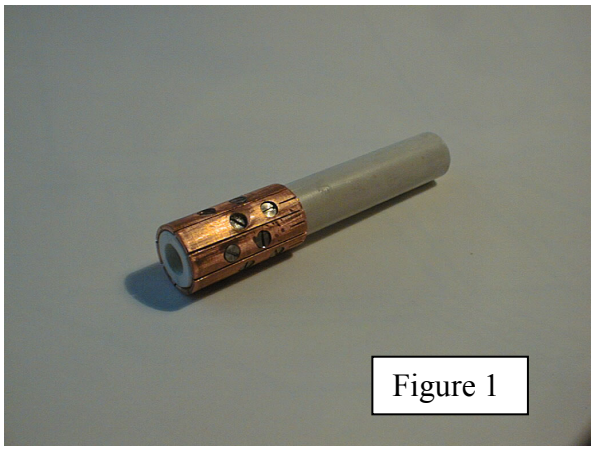

The Gundestrup probe design has been improved ("Ideal Gundestrup Probe", IGP) and tested in order to render it attractive for flow measurements even in unbiased edge plasmas. The ion collecting surface is a nearly continuous cylindrical conductor (made of Cu-tube of diameter 11.7 mm) divided into eight segments separated by 0.2 mm gaps, as shown in **Fig. 1**. The

collecting area, determining the radial resolution (2.2 mm) is defined by an insulating quartz sleeve that is slightly shorter than the central conductors. The eight collectors are biased negatively into ion saturation in order to construct polar diagrams with good temporal resolution. All signals are sampled at 1 MHz.

This optimized design has been validated in the CASTOR tokamak (R=40 cm, a= 8.5 cm, B_T =1 T) in ohmic and biasing discharges. The poloidal and toroidal flows are measured simultaneously at the same radius by the IGP and rotating Mach probe (RMP) [2]. The electrode is located at the separatrix (r_b = 75 mm), and is positively biased with respect to the vacuum vessel. It has been shown recently [3] that such a biasing scheme effectively modifies the radial electric field not only in the scrape-off layer, but also in front of the electrode in the region of open magnetic field lines. The radial profile of the floating potential is monitored at the plasma edge by a rake probe [4] to derive the radial electric field in the edge plasma. All these tools are located at the same poloidal angle (at the top of the torus) to assure their respective radial positioning with a sufficient precision.

Comparison of IGP and RMP

Polar diagrams of the ion saturation current measured by the IGP and RMP at the same radial position are compared in **Fig. 2**. The data are recorded in the same shot, during the biasing period of the discharge. Both probes are positioned inside the separatrix, at the radial electric field maximum, and consequently are not connected to any material element of the discharge chamber.

It is well seen that experimental data are reasonably fitted by the fluid model [2] and the resulting Mach numbers are shown in the table:

	$M_{\parallel}$	$M_{\perp}$
IGP	-0.2	-0.18
RMP	+0.0	-0.24

From this table and even from the visual inspection of the diagrams, a different shape of the diagrams, in particular in the toroidal direction is apparent. It is possible that toroidal asymmetries of the ion flow could exist in the CASTOR tokamak. Local recycling from different objects in the SOL (for example the biasing electrode or the poloidal limiter), plus viscous propagation of parallel flow from the various pre-sheaths into the core could lead to such asymmetries. One can not exclude that the difference in the $M_{\parallel}$ determination is partially caused by a misalignment of the probes with respect to the magnetic field lines [1].

Alternatively, the probe data are processed by the model developed by H. Van Goubergen [5]. An advantage of this method is that it provides an analytic formula for the ratio of upstream and downstream currents. However, only four pins of eight are used for processing of the raw data. Consequently, we have only two points from which we derive the Mach number using linear regression.

Systematic measurement of $M_{\perp}$ and $M_{\parallel}$- radial profiles

The IGP and RMP probes were moved radially by steps of 3 mm between shots. The electrode was biased to +150 V. The ExB velocity at the probe position is deduced from radial profile of the floating potential, $v_{ExB} = (-\nabla_r V_{FL} - 2.5\nabla T_e)/B$ and normalized by the sound velocity $M_{\perp}^{ExB} = v_{ExB}/c_s$.

A reasonable agreement between the $M_{\perp}$, measured by both probes is observed. This indicates the toroidal symmetry of perpendicular flow. Note that the ExB velocity is systematically lower in the SOL, if the actual profile of the electron temperature is taken into account. Both probes are located on different sides of the stagnation point in the SOL, therefore the opposite sign of the $M_{\parallel}$ is measured there as expected. The exceptional region appears in the proximity of the separatrix (r=75 mm), where the RMP is directly connected with the electrode and the parallel flow reverses in this region during biasing.

Conclusions

The physics basis for this Gundestrup probe design has been validated by detailed measurements of ion

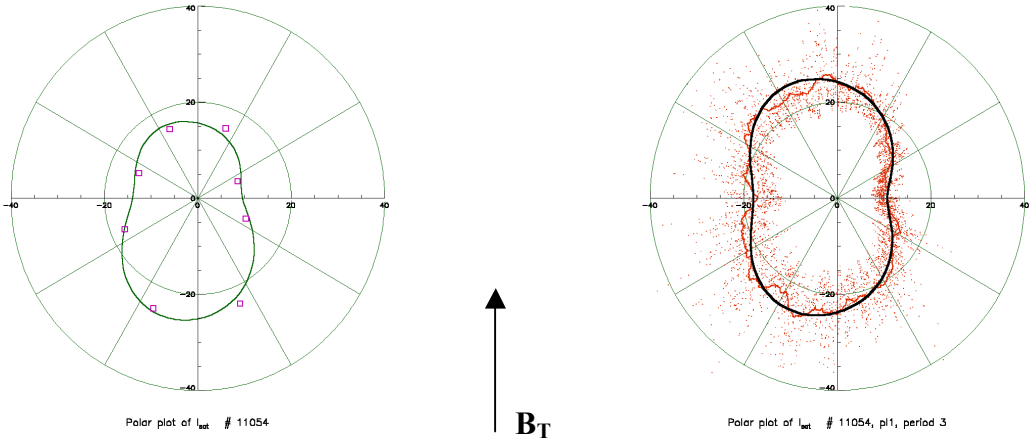

Figure 2 *Polar diagrams of the ion saturation current as measured in the same shot #11054 by the IGP (left) and the RMP (right) located inside the separatrix (r= 70 mm). The experimental points are fitted to the KD model [2] (solid lines).*

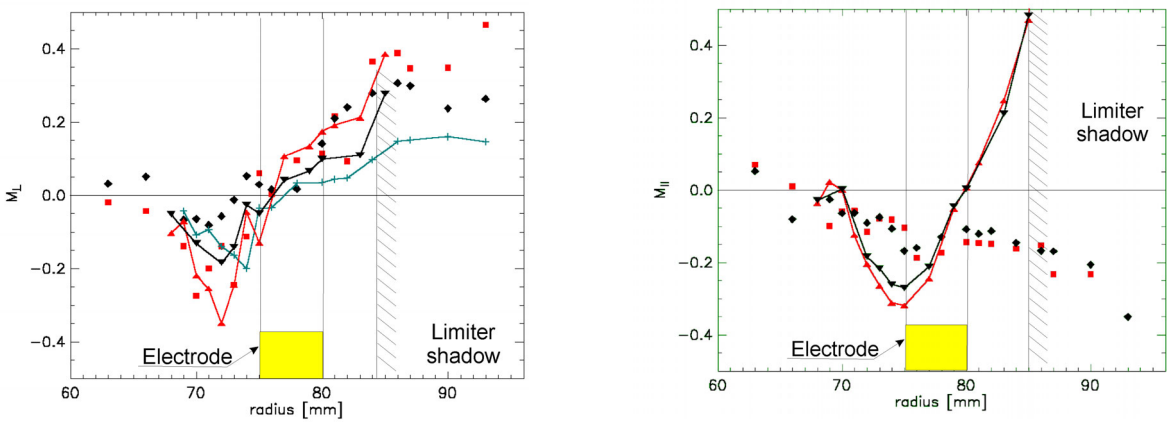

Figure 3 *Radial profiles of perpendicular and parallel Mach numbers during electrode biasing as measured simultaneously by the RMP and the IGP. Electrode occupies the range of radii 75-80 mm, i.e. separatrix biasing with U_b= 150 V. Radial profile of the ExB velocity is shown for comparison in the left panel. Probe data are processed by two methods (denoted as KD [2] and VG [5]). #11027-51.*

collection by a rotating planar Mach probe in bias-controlled edge flows in the CASTOR tokamak. In principle, Gundestrup probes present advantages over rotating Mach probes due to their simpler mechanical design (no sliding contacts) and better temporal resolution. The absolute magnitude of the poloidal velocity is in a good agreement with the ExB drift velocity deduced from the measured radial electric field, when the E_r and flow measurements are carried out in the same plasmas.

References

[1] J.P. Gunn et al.: Edge flow measurements with Gundestrup probes. *Phys Plasmas* **8** (2001) 1995.

[2] K. Dyabilin et al: Ion flows measurements using a rotating Mach probe on the CASTOR tokamak. 27th EPS Conf. Contr. Fusion and Plasma Physics, Budapest, 2000, p. 1653.

[3] G. Van Oost et al.: Potential Structures and Flow Measurements with Separatrix Biasing in the CASTOR tokamak. ITC-11, Toki 2000, *J. Plasma Fusion Research Series* **4** (2001) 29-35.

[4] J. Stockel et al.: Magnetic and electrostatic fluctuations in the CASTOR tokamak. *Plasma Phys. Contr. Fusion* **41** (1999) A577.

[5] H. Van Goubergen et al.: *Plasma Physics Contr. Fusion* **41** (1999) L17.

Thomson Scattering System

Item II.2/c

P. Plíšek, F. Žáček, V. Badalec,
J. Brotánková

Institute of Plasma Physics, Prague

On the first session of International Adviser Board of Tokamak CASTOR in 1999, it was recommended to install a Thomson scattering system to increase a credibility of all experimental works made on this experimental device. Thomson scattering system should measure mainly electron temperature and its profile over a plasma column.

Possibility of getting a suitable high power diagnostic laser from FOM Nieuwegein, The Netherlands, was found after discussion of this board. It was also recommended to get the best possible detection system (monochromator and photomultipliers) from CEA Cadarache, France.

J. Brotánková from IPP Prague has been on the one month stay at FZJ Jülich, Germany, to cooperate with the Dutch TS group from FOM Nieuwegein in installation of Thomson Scattering system and to work under the real experimental conditions on the TEXTOR – 94 tokamak. Valuable experiences has been acquired.

Layout of the experiment and many detail calculations of primary beam path, stray light suppression, needed focussing optics, requirements on optimisation of detection etc. have been proposed and done in collaboration with R. Barth from FOM Nieuwegein and P. Platz from CEA Cadarache.

Primary laser beam will go through the Tokamak CASTOR (R/a=0.4/0.1m) vertically. It will enter tokamak through a vacuum window (BK7) from the top at position 1200 mm above the plasma centre (diameter of the beam on the window is 17 mm) and it will exit tokamak through a similar window at position 900 mm below the plasma centre (diameter of the beam on this window is 14 mm). The vacuum windows are installed in a tubes with the system of apertures and diaphragms, which will suppress the stray light from the primary beam.

For focussing of the primary beam a telescope with focal length 1500 mm will be used. It will consist of two lenses: converging and diverging with focal length ± 500 mm. The lenses have been delivered by Optical Workshop of the Academy of Sciences of the Czech Republic in March 2001.

After passage through the tokamak, the beam will be absorbed in a dump from black glass with a monitoring of the beam energy.

Light scattered at 90 degrees angle will be detected through a horizontal port (80x200mm) and collected by a large detection lens. Then the light will be dispersed in monochromator and displayed to the 10-channel glass fibre-optic array. Fibres lead light to the photomultipliers, where the scattered light will be detected.

P. Plíšek from IPP Prague has been on the two days stay at FOM Nieuwegein to take over the high power ruby laser mentioned above (see **Fig. 1**) and to learn details about its alignment and operation. The whole system, including laser head, power supplies, remote controls and water cooling were transported to the tokamak CASTOR in October 2000.

Figure 1 *Laser system.*

The laser system is made by Holobeam Laser, Inc. It consists of a Q-switched oscillator and one amplifier. Laser works on the line (λ = 694,3 nm) and it produces one giant 10 J pulse with length 10-20 ns. The laser output light is vertically polarised. For CASTOR experiment will be the polarisation changed to horizontal one (parallel to the confining magnetic field) using a Half Waveplate already bought from CVI Laser Corporation.

By the end of year 2000 the laser system was adapted and some small repairs were done. Afterwards the system was successfully activated. However, because a small damage on the input face of an amplifier ruby rod has been found (see **Fig. 2**) and because this damage has been expanding very quickly, an operation of the laser could result in destruction of the whole ruby rod. Damaged ruby rod has been therefore sent to Radiate Hamburg to be repolished and recoated.

Detection system, including large collecting lens (diameter 100 mm, focal length 200 mm), monochromator (Czerny-Turner type, entrance slit 15 mm x 0-5mm, focal length 300 mm, gratings 1200 or 1800 lines/mm with dimensions 64x64 mm [type 70 HSM

Figure 2 *Damaged face of the laser rod.*

27] and dispersion about 2,7 nm/mm or 1,8 nm/mm, respectively), ten photomultipliers (56 TVP, S20, quantum efficiency 3,6%), connecting fibre optics (10 pieces, length 1500 mm, input face 1,5 x 4,5 mm, output face rounded) and some other accessories, have been sent to IPP Prague from CEA Cadarache.

Simultaneously with laser adjustment, detail calculations of detection system efficiency and total throughput, including estimate of potential errors of measurement have been processed. These calculations show that on Tokamak CASTOR, with relatively small dimensions (R = 0,4 m, a = 0,1 m) and low plasma density (maximum value in the centre is about $2 \cdot 10^{19}$ m^{-3}), detection system with photomultipliers will not be sensitive enough to measure at the plasma edge or even not sensitive enough in the plasma centre if a high spatial resolution will be required. The estimations show that probably only measurement in the plasma centre (with no spatial resolution) will be possible. Therefore, it would be desirable to extend this detection system with intensified CCD detector for measurement of the whole profiles of plasma temperature and density with sufficient spatial resolution in the future.

With account of space situation around the Tokamak CASTOR, a final experiment layout of the whole diagnostics and setting of all optical as well as other components has been decided.

Vacuum tubes of primary beam with all apertures and diaphragms have been designed and their manufacturing are nearly finished. Also the frames for fixing of the laser itself as well as for fixing of laser focusing system, detecting system, tubes with apertures and diaphragms and both back viewing optical and primary beam dumps are under construction.

Fast electronic gating for the detecting photomultipliers and fast electronic circuits for signal integration are still to be designed and manufactured.

Partial installation of the system on the CASTOR tokamak took place during year 2001, and the first preliminary measurements are envisaged at the end of year 2002.

3 Wave Interactions in Plasmas

Propagation of LH Waves in Tokamaks

Item II.3/a

P. Pavlo, L. Krlín, R. Pánek, R. Klíma

Institute of Plasma Physics, Prague

Lower Hybrid Waves (LHW) have been successfully used for auxiliary heating and non-inductive current drive in tokamak experiments already for two decades. Experimentally observed characteristics (e.g., the current drive efficiency) have been found to agree well with the theoretical predictions based on the quasilinear theory and a resonant interaction of LHW with electrons. Despite of that, there still remain some open questions, e.g., the disparity between the relatively high phase velocity compared to the velocity of tail electrons for usual plasma temperatures has never been fully explained.

1 Test-particle simulations

We have shown earlier [1] that if the spatial localization of the LHW (lower hybrid cones) is taken into account, the energy density of the wave may exceed the limit of applicability of the quasilinear theory, and nonlinear effects become significant. In particular, we have assumed that the LHW exists only in a small fraction of the magnetic surface, and looked for the spread of final velocities of particles passing through a rectangular area of length L (cf. **Fig. 1**) by direct numerical integration of the equations of motion.

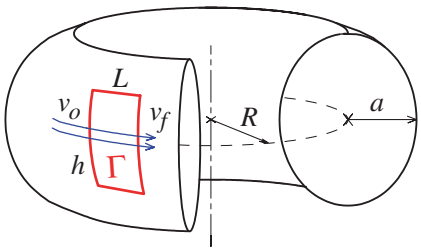

Figure 1 *Sketch of the model geometry.*

Further analysis revealed that the electrons with velocities above a certain threshold, and for high enough wave amplitude, are fast dragged into the resonant region (see **Fig. 2**).

These electrons however do not stay trapped in the middle of this region (at the resonant phase velocity) but are expelled above or below this velocity. As a result, a bump is formed on the tail of the electron distribution function, see **Fig. 3**.

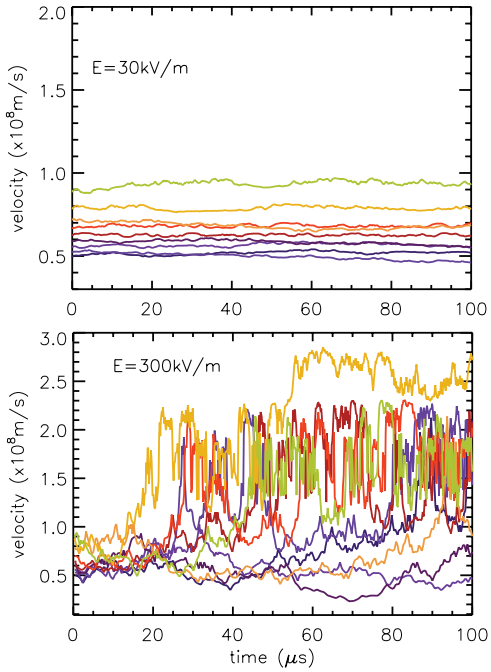

Figure 2 *End velocities of several particles when leaving the RF region of length* L = 0.3 m; *parallel refractive index* $N_{||}$ = 2 (phase velocity $v_{ph} = 1.5 \times 10^8$ ms^{-1}). *For the lower amplitude, there is no interesting change of the velocity for initial values* $v_0 \le v_{ph}/2$. *For* E_0 = 300 kV/m, *the acceleration of particles is dramatic even for* $v_0 \approx v_{ph}/4$.

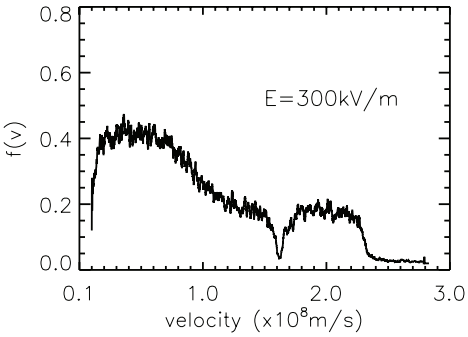

Figure 3 *Steady state distribution of electrons calculated for a large number of electrons initially homogeneously distributed in the region* $1\times10^7 < v_0 < 1.5\times10^8$. E_0 = 300 kV/m.

More details were presented in [2].

2 Absorption of LHW

To get a more global view of the above mentioned effects, we have developed a novel approach for

calculation of the absorption of LHW, based upon the detailed test-particle statistics. Full description was given in [3]; here, we give only a brief outline of the method.

The interaction of lower hybrid waves with electrons is usually described by the Fokker-Planck equation which – in its most simple, 1D form – reads

$$\partial/\partial v_{||}\,[D_{LH}(v_{||})\,\partial f_{||}/\partial v_{||}] + (2+Z_{eff})\,\partial/\partial v_{||}\,[\nu(v_{||})(v_{||} f_{||} + T_e m_e\,\partial f_{||}/\partial v_{||})] = -\partial f_{||}/\partial t\ . \quad (1)$$

Here, $f_{||}$ is the electron distribution function, $v_{||}$ is the velocity parallel to the magnetic field, ν is the collision frequency, m_e and T_e are the electron mass and temperature, respectively, and Z_{eff} is the effective charge. D_{LH} is the usual quasilinear diffusion coefficient. Equation (1) is spatially 0-dimensional, i.e., it applies to a distribution function averaged over the magnetic surface. To take into account the spatial localization of the LHW (only within the LH cone), without actually introducing the spatial dependence, we will proceed as follows. In the RF region Γ (of length L and height h, cf. Fig. 1), particles with the initial velocity v_0 are scattered to final velocities v_f with a probability $P(v_0, v_f)$. Thus, the original distribution $f_{||}$ is mapped onto f_1,

$$f_1(v) = \int P(v, v')\, f_{||}(v')\, dv'\,. \quad (2)$$

The scattering event occurs for the fraction $h/(2\pi a)$ of all particles, and that once in an orbit time $v_0/(2\pi R)$, where a and R are respectively the minor and major radii. The influence of the LHW on the distribution function can be then described by Eq. (1) but with the diffusion term replaced by a sink/source term,

$$(h/2\pi a)\,(v/2\pi R)\,(f_1 - f_{||}) + (2+Z_{eff})\,\partial/\partial v_{||}\,[\nu(v_{||})(v_{||} f_{||} + T_e m_e\,\partial f_{||}/\partial v_{||})] = -\partial f_{||}/\partial t. \quad (3)$$

Further, for conservation of particles, we must request

$$\int_v f_{||}\, v\, dv = \int_v f_1\, v\, dv,\ \text{i.e.,}\ 1/v \int_{v'} P(v, v')dv' = 1,\ \text{for all } v.$$

$P(v, v')$ can be determined statistically by direct integration of the equations of motion for the chosen combination of spatial modes, and a sufficient number of samples, cf. **Fig. 4**.

In what follows, Eqs. (1) and (3) are solved in variable $N = c/v_{||}$, on an equidistant grid with $\Delta N = 0.01$, $N \in (1, 31)$ (3000 grid points) unless specified otherwise by a finite difference method. The boundary conditions are $f(c/1) = 0$, $f(c/31) = f_M(c/31)$, f_M is the Maxwellian. Initial distribution $f_{||}(t) = f_M$, the timestep $\Delta t = 10^{-8} - 10^{-6}$ s.

Figure 5a shows the evolution of the distribution function as obtained from Eq. (3), using the scattering matrix as in Fig. 4. The steady state is reached in ≈ 10 ms for the parameters chosen. The curve 1 of **Fig. 5b** shows the steady-state distribution obtained for the same case but using Eq. (1) with the quasilinear diffusion coefficient for the spectrum used [3]. The staircase structure is due to zeros in this spectrum. If one takes into account the overlap of modes, the distribution function becomes close (within a factor of 2) to the steady state value (t = 20 ms) shown in Fig. 5a.

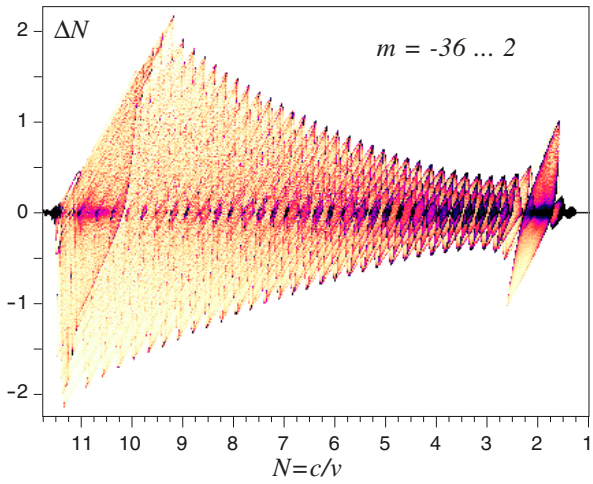

Figure 4 *Probability of the change of $N = c/v$* (scattering matrix) for E_{mono}= 300 kV/m, N_0 = 2, L = 0.324 m, f = 3.7 GHz, *and the spatial harmonics* m = 2 - 36, ΔN = 0.01, 1000 *samples per grid point.*

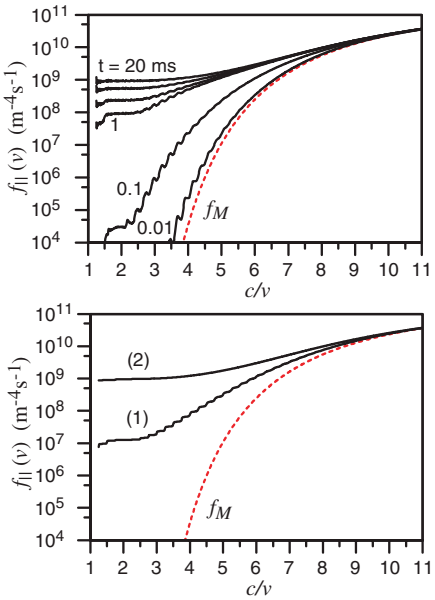

Figure 5 a) *Electron distribution function $f_{||}$ calculated by Eq. (3), at t* = 0.01, 0.1, 1, 2, 5, 20 ms; b) *Quaslinear results by Eq. (1) - steady state distribution function* (t = 20 ms): *curve 1 - the linear spectrum [3]; curve 2 - smoothed spectrum $W_k \sim 1/(k_0 - k)^2$.* E_{mono}=300 kV/m, $N_{||0}$=2, L=0.324 m, f=3.7 GHz, m = 36, ..., 2 (i.e., N_{min}=1.25, N_{max}=11.25), n_e=1×10^{19}m^{-3}, T_e=1 keV.

Temporal evolution of the absorbed power, and the power transferred collisionally to the bulk is shown in **Fig. 6a**. The absorption sets on instantly, then increases while the plateau is being built and finally saturates. The collisions first tend to fill the "hole" in the distribution function caused by the RF field (the transferred power is negative), then the collisional transfer increases to a steady state value. The patterns are similar for the nonlinear and the quasilinear approach if a smooth spectrum is used in the latter case.

The non-monotonous shape of the distribution function which is well apparent in the early stages of the built-up of the plateau (cf. Fig. 5a) and which still persists in the steady state as well. It should lead to destabilization of Langmuir waves with $\omega_L \approx \omega_{pe}$, $\omega/k = v_{||}$ wherever $\partial f_{||}/\partial v_{||} > 0$. Because the form of $P(v, v')$ is independent of $f_{||}$, these waves cannot fully eliminate the positive slopes of $f_{||}$, and the electrostatic energy will steadily grow. This is shown in **Fig. 6b**.

Here, Eq. (1) has been complemented by calculation of the electrostatic energy, using quasilinear growth rates [1], and the quasilinear diffusion term corresponding to the generated Langmuir waves energy has been added. Though the power spent on excitation of these waves is moderate (see Fig. 6a), due to the "accumulation", the spectral energy density of the Langmuir waves $W_{es,k}$ can fast exceed the spectral energy density of the primary LH wave. This opens the possibility of other nonlinear interactions which we will address in the future.

3 One-Dimensional Particle-In-Cell Simulation

A one-dimensional PIC code was constructed primarily to verify the effects observed in test particle simulations. The main advantage is the possibility to include self-consistent electrostatic field resulting from the charge separation. LH wave can accelerate electrons up to relativistic velocities, therefore, also relativistic effects were taken into account in the PIC simulations. Preliminary results, presented in [4], basically confirmed the picture obtained from the test-particle models; the effect of the charge separation and relativistic corrections appear rather insignificant in this case.

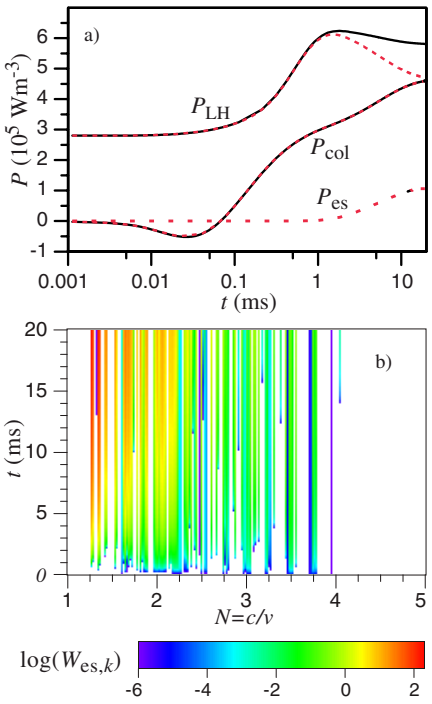

Figure 6 *Temporal evolution of* a) *the LH power absorbed and that transferred to the bulk by collisions without (full lines) and with (dashed lines) the account of generation of Langmuir waves, for the same case as in Fig. 5a); and* b) *the spectral energy density of the Langmuir waves* $W_{es,k}$.

References

[1] P. Pavlo and L. Krlín: Limits of applicability of the quasilinear approximation to the lower hybrid wave-plasma interaction. *Plasma Phys. Contr. Fusion* **41** (1999) 541.

[2] R.Pánek, L.Krlín, P. Pavlo, R. Klíma, V. Petržílka: The Role of Nonlinear Effects in LH Wave-Plasma Interaction, 27*th EPS Conf. CFPP*, Budapest, p. 1208.

[3] P. Pavlo and L. Krlín: Nonlinear effects in lower hybrid heating and current drive. *Czechoslovak Journal of Physics* **50** [S3] (2000) 25-32.

[4] R. Pánek, L. Krlín, P. Pavlo, V. Fuchs, R. Klíma, V. Petržílka, D. Tskhakaya, S. Kuhn: One-Dimensional Particle-In-Cell Simulation of Electron Acceleration in a Spatially Localized LH Wave, *28th EPS Conf. CFPP,* ECA Vol. **25A**, p. 341.

Measurements of Suprathermal Electrons in front of the Grills in CASTOR and Tore Supra Tokamaks

Item II.3/b

F. Žáček, K. Jakubka, J. Stöckel, I. Ďuran, M. Hron, V. Petržílka

Institute of Plasma Physics, Prague

A whole range of methods utilising absorption of RF waves momentum or energy is applied for electric current generation as well as for additional heating of plasma in tokamaks. Because a high RF power is often used, the wave-plasma interaction can be accompanied by a number of non-linear effects [1]. Commonly observed damages of limiter parts and divertor plates, which are connected directly with the antenna by lines of force of the confining magnetic field, can be result of such interaction. Theory explains this undesirable phenomenon by acceleration of particles due to the processes taking place just in front of the antenna. To verify this theory prediction experimentally, a fruitful experimental co-operation started in the year 2000 with CEA Cadarache, France. In the frame of this experimental co-operation four actions have been undertaken in the year 2000:

1) extensive probe measurements of plasma parameters in front of the CASTOR LH grill (frequency 1.25GHz, power up to 50kW) using a new movable double Langmuir probe (see Fig.1) have been carried out;

2) preparation of experiment using coaxial RF probes in front of the new launcher on tokamak Tore Supra has begun;

3) to identify the cause of damage, a surface analysis (SEM and SIMS) of the eroded graphite tile from the Tore Supra grill guard limiter has been made in Prague;

4) adaptation work for measurement of particle distribution functions (both electrons and ions) using the French Retarding Field Analyser (RFA) in tokamak CASTOR has started.

In the following the physical results obtained and the progress of the construction works are described in more details.

1. Probe measurements in front of the CASTOR tokamak grill

For the measurements in CASTOR tokamak (major radius 400mm, limiter radius 85mm, wall radius 100mm) a miniaturised movable Langmuir probe has been constructed, see **Fig. 1**. The probe consists of two tips of the length 1.5mm and diameter 1mm, spaced in tokamak toroidally by 3.5mm.

The lines transmitting the signal detected by the tips are performed as RF coaxial ones (with transmission up to 10GHz) with the characteristic impedance 50 Ohms. The outer conductors of the lines (stainless steel) are covered by corundum (Al_2O_3) using the technology of plasma spraying to prevent the electric field short circuiting. The probe has been fixed in a spherical joint located about 500mm above the centre of the tokamak small cross section where the grill is placed. This arrangement enabled us (by a tilting of the probe) to change the radial as well as the toroidal position of the measuring tips on the shot-to-shot basis, see **Fig. 2**. Further, vertical shift of the probe along its axis enabled to change the position of the tips also in the third dimension, denoted in figure 2 as *h* (height above the equatorial plane of the torus).

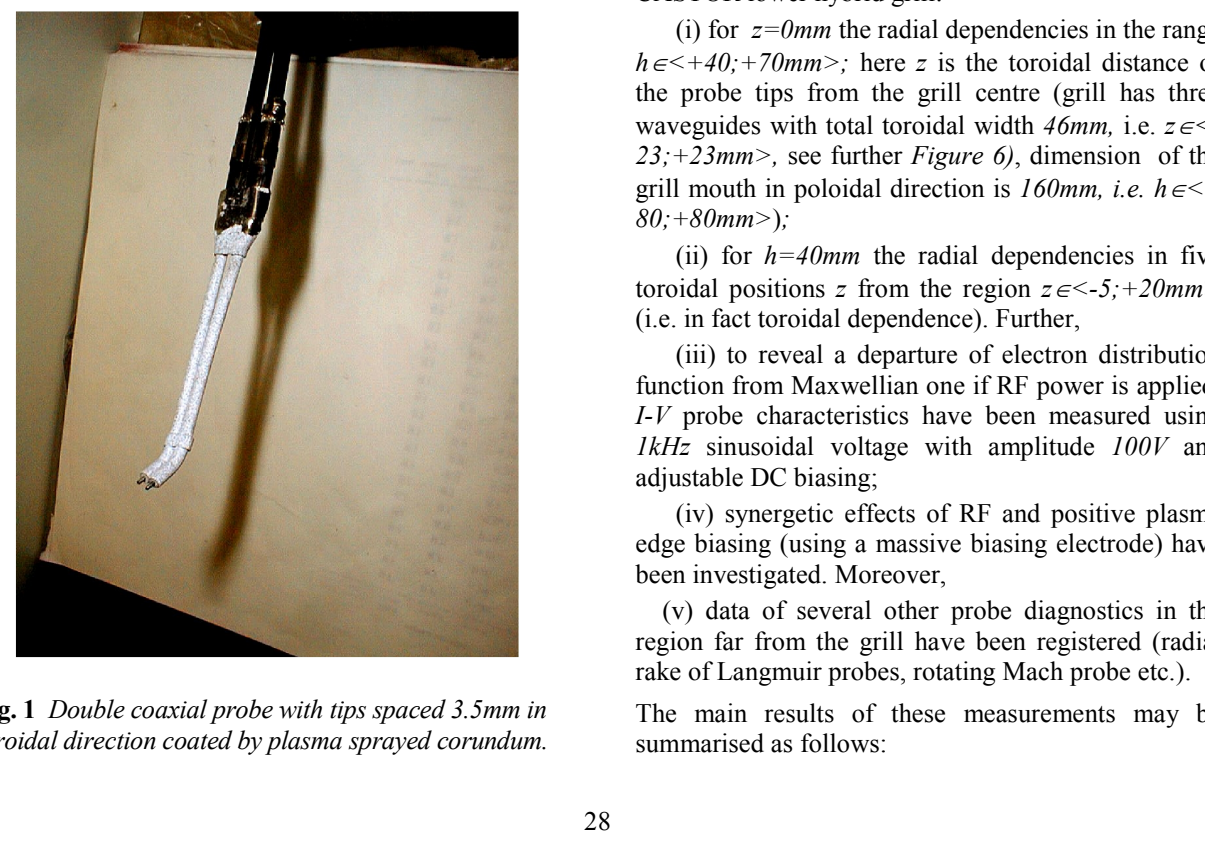

Fig. 1 *Double coaxial probe with tips spaced 3.5mm in toroidal direction coated by plasma sprayed corundum.*

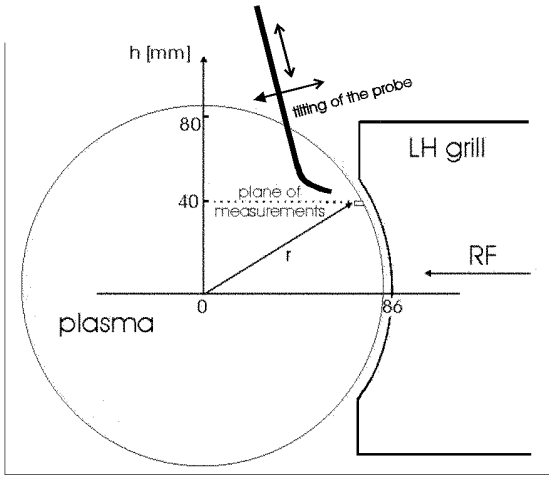

Figure 2 *Schematic of CASTOR small cross-section with the lower hybrid grill (radius of the grill circular shaping 86mm, aperture limiter radius 85mm).*

All the signals measured have been registered by the sampling frequency 1MS/s for the whole CASTOR discharge period (32ms).

Using of the probe described, the following spatial measurements of the plasma floating potential and ion saturated current have been done in front of the CASTOR lower hybrid grill:

(i) for *z=0mm* the radial dependencies in the range $h \in <+40;+70mm>$; here *z* is the toroidal distance of the probe tips from the grill centre (grill has three waveguides with total toroidal width *46mm,* i.e. $z \in <-23;+23mm>$, see further *Figure 6)*, dimension of the grill mouth in poloidal direction is *160mm, i.e.* $h \in <-80;+80mm>$);

(ii) for *h=40mm* the radial dependencies in five toroidal positions *z* from the region $z \in <-5;+20mm>$ (i.e. in fact toroidal dependence). Further,

(iii) to reveal a departure of electron distribution function from Maxwellian one if RF power is applied, *I-V* probe characteristics have been measured using *1kHz* sinusoidal voltage with amplitude *100V* and adjustable DC biasing;

(iv) synergetic effects of RF and positive plasma edge biasing (using a massive biasing electrode) have been investigated. Moreover,

(v) data of several other probe diagnostics in the region far from the grill have been registered (radial rake of Langmuir probes, rotating Mach probe etc.).

The main results of these measurements may be summarised as follows:

(i) radial gradient of floating potential becomes to be steeper (i.e. the radial electric field increases) in the whole tokamak periphery during the RF application, see **Fig. 3**, where three time averaged profiles of floating potential are shown: one in ohmic regime (just before the RF application – triangles, connected by the full line) and two during RF – asterisks and circles); this macroscopic effect is undoubtedly reason of the particle confinement increase observed on CASTOR under RF;

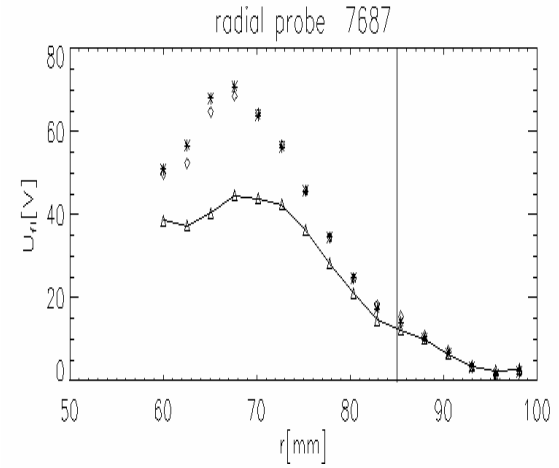

Figure 3 *Radial profiles of the probe floating potential during ohmic (triangles) and RF (in two times differing by 1ms – diamonds and asterisks) regimes, measured during the shot # 7687 by a radial rake of 16 probes in the toroidal position 180° away from the grill. The values of the floating potential given in the figure are averaged over 10^3 samples (=1ms).*

(ii) a radially very narrow layer (several mm only) of the plasma floating potential drop (negative potential „well“) has been found close to the grill mouth if RF is applied, see example in **Fig. 4**; such

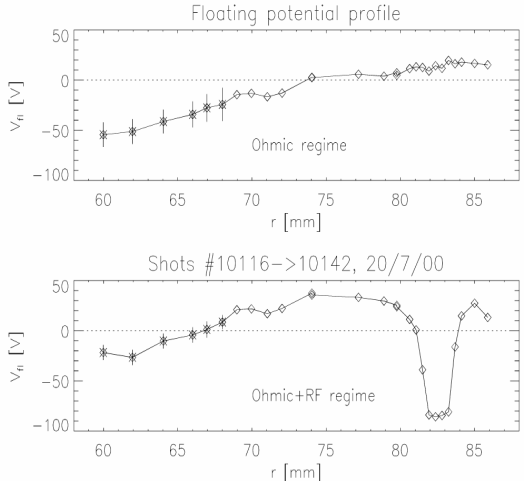

Figure 4 *Radial profiles of the probe floating potential measured by movable probe in the centre of the grill (i.e. z=0mm) at h= 40mm.*

potential „well“ could indicate existence of the fast electrons generated in this layer by the launched wave;

(iii) the depth of the potential „well“ decreases in poloidal direction (i.e. along the longer wall of the waveguides) from the grill centre, in concordance with the second power of sinusoidal distribution of the electric field in the grill waveguides, see **Fig. 5**;

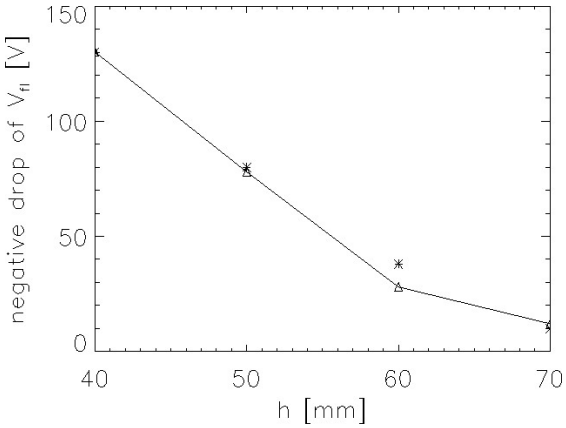

Figure 5 *Comparison of the measured radial maximum of V_{fl} drop (triangles – full line) with square of the electric field value in waveguide normalised to the value of V_{fl} at h=40mm (asterisks), in dependence on the vertical probe position h.*

(iv) however, similar dependence of the floating potential drop has been found also in the toroidal direction (i.e. the depth of the potential „well“ decreases on the both sides from the centre of the middle waveguide, where it reaches its maximum), see a 3D picture of the situation given in **Fig. 6** and later in figure 11 as well; this fact seems to be in disagreement with the assumption of equal power distribution among the all three waveguides and it is also in contradiction with the theory, predicting just in the centre of the antenna a zero acceleration of electrons [2];

(v) measurement of power dependence proved that floating voltage drop depends linearly on the RF power applied, see **Fig. 7**;

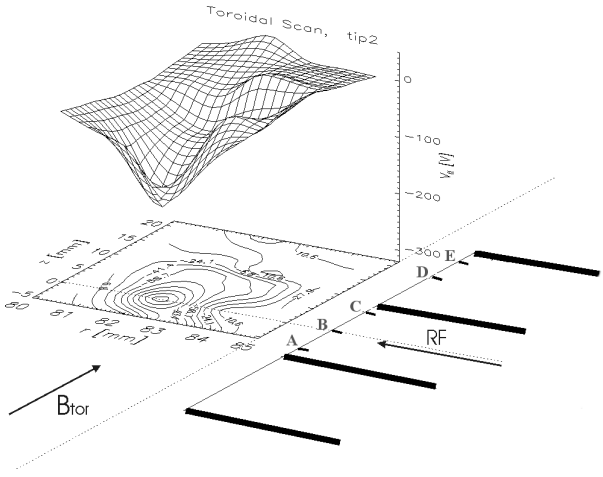

Figure 6 *Toroidal versus radial plot of the floating potential V_{fl} (averaged over 1ms period) under RF application, obtained by radial scan of the probe in five different toroidal positions denoted in the figure as A, B, C, D and E (measured at h=40mm).*

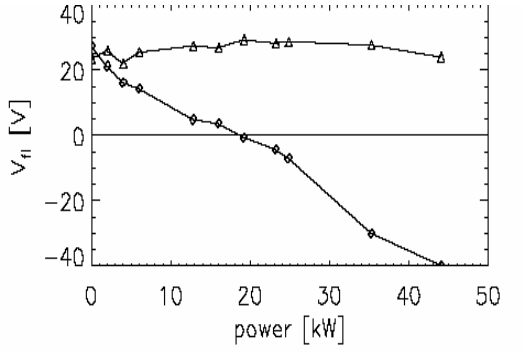

Figure 7 *Dependence of the probe floating potential V_{fl} measured during RF pulse on RF power (diamonds); V_{fl} in ohmic regime just before RF application (triangles).*

(vi) biasing of the plasma can result, in certain range of experimental parameters, in some reduction of the plasma density fluctuations (see e.g. lower trace in **figure 9** below) linked with an observed improvement of global particle confinement (note that biasing is accompanied by substantial change of the plasma potential in the whole edge plasma); however, investigation of floating voltage drop during simultaneous positive biasing and RF application didn't prove that reduction of density fluctuations brings down the generation of the fast electrons by RF as it is supposed by theory and as it could be erroneously deduced from figure 9; only a small radial shift (about 1mm inward) of the floating potential „well" has been found, see the lower right trace in **Fig. 8**.

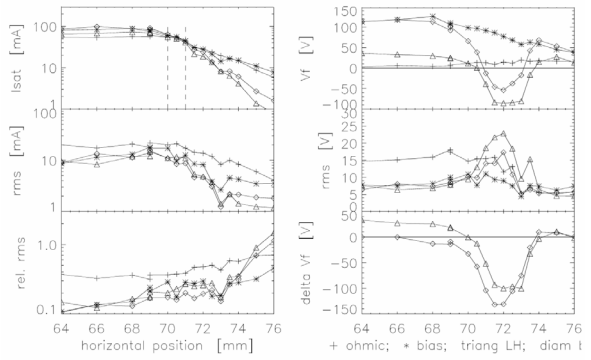

Figure 8 *Upper traces: time averaged radial profiles of ion saturated current I_{sat} and probe floating potential V_{fl} (measured simultaneously by the two tips spaced toroidally 3.5mm on the same radius) in pure OH (crosses), edge plasma biasing +150V (asterisk), LH (triangles) and simultaneous biasing and LH regimes (diamonds);*
middle traces: RMS values of both quantities;
lower traces: left – *relative RMS value of the ion saturated current,* right – *triangles: drop of V_{fl} during LH (relative to OH), diamonds: drop of V_{fl} during LH and simultaneous biasing (relative to biased case).*

To elucidate better the situation, the time development of floating potential and ion saturated current (at the radius of maximum V_{fl}) are shown in Fig. 9 (it may be seen that biasing has been applied in the period 8-10ms, RF in the period 9-11ms, i.e. there is 1ms overlapping).

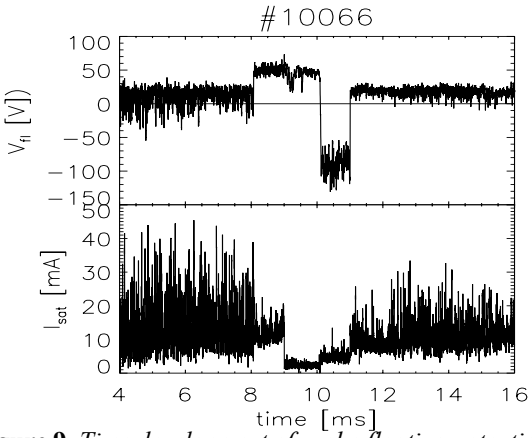

Figure 9 *Time development of probe floating potential and ion saturated current during edge plasma biasing and LHW applications with a partial overlapping.*

(vii) an attempt to find origin of the negative „well" formation by analysis of probe *I-V* characteristics (see **Fig. 10**), measured just in the place of the „well" formation, didn't bring expected result up to now; fitting of the electron temperature to the measured characteristics indicates rather bulk electron temperature increase as an existence of a some measurable group of accelerated electrons; it is clear that more care must be paid to interpretation of these measurements (at the first to take into account properly the observed effect of non-saturation of the ion current with the increasing negative voltage, see the figure 10; namely this effect can the contribution of the fast electrons quite overlap).

The experimental results given above indicate the complexity of the problem under study. First of all we hit upon the fact that while theory is speaking about the plasma potential changes (a positive increase is predicted due to the acceleration and subsequent escape of electrons), we are measuring the probe floating potential, which value can be influenced by many factors. Nevertheless, experimentally detected negative drop of V_{fl} may be taken surely as a certain indication of fast electrons existence. However, to make some qualitative estimates is hardly possible. Especially to judge from these measurements on the plasma potential is impossible. In addition, the value of V_{fl} may be influenced by a possible asymmetry of electron acceleration in front of the launcher (as a results of the launcher power spectrum asymmetry). Such effect could e.g. explain an interesting fact shown in **Fig. 11**: if the both tips of the probe shown in figure 1 are measuring V_{fl}, the both values of V_{fl} differ more as three times during RF pulse while they are identical during OH. More light on this strange phenomenon could bring the planned measurements of particle distribution functions using RFA, see paragraph 4 below.

In addition to the low frequency plasma measurements (up to several hundreds of kHz, given by Data Acquisition System used), an RF circuit for direct measurement of launched RF wave properties in plasma has been prepared and tested as well. **Fig. 12** shows RF signal detected simultaneously with V_{fl} by one probe

(out of the V_{fl} „well“ in this case), while the second probe detected I_{sat}. It may be seen high level of RF signal fluctuations, generally ascribed to the plasma density fluctuations, see e.g. [3].

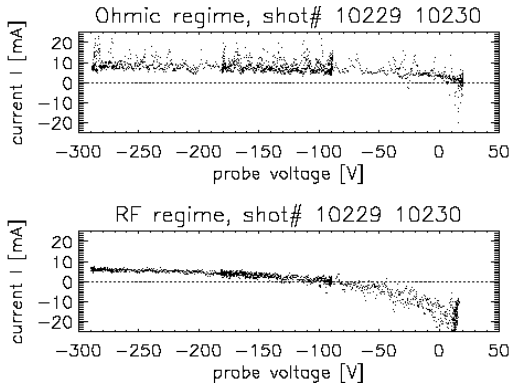

Figure 10 *Example of I-V probe characteristics measured at the radius of maximum V_{fl} drop (if RF is applied): upper trace – without RF, lower trace – RF applied (note the shift of V_{fl} by about –150V).*

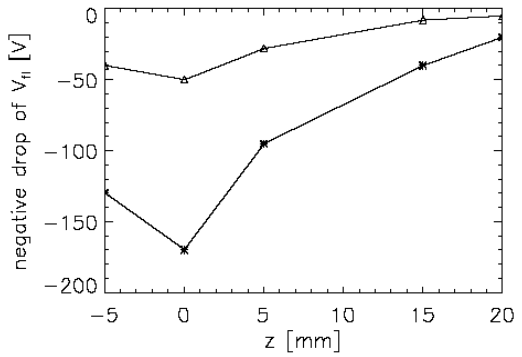

Figure 11 *Toroidal dependence of the maximum V_{fl} drop measured by two each other toroidally shadowing probes shown in Figure 1.*

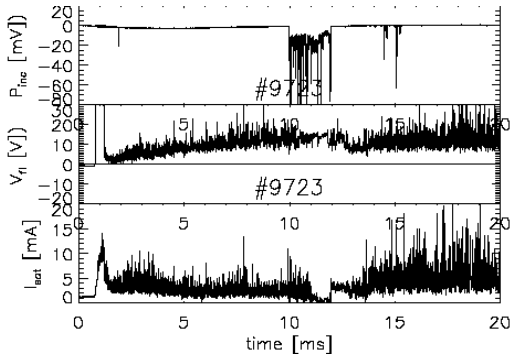

Figure 12 *Time dependencies of a) RF signal detected in the plasma (upper trace), RF applied at 10-12ms, b) floating potential (middle trace) and c) ion saturated current (lower trace).*

2. Detection track for measurement of lower hybrid wave properties in tokamak Tore Supra (TS)

The following preparatory construction works have been already done for the future common RF experiments planned to be carried out on the French tokamak TS:

(i) a receiving 50 Ohm RF antenna has been designed in IPP Prague for detection of RF field on the edge of the new TS launcher developed for 1000s pulse operation (Project CIMES); the construction is fully compatible with requirement of high thermal load expected, manufacturing will be made by the French part; two such antennas will be fixed on the edge of TS launcher;

(ii) IPP Prague purchased two special RF SiO_2 50 Ohm coaxial cables (from KAMAN Co., USA, length 3.8m, equipped by SMA connectors, price 2x600 US $) for transmission of detected RF signals from the TS launcher edge to the vacuum bushing; these cables have been already installed in the TS tokamak;

(iii) a small chamber with two double vacuum sealed RF 50 Ohm bushing (with possibility of interspace differential pumping) has been designed in IPP Prague for output of detected RF signal from TS tokamak to atmosphere for data acquisition; manufacturing of this part will be made in IPP Prague after delivering of special low cobalt stainless steel from CEA Cadarache.

3. Surface analysis of eroded Tore Supra graphite tiles

Scanning Electron Microscope (SEM) and Secondary Ion Mass Spectrometry (SIMS) analysis of eroded locations of the graphite tile exposed to the fast particle beam in the guard limiter to the Tore Supra LH grill have been done in Institute of Physical Chemistry of the Academy of Sciences of the Czech Republic in Prague [4]. Erosion of this type may be caused either by overheating of the tile's material by the electron and/or ion beams or by sputtering of the tile materials by accelerated ions (the electrons with energy less than 5 keV have too low momentum for sputtering). The results of the analysis have proved presence of the plasma ions (H and D) in the tile surface. However, the resolution of the SIMS apparatus was too low to make conclusion from the curve profiles if the plasma ions found in the tile material originate from the accelerated ions impact or, maybe, simply from exposition of the surface by plasma thermal ions. Next SIMS observations should therefore be performed with a SIMS device, which would allow a higher spatial resolution.

4. RFA measurements planned in CASTOR

Two-side RFA has been developed in CEA Cadarache for determination of electron and ion distribution functions in tokamak TS. Because the first application of this device is planned in CASTOR tokamak during spring 2001, an adaptation construction has to be designed and manufactured in IPP Prague. This construction is ready and instalment of RFA in CASTOR and performance of the common experiments are envisaged in the nearest future. The analyser will be placed in horizontal port 45° toroidally away from the grill and will be movable in the radial direction.

References

[1] V. Petržílka, K. Jakubka, R. Klíma, L. Krlín, P. Pavlo, J. Stöckel, F. Žáček, D. Tskhakaya, S. Kuhn, J.A. Tataronis, V. Fuchs, M. Groniche: Plasma biasing by fast particles generated in front of the CASTOR and TORE SUPRA LH grills. *Czech. J. Phys.* **49** , Suppl. S3 (1999) 127-140.

[2] F. Žáček, V. Petržílka, K. Jakubka, J. Stöckel, D. Tskhakaya, S. Kuhn: Radial variations of the floating potential in front of the lower hybrid grill of the CASTOR tokamak. *27th EPS Conf. Contr. Fusion and Plasma Phys.*, Budapest, 2000, p. 349.

[3] F. Žáček, R. Klíma, K. Jakubka, P. Plíšek, S. Nanobashvili, P. Pavlo, J. Preinhaelter, J. Stöckel, L. Kryška: Spectrum broadening and fluctuations of lower hybrid waves observed in CASTOR tokamak. *Plasma Phys. Contr. Fus.* **41** (1999) 1221.

[4] V. Petržílka, F. Žáček, B. Kolman, F. Kroupa, K. Jakubka, J. Stöckel, R. Klíma, L. Krlín, P. Pavlo: On the fast electron beam, consequent generation of electrostatic fields and fast ion production in front of LH grills: measurements and theory. *18th IAEA Fusion Energy Conf.*, Sorrento, Italy, 4-10 October 2000.

Design Aspects of Advanced Grills

Item II.3/c

J. Preinhaelter, F. Žáček, P. Pavlo

Institute of Plasma Physics, Prague

During the year 2000 we paid the main attention to our codes describing the wave propagation in tokamak plasma. In collaboration with Physico-Technical Institute of Petersburg and universities William&Mary and the Old Dominion University in Virginia, we implemented the finite shear of magneto-static field into our both codes:

1) the cold plasma code treating the plasma as a two fluid medium, where the wave absorption at the upper hybrid resonance due to an artificially introduced collisions stand for the true process of X-mode conversion into the electron Bernstein wave. This code was applied to the MAST 60GHz ECRH experiment.
2) the warm plasma code where we included the finite Larmore radius effects into our system of equations describing the wave propagation in an inhomogeneous plasma. The results of this code were used for the design of 18GHz experiment on CASTOR. Application to MAST prevents the restriction to the frequencies lower then the second harmonics of the electron cyclotron frequency.

Results of the absorption of RF power in MAST were described in four publications and presented on two conferences. We concluded that, in the overdense MAST plasma, only O-X-EBW conversion works and thus the 60GHz wave must be launched obliquely with respect to the direction of the magnetostatic field to be converted into the Bernstein modes. We also showed that for envisaged H-mode regime of MAST discharge, where the density gradient in the plasma transport barrier region is very large, the requirements on the incident beam divergence can be met by the mirror system used for wave launch. It looks like the highest efficiency can be reached for circularly polarized wave (see **Fig. 1**) [1]. The direct X-mode conversion into the EBW can be possible only for longer incident waves having the frequency below 30GHz (see **Fig. 2**).

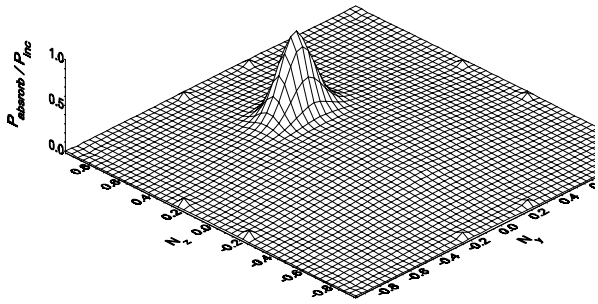

Figure 1 *Power absorbed in a MAST plasma at oblique incidence of the right-handed circularly polarized electromagnetic wave (f=60GHz); launch from low field side; the optimum is reached for N_y =0, N_z=0.4 (the angle of incidence α=24°); narrow flat density profile (pde1=6). $N_{y,z}=k_{y,z}/k_{vac}$ are the normalized component of the wavevector.*

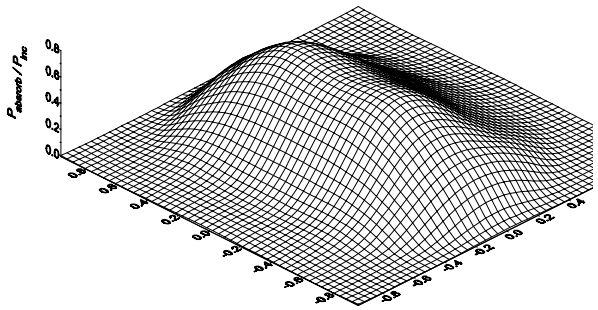

Figure 2 *Power absorbed in a MAST plasma at oblique incidence of linearly polarized electromagnetic wave (f=30GHz, $E^{inc} \perp B_{surface}$); the optimum is reached for N_y =-0.1, N_z=±0.1, very dense plasma $n_0=2x10^{14}cm^{-3}$.*

We also investigated the effect of bootstrap current on the mode conversion at the upper hybrid resonance region for twin peaked density profile of H-mode in

MAST. Here, for 1MA discharge, the very large density gradient develops in the transport barrier region producing the bootstrap current of the order several hundreds of kA. Even such large current (and the corresponding strong inhomogeneity of the magnetic field) do not influence substantially the distance between the R cut-off and the upper hybrid resonance.

We also consulted with V. Shevchenko its ECE detection equipment on MAST, because we prepare to measure this effect on the CASTOR tokamak in Prague.

The main part of this work was done during the two-month visits of J. Preinhaelter in EURATOM/UKAEA Culham Laboratory.

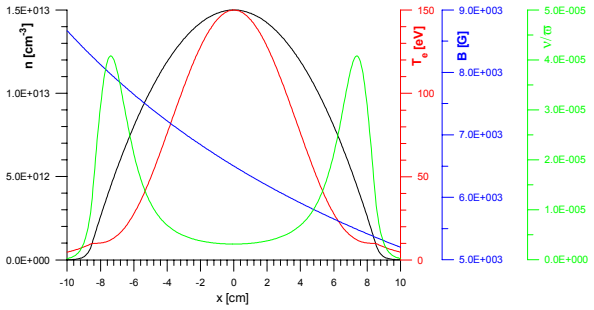

Figure 3 *The profiles of the plasma density, the electron temperature, the magnetostatic field and electron-electron collisions used in computation of RF absorption in CASTOR.*

A preliminary study of possibility of the electron cyclotron resonance heating (ECRH) in an overdense plasma of CASTOR tokamak was done. The 18GHz klystron giving 10kW in a 10ms pulse will be available and the sustainable discharge regime exists in CASTOR (small Prague tokamak, R=40cm, a=10cm) for the magnetic fields B_z=6.5kG on plasma column axis (the first electron cyclotron resonance is than situated at the plasma column center). Such a situation is ideal for the study of ECRH based on the conversion of the X and O modes into the electron Bernstein waves (EBW).

The obliquely incident linearly polarized wave having the electric field perpendicular to the toroidal magnetic field (the shear in CASTOR is negligible) can be partially absorbed in tokamak either due to the direct X-EBW conversion (25% of the incident power can be absorbed if N_y=-0.22 and N_z=0 or due to O-X-EBW conversion (41% of the incident power can be absorbed if N_y =0.05 and N_z =±0.68).

The efficiency of X-EWB conversion increases with increasing central density (at the same time, the density gradient grows in UHR region) (**see Fig.5**).

The most intensive absorption (95%) can be reached when the incident wave has the circular polarization (for the right-handed orientation the wave must be incident obliquely having N_y =0.0 and N_z =0.678).

References

[1] J. Preinhaelter, V. Shevchenko, M.A. Irzak, L. Vahala, G. Vahala: ECRH in Spherical Plasmas:- O-X-EBW Mode Conversion in MAST. Report UKAEA, FUS 444, Culham Sci. Centre, UK, 2000.

[2] J. Preinhaelter: O-X-EBW mode conversion of 60GHz wave in MAST H-mode twin peak density profile. MAST OPS NOTE No: 00.36, UKAEA Fusion, Culham Science Centre, UK, 2000.

[3] J. Preinhaelter, M.A. Irzak, L. Vahala, G. Vahala: O-X-EBW conversion in MAST. *13th Topical Conf. High-Temp. Plasma Diag.*, Tucson, Arizona, June 2000. *Rev. Sci. Instrum.*. **72** (2001) 391.

[4] J. Preinhaelter, M.A. Irzak, P. Pavlo, L. Vahala, G. Vahala: Excitation of Electron Bernstein Waves in MAST. *27th EPS CCFPP,* Budapest, 2000.

[5] J. Preinhaelter, F. Žáček, M.A. Irzak, L. Vahala, G. Vahala: ECRH on CASTOR. 19th *SPPT Prague*, 2000. *Czech J. Phys.* **50**/S3 (2000) 51.

[6] J. Preinhaelter, M.A. Irzak, E. Tregubova, L. Vahala, G. Vahala: Prospects of 18GHz ECRH experiment on CASTOR. *42th Annual Meeting of the Division of Plasma Physics*, Quebec, October, 2000, *Bull. Am. Phys. Soc.* **45** (2000) 254.

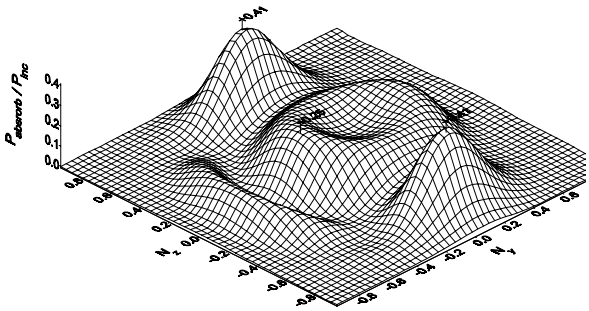

Figure 4 *Power absorbed in CASTOR plasma at oblique incidence of linearly polarized electromagnetic wave ($E^{inc} \perp B_{surf}$ and f=18 GHz).*

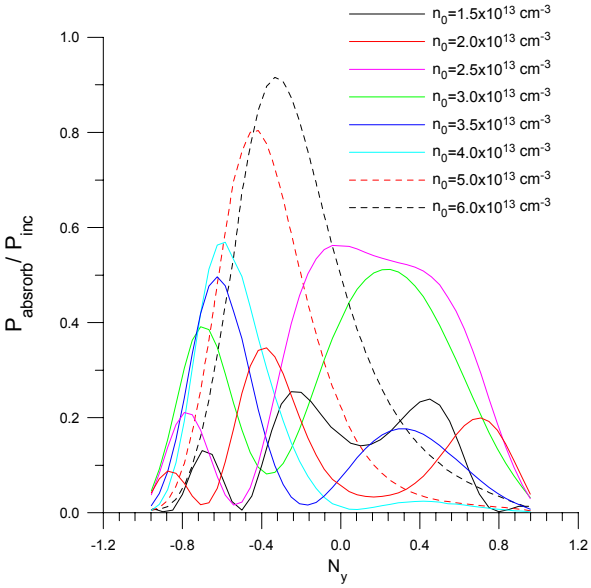

Figure 5 *Power absorbed in CASTOR plasma at oblique incidence of linearly polarized electromagnetic wave ($E^{inc} \perp B_{surf}$ and f=18 GHz) for different central densities n_0 and N_z=0 (direct X-EBW.*

Generation of Fast Electrons in front of LH Grills

Item II.3/d

V. Petržílka, L. Krlín, R. Klíma, P. Pavlo, F. Žáček, V. Fuchs

Institute of Plasma Physics, Prague

Collaboration:
S. Kuhn, D. Tskhakaya, University of Innsbruck:
M. Goniche, J. Gunn, P. Devynck, CEA Cadarache

Let us first describe amendment of the theoretical model of the vortex in front of LH grills, which we did during the last year. The term plasma vortex is an expression used for a rather complicated configuration of plasma flows, plasma density variations and electrostatic fields, which arise in front of an active lower hybrid (LH) grill in tokamaks.

We performed MHD analysis of the plasma vortex, which arises because of local generation of fast electrons by LH waves in a thin layer just in front of the grill mouth: As the electrons are pushed away from the grill mouth along the magnetostatic field lines, they leave the heavier ions behind, and thus an electrostatic field and consequent plasma flows are generated. Without the presence of spontaneously generated fields in front of the grill, this acceleration is limited to a narrow layer in front of the grill mouth, where higher LH harmonics can propagate. However, the electron acceleration and the radial width of the acceleration layer may be significantly enhanced by random fields, which are spontaneously generated near the antenna. By using test particle simulation of electron acceleration and its enhancement by random field effects for parameters relevant to conditions of the Tore Supra and Castor LH grills, it is possible to determine an effective potential W, which expels and accelerates electrons [1]. It is useful to note that the value of W is much larger than the value of the well-known ponderomotive potential of the gradient ponderomotive forces in front of the grill. Consequently, and namely at enhanced acceleration due to the presence of the random fields, a strong stationary toroidal z-directed electrostatic field arises, which is able to accelerate ions. The potential U of this electrostatic field varies along the radial coordinate x and along the poloidal coordinate y. Therefore, also strong radial and poloidal electrostatic fields appear in front of the grill mouth.

As our previous 1-d and 2-d particle-in-cell (PIC) simulations of the plasma vortex were very time consuming because of the large region, which has to be modeled, we now concentrated on two-fluid MHD modeling. We prepared a first version of a 3-d MHD numerical model of a plasma vortex. We also obtained first results on the 3-d vortex configurations in front of an active grill mouth. This first version of the 3-d MHD code computes the plasma flows and electrostatic fields according to the following algorithm: It is assumed that the forces along the magnetostatic field lines and the corresponding parallel plasma flux are dominant in the momentum and continuity equations, and then the parallel flows and corresponding plasma density perturbations are computed. Because of the above described simplifying algorithm used in the computations, the results are fully valid only for rather quickly toroidally rotating plasmas. Typical results of computations are shown in **Figures 1-7**. The large initial unperturbed rotation velocity might occur in beam heated plasmas.

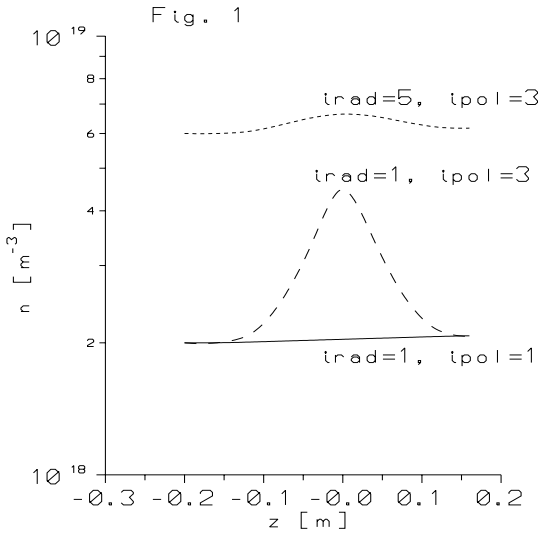

Figure 1 *Profiles of the plasma density in front of the grill mouth.*

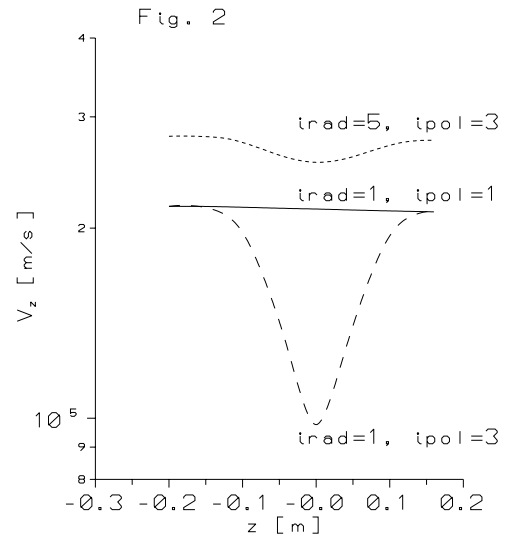

Figure 2 *Profiles of the toroidal plasma velocity front of the grill mouth.*

To speed up the program execution in the first series of computations reported here, we computed the z-profiles in only five points of the x (irad = 1,…,5) and y (ipol = 1,…,5) mesh. The value irad = 1 corresponds to x = 0 just at the grill mouth, while irad = 5 corresponds to the radial distance of x = 2 cm from the grill mouth. The remaining values irad = 2, 3, 4 then correspond to x = 0.5, 1, 1.5 cm, respectively. Similarly, ipol = 1 corresponds to the value of the poloidal coordinate y = 0 at the grill row boundary (poloidally), the value ipol = 5 corresponds to the

other poloidal boundary of the row (to y = 10 cm in our model computations). The values ipol = 2, 3, 4 then correspond to y = 2.5, 5, 7.5 cm, respectively.

Let us comment some specific features of the results. We can see in Fig. 1, how the plasma density grows near z = 0, namely radially at the grill mouth and in the poloidal maximum of the rf field amplitude, i.e., for irad = 1 and ipol = 3. This growth is related to the decrease of the toroidal plasma flow velocity in the same place, cf. **Fig. 2**. This flow velocity decrease is due to the slowing down of the electron component by the expelling force of the rf field in the left half of the grill for z < 0. By the toroidally directed component of the charge separation electrostatic field, the ions are also braked for z < 0, and the flow velocity decreases. The absolute value profiles of the charge separation field are shown in **Fig. 3**. Let us note that the dashed lines in the left half of the grill (for z < 0) correspond to negative values of the toroidal z- component of the electrostatic field.

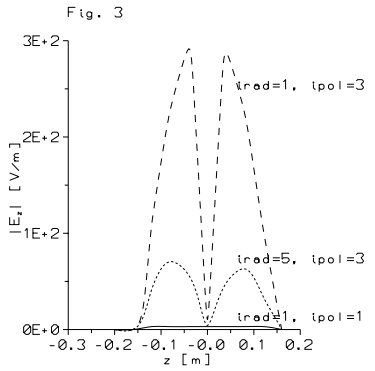

Figure 3 *Profiles of the absolute value of the toroidal component of the electrostatic charge separation field.*

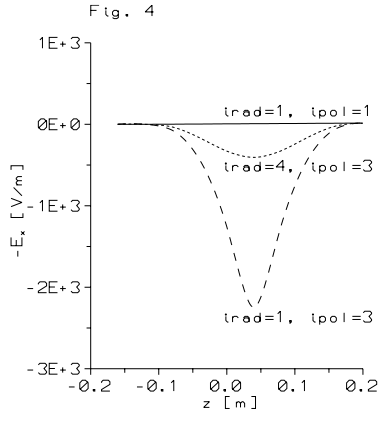

Figure 4 *Profiles of the radial component of the charge separation electrostatic field in front of the grill mouth.*

Profiles of the remaining components of the electrostatic field and of the plasma flow velocity are shown in Figures 4-7.

The plasma density growth shown in Figure 1 would result in changes in the wave coupling (in variations of the reflection coefficient), and in growth of the energy carried by the accelerated electrons – because of the large number of accelerated electrons in a higher density plasma.

This plasma density growth would in turn further amplify the intensity of the vortex. The plasma density growth might result also in a change of the launched LH wave spectrum.

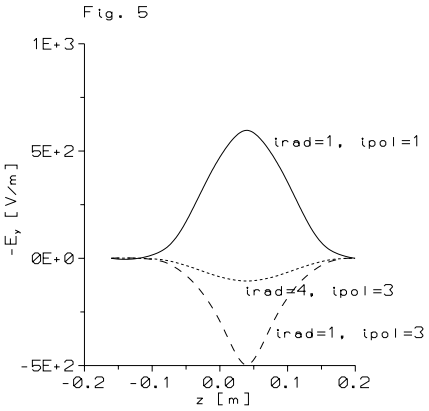

Figure 5 *Profiles of the poloidal component of the electrostatic charge separation field..*

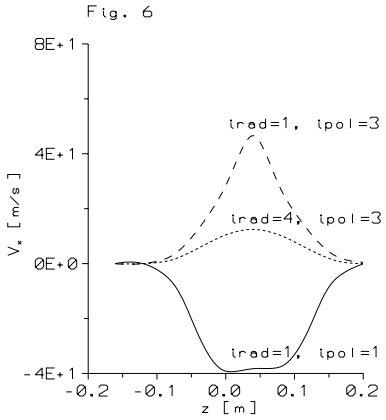

Figure 6 *Profiles of the radial plasma flow velocity.*

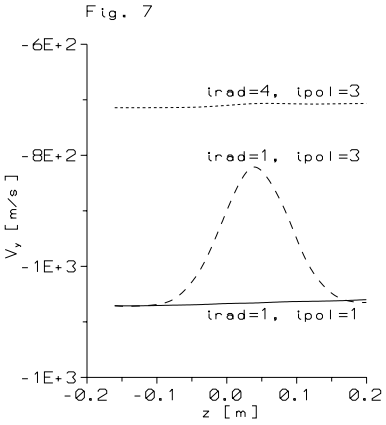

Figure 7 *Profiles of the poloidal plasma flow velocity.*

For larger values of the tilt of the magnetostatic field, the density growth would not be limited to the region around z = 0, but would acquire form of a toroidally oriented “sausage” along the poloidal plane of symm-

etry (ipol = 3) of the grill row. This would mean that consequences of the density growth would be more significant in a larger area in front of the grill mouth. Corresponding computations are envisaged in a continuation of this study.

In conclusion, we found that the acceleration of electrons in front of the LH grill mouth by the field of the LH wave results in important growth of the plasma density in front of the grill, which should lead to ensuing further amplification of the vortex, and to changes in the LH wave launched spectrum. The results have been presented at the 28th EPS Conference on Plasma Physics and Controlled Fusion, Madeira, 18-22 June 2001 [2].

The density variation is sensitive to the value of tilt of the magnetostatic field in front of the grill – the corresponding computations will be performed in a continuation of this task. However – according to the simplifying algorithm used in the computations – the first results of the 3-d MHD code are valid only for rotating plasmas. The corresponding further amendment of the code will be a topic of our further efforts.

In addition to the work on the 3-d MHD model, we explored momentum and heat transfer from LH grills to tokamak edge plasma in frame of quasilinear theory, because of production of fast particles in front of the grill. We calculated the resulting electrostatic charge separation field in equilibrium with the ambient plasma. We also identified terms which are likely to modify the ion dynamics [3].

We also studied the influence of the fast particle production on Langmuir probe measurements of the floating potential in front of a LH grill mouth [4,5], which were performed in order to check our theoretical conclusions concerning fast particle production in front of LH grills. Measurements of the floating potential by a special Langmuir probe in front of the Castor tokamak LH grill demonstrated a strong decrease of the floating potential in front of the active LH grill [4]. This decrease is radially localized in a very narrow layer just in front of the grill. The depth of this potential well in the layer depends linearly on the launched LH power and reaches the magnitude of about 80 Volts for the maximum LH power of 50 kW accessible in Castor. These facts indicate presence of fast electrons in the thin layer in front of the grill mouth.

To explain the magnitude of the floating potential decrease, we performed series of 2-d PIC simulations of the plasma layer in front of the grill [4,5]. We considered a 2-d (in radial and toridal directions) plasma slab in front of the grill mouth. In the radial direction, the boundary conditions were periodical. The electron-wave interaction was again (as in the above described 3-d MHD modeling) represented by an effective ponderomotive potential W [1], which expels electrons from the space in front of the grill mouth. The large size of the plasma region under consideration (more than 1000 Debye lengths in the toroidal direction) does not allow to simulate the real size Castor system, and therefore the simulated region was shortened by a factor of four in the computations. We ran simulations till the stationary state was reached. We found that both electrons and ions are accelerated in the rf active region. While the electrons are accelerated directly by the rf wave (through the effects of the effective ponderomotive potential W), ions are accelerated by the electrostatic field of the charge separation. In the region magnetically connected to the rf active region, the energetic electron beam has the same radial width as is the width of the rf active region (chosen as 2 mm in the computations), whereas the ion beam width is four times larger (8 mm). A strong radial electrostatic field (about 20000 V/cm) is created in the rf region, which can cause poloidal rotation of the plasma by the drift in the toroidal magnetostatic field. Using the simulation results, we can estimate the drop in the floating potential measured by the Langmuir probe inserted into the rf active region. By calculating the electron current to the probe and by taking it equal to the ion current, we obtain the potential drop across the probe sheath of about 20 Volts, in qualitative agreement with the CASTOR measurements.

References

[1] V. Petržílka, F. Žáček, B. Kolman, F. Kroupa, K. Jakubka, J. Stoeckel, R. Klíma, L. Krlín, P. Pavlo, J. Gunn, M. Goniche, V. Fuchs, D. Tskhakaya, S. Kuhn, J.A. Tataronis, and J. Loerinčík: On the fast electron beam, consequent generation of electrostatic fields and fast ion production in front of LH grills - experiment and theory, *18th IAEA Fusion Energy Conference*, Sorrento, Italy, October 4-10, 2000, paper CN-77/EXP4/07, p. 253.

[2] V. Petržílka, V. Fuchs, R. Klíma, L. Krlín, P. Pavlo, M. Goniche, J. Gunn, D. Tskhakaya, S. Kuhn: A 3-d model of the plasma vortex in front of LH grills, *28th EPS Conference on Plasma Physics and Controlled Fusion*, Madeira, Portugal, 18-22 June 2001, p. 289.

[3] V. Fuchs, V. Petržílka, M. Goniche, J. Gunn: Momentum and heat transfer from lower hybrid antennas to the tokamak edge plasma, *28th EPS Conference on Plasma Physics and Controlled Fusion*, Madeira, Portugal, 18-22 June 2001, p.317

[4] F. Žáček, V. Petržílka, K. Jakubka, R. Klíma, J. Stoeckel, D. Tskhakaya, S. Kuhn, S. Nanobashvili: Radial variations of the floating potential in front of the lower hybrid grill of the Castor tokamak, *27th EPS Conference on Plasma Physics and Controlled Fusion*, Budapest, Hungary, June 12-16, 2000, Book of Abstracts p. 349.

[5] D. Tskhakaya, S. Kuhn, V. Petržílka: Simulation of particle acceleration in front of a LH grill, *27th EPS Conference on Plasma Physics and Controlled Fusion*, Budapest, Hungary, June 12-16, 2000, Contributed Papers, p. 1028.

4 Atomic Physics and Data for Edge Plasma and Plasma Wall Interactions

Energy Transfer in Collisions of Ions with Surfaces

Item II.4/a
Zdenek Herman, Z.Dolejšek, J. Hrušák, J. Žabka

Institute of Physical Chemistry

A. Energy partitioning in collisions of slow polyatomic ions with carbon surfaces

1. Introduction

Collisions of hyperthermal ions with surfaces are of interest because of a wide range of applications in both science and technology. Surface-induced dissociations (SID) of ions have been used to characterize structural properties of polyatomic ions. Moreover, surface-induced chemical reactions are of growing interest not only as a class of chemical reactions of ions, but also as a tool of characterizing the nature of surfaces. Besides of being of fundamental importance, polyatomic ions - surface interactions are also relevant to technological applications in a variety of fields like surface analysis, surface modifications for preparation of new materials (including plasma processing), and – quite significantly – plasma-wall interactions in discharges and fusion devices .

Energy transfer in the ion-surface collisions is of prime importance. The question of what fraction of collisional energy of the incident ion is transformed into its internal energy (and may lead to its further dissociation), what fraction is retained as translational energy of the scattered collision products, and what is absorbed by the surface is of fundamental importance.

The entrance channel is the translational energy of the incident projectile ion, E_{tr} , possibly complemented by the initial internal energy content of the ion, E_{int}. This energy is distributed (product energies primed) into the internal energy excitation of the product(s) (E'_{int}), translational energy of the product(s) (E'_{tr}), and energy absorbed by the surface (E'_{surf}). The various energy fractions are characterized by the respective distribution functions, $P(E'_{int})$, $P(E'_{tr})$, $P(E'_{surf})$.

Here we describe results of experiments on energy partitioning in collisions of a model polyatomic ion with specific carbon surfaces [1,2]. The aim of this set of experiments was to determine energy transfer for surfaces relevant to fusion research. Therefore, the carbon surface used was the surface of a TORE SUPRA carbon tile. The results were compared with data obtained with a standard HOPG (highly oriented pyrolytic graphite) carbon surface. Both surfaces were kept at ambient temperatures (about 300 K) during the experiments. The model polyatomic ion used was the ethanol molecular ion $C_2H_5OH^+$. It should be emphasized that the exact quality of the projectile ion is of secondary importance in these studies. The ethanol molecular ion represents here only a suitable polyatomic moiety of about 10 chemically bound atoms of well-characterized properties.

We describe here results of projectile ion - surface collisions on the two carbon surfaces at incident energies of 12 and 23 eV. The incident angle was 60^0 (measured from the surface normal, i.e. 30^0 with respect to the surface). Mass spectra of the product ions, product ion angular and translational energy distributions were measured and from the results the partitioning of energy in the surface collision was derived.

2. Experimental

The experiments were carried out using the Prague beam scattering apparatus EVA II, built originally for studies of gas-phase ion-molecule collision dynamics, and modified for the ion-surface collision studies[1)] (Fig. 1). The modification consisted in replacing the crossed beam arrangement with a carbon surface target from which projectile ions were scattered and detected. In the present experiments, projectile ions were formed by bombardment of the ethanol molecules in a low-pressure ion source by 120 eV electrons. The ions were extracted, accelerated to about 140 eV, mass analyzed by a 90^o permanent magnet, and decelerated to a required energy in a multi-element deceleration lens. The resulting beam had an energy spread of 0.2 eV, full-width-at-half-maximum (FWHM), and angular spread of 1^o, FWHM, and geometrical dimensions of 0.4x1.0 mm. The beam was directed towards the surface under a pre-adjusted incident angle Φ_N. Ions scattered from the surface passed through a detection slit (0.5x1 mm), located 25 mm away from the target, into a stopping potential energy analyzer; they were then accelerated to 1000 eV into a detection mass spectrometer (a magnetic sector instrument) and detected with a

[1)] J. Kubišta, Z. Dolejšek, and Z. Herman, *Eur. Mass Spectrom.* **4**, 311 (1998).

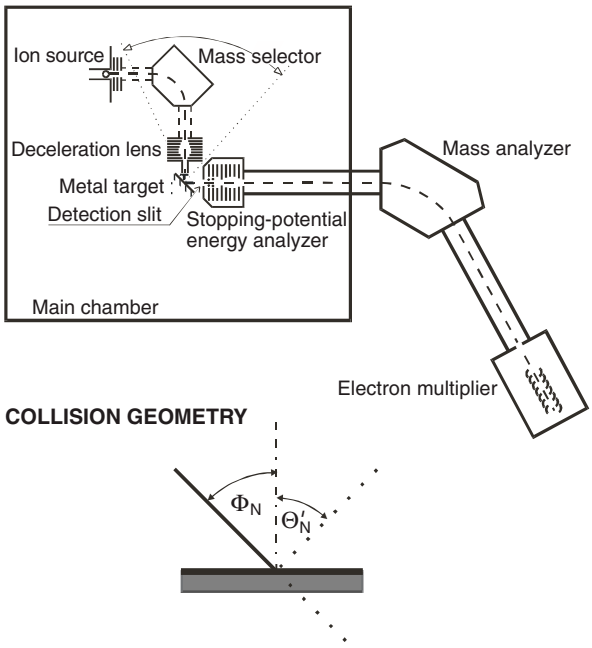

Figure 1 *Schematic of the experimental arrangement. Inset shows the collision geometry.*

Galileo channel multiplier. The primary beam exit slit, the target, and the detection slit were kept at the same potential during the experiments and this equipotential region was carefully shielded by μ-metal sheets. The primary beam - target section could be rotated about the scattering center with respect to the detection slit to obtain angular distributions.

The energy of the projectile ions was measured by applying to the target a potential exceeding the nominal ion energy by about 10 eV. The target area then served as a crude ion deflector directing the projectile ions into the detection slit. Their energy could be determined with accuracy better than about 0.2 eV. The impact angle of the projectile ions was adjusted before an experimental series by a laser beam reflection with a precision better than about 1°. Incident (Φ_N) and scattering (Θ'_N) angles were measured with respect to the surface normal (see inset in **Fig. 1**).

The carbon surface target was

1) a 5x5 mm carbon plate about 1 mm thick cut from a TORE SUPRA carbon tile and polished by diamond powder; the sample was cleaned in an ultrasonic cleaner successively in an acetone, methanol, and water bath before being placed into vacuum;
2) a 5x5 mm sample of highly oriented pyrolytic carbon (HOPG) sample from which the surface layer was peeled-off immediately before placing it into vacuum.

Both samples were mounted into a stainless steel holder located 10 mm in front of the exit slit of projectile ion deceleration system. The incident angle of the projectile ion beam Φ_N was set with an accuracy of $\pm$ 1°. The experiments described in this communication were carried out with target surfaces kept at ambient temperature. The background pressure in the scattering apparatus was about 5×10^{-7} Torr, and during the experiments the pressure was about 3×10^{-6} Torr due to the leakage of the source vapor into the scattering chamber.

3. Results

Measurements of the mass spectra (fragmentation patterns), translational energy distributions, and angular distributions of product ions from interactions of a model polyatomic projectile ion (ethanol molecular ion) with carbon surfaces (TORE SUPRA carbon tile, HOPG surface) were used to determine the distribution functions for partitioning of incident energy of the projectile ion energy in slow polyatomic ion-surface collisions. The results were compared with results of analogous measurements using as a target surface stainless steel (covered by a multilayer of hydrocarbons) [3] and self-assembled monolayer of C_{12} alkane chain on a metal surface.

Distribution of energy transformed into internal energy of the projectile ion, $P(E'_{int})$, was determined from the extent of its fragmentation with the help of the break-down pattern of the projectile molecular ion. Distribution of energy covered into product ion translational energy, $P(E'_{tr})$, was obtained from direct measurements. Distribution of energy absorbed by the surface, $P(E'_{surf})$, was obtained as a difference of the sums of the latter two terms and the incident energy of the projectile ion (with the estimated initial internal energy of the projectile ion included).

Fig. 2 is a summary of the energy partitioning: at the collision energy of about 22.5 eV and incident angle of 60° (with respect to the surface normal) the peak value of $P(E'_{int})$ was 6 % of the incident projectile energy, the peak value of $P(E'_{tr})$ was 24-28% for the carbon surfaces (to be compared with 32% of hydrocarbon-covered stainless steel surface), and the peak value of $P(E'_{surf})$ was 70-66% (62% for the stainless steel surface).

The similarity of the charge transfer results and the chemical reactions observed at the surface (hydrogen atom transfer processes) for both carbon surfaces, for the stainless steel covered by a layer of hydrocarbons, and for the C_{12} alkane SAM surface suggests that the studied carbon surfaces were covered by a layer of hydrocarbons.

The conclusion that the carbon surfaces, used in the presented experiments, were covered by a layer of background hydrocarbons does not diminish the value of the results with respect to the exploitation as information for fusion research. In fact, a considerable effort has been directed recently to covering the walls of nuclear devices by hydrocarbon films to control the impurity level of the fusion plasmas caused by erosion of the first wall. The growth of hydrocarbon C:H films by plasma chemical vapour deposition and the properties of these films has been given, therefore, considerable attention.

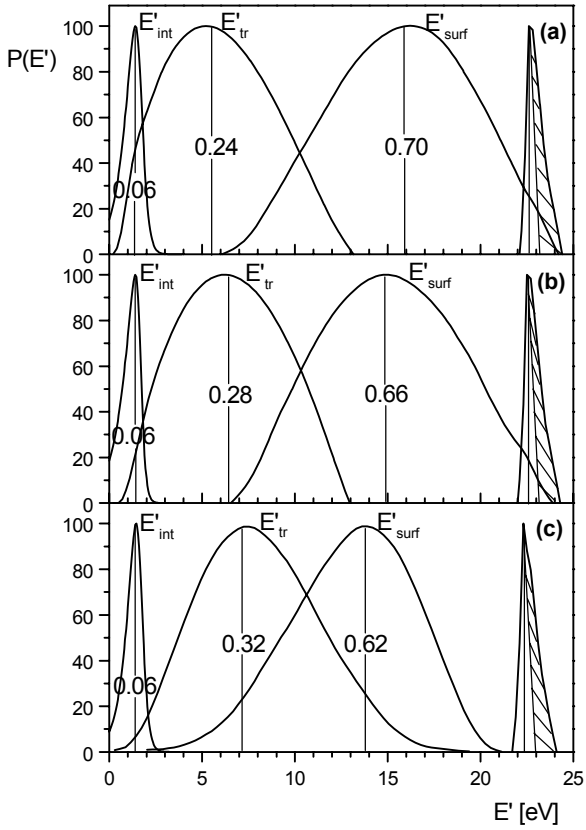

Figure 2 *Distribution functions for energy partitioning into E'_{int} , E'_{tr} and E'_{surf} on interaction of projectile ions* $C_2H_5OH^+$ *with (a) TORE SUPRA sample, E_{tr}=* 22.7 eV *(b) HOPG sample, E_{tr}=* 22.6 eV *(c) stainless steel, E_{tr}=* 22.3 eV. *Incident angle Φ_N =* 60°. *The narrow peak in the right part of the figures indicates the energy distribution of the incident projectile ions, its shaded area denotes their internal energy distribution.*

The presented results on energy transfer in collisions of slow polyatomic ions with carbon surfaces, covered by background hydrocarbons, thus may be regarded as a first step in obtaining information on energy partitioning in ion-surface collisions with materials important in fusion research.

In 2001, further work, oriented towards collisions of simple ions with surfaces, collisions with surfaces at elevated temperatures, and with surfaces covered by specially deposited films has started. Interaction of small hydrocarbon ions, CD3+, CD4+, CD5+, and their isotopic variants CHn+ and (CHn+)-C-13 (n = 3, 4, 5), with room-temperature and heated carbon (highly oriented pyrolytic graphite, HOPG) surfaces was investigated over the collision energy range 16-52 eV. Mass spectra, translational energy distributions, and angular distributions of product ions were determined. Collisions with room-temperature surfaces showed both surface-induced dissociation of the projectiles and chemical reactions with the surface material. First results were summarized in [5].

Acknowledgments

The support of this research by a grant of the Grant Agency of the Czech Republic No. 203/00/0632 is gratefully acknowledged. The work was carried out within the framework of the Ass. EURATOM/IPP.CR in cooperation with the Association EURATOM-ÖAW, Wien (Prof. T.D.Märk, Institut für Ionenphysik, Universität Innsbruck).

B. Elementary Collision Processes of Multiply-Charged Ions with Neutrals in the Gaseous Phase

Dynamics of chemical and charge transfer reactions of molecular dications - Beam scattering and total cross section data for processes in the system CO_2^{2+} + D_2

Atomic and molecular doubly-charged ions are highly energy-rich species which in collisions with neutrals deposit this energy in the reaction products formed. In a long-term program we investigate the kinetics and dynamics of various elementary collision processes to obtain general information on the way this high energy of dications is deposited. As a precent part of these efforts, chemical reactions and charge transfer processes in the system CO_2^{2+} + D_2 were investigated in crossed beam scattering experiments [3,4]. Theoretical calculations of stationary points on the dication potential energy surface $(CO_2D_2)^{2+}$ were carried out to complement the experiments. The main ion products identified were CO_2D^+, COD^+, CO_2^+, CO^+, and O^+. The relative cross sections for reactions with D_2 (H_2) were in the ratio CO_2^+: COD^+: CO_2D^+ = 100 : 10 : 1, and almost independent of the collision energy over 0.5 and 4 eV (center-of-mass, CM) (Fig. 3).

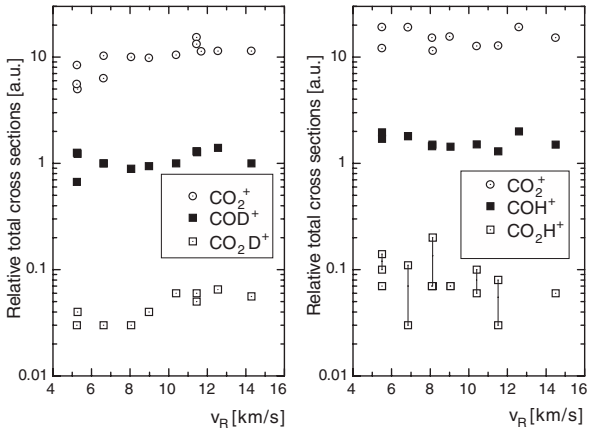

Figure 3 *Dependence of the relative total cross sections for the formation of* CO_2D^+, COD^+, CO_2^+, COD^+ (COH^+),CO_2D^+ (CO_2H^+) *in collisions of* CO_2^{2+} *with* $D_2(H_2)$ *on the relative velocity of the reactants, v_R.*

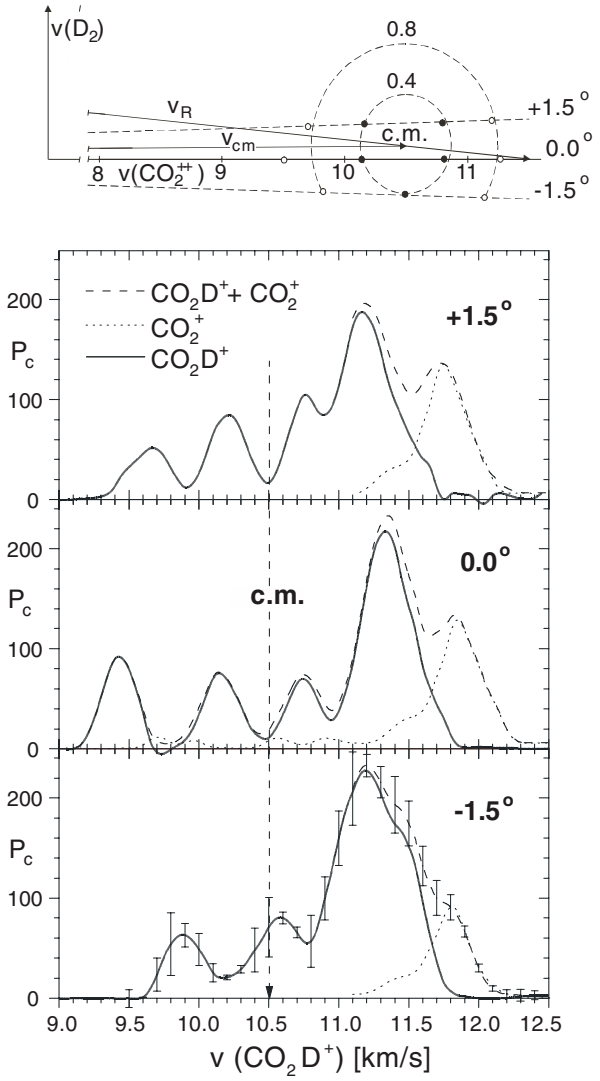

Figure 4 *Velocity profiles of* CO_2D^+ *at the laboratory scattering angles of* +1.5°, 0.0°, *and* -1.5°, *respectively. The dashed lines refer to measured data, the solid lines are data obtained after subtraction of the isotopic contribution of* $^{12}C^{18}O^{16}O^+$ *at the same mass (dotted). The Newton diagram in the upper part of the figure shows the locations of the maxima with respect to the center-of-mass (c.m.)*

The chemical product CO_2D^+ was formed in a non-dissociative chemical reaction leading to $CO_2D^+ + D^+$ in two channels of different translational energy release via decomposition intermediatesr $(CO_2D_2)^{2+}$ (**Fig. 4**); the high translational energy release channel (peak value 4 eV) is consistent with energetics of the formation of a D-C bonded isomer DCO_2^+ which dissociates further to form $DCO^+ + O$. The charge transfer product CO_2^+ (**Fig. 5**) is formed prevailingly in the excited states A and B; a small amount of it is also formed by further dissociation of the product CO_2D^+ (formed in the low translational energy release channel presumably in an excited state) to $CO_2^+ + D$. The product CO^+ results from two different processes: from charge transfer leading to $CO_2^+(C^2\Sigma_g^+) + D_2^+$ and predissociation of the C-state to $CO^+(X^2\Sigma^+) + O(^3P)$, and in spontaneous dissociation of the projectile CO_2^{2+} (vibrationally excited to its predissociation barrier) to $CO^+ + O^+$.

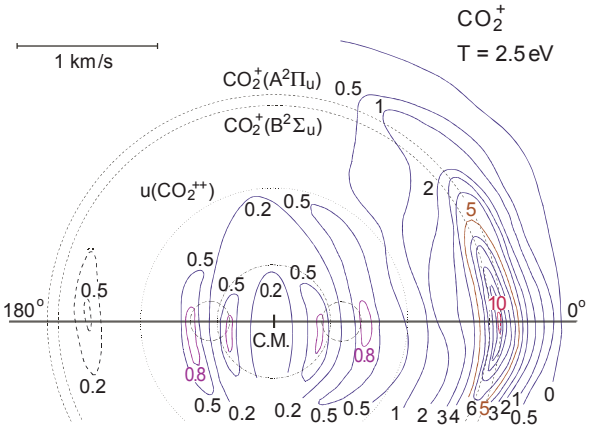

Figure 5 *Contour scattering diagrams of* CO_2^+ *at the collision energy of* 2.5 eV. *The solid line denotes the direction of the relative velocity vector, c.m. denotes the position of the tip of the center-of-mass velocity vector. The dotted circle denotes the initial center-of-mass velocity of the reactant* CO_2^{2+}. *The dashed circles show the loci, where the product* CO_2^+ *should appear if formed in charge transfer reaction in the vibrationally ground states of the excited electronic states* A *and* B *of* CO_2^+.

Publications

[1] J. Žabka, Z. Dolejšek, J. Roithová, V. Grill, T.D. Märk, Z. Herman: Energy partitioning in collisions of slow polyatomic ions with carbon surfaces, submitted to Int.J.Mass Spectrometry (appeared in 2002, IJMS **213** (2-3): 145-156 FEB 1).

[2] Z. Herman, 18th Informal Meeting on Mass Spectrometry, Prague 2000 (Invited Lecture).

[3] L. Mrázek, J. Žabka, Z. Dolejšek, J. Hrušák, and Z. Herman, J. Phys. Chem. A**104,** 7294 (2000).

[4] L. Mrázek, J. Žabka, Z. Dolejšek, J. Hrušák, and Z. Herman, Book of Abstracts, 13th Eur. Conference on Dynamics of Molecular Collisions MOLEC 2000, Jerusalem, 2000, p. C.8.

[5] J. Roithová, J. Žabka, Z. Dolejšek, Z. Herman: Collisions of slow polyatomic ions with surfaces: Dissociation and chemical reactions of CD5+, CD4+center dot, CD3+, and their isotopic variants on room-temperature and heated carbon surfaces, submitted to *Journal of Physical Chemistry.*

Studies of the Rate Coefficient for the Recombination Reaction of H_3^+ Ions with Electrons

Item II.4/b

J. Glosík, R. Plašil, M. Tichý, V. Poterya, P. Kudrna, A. Pysanenko

Charles University in Prague, FMP

The H_3^+ is an important ion in many plasmas including cold periphery of magnetically confined plasma. The rate coefficients (cross sections) are necessary for understanding and modelling of phenomena in fusion edge plasmas ([2]). Over past 50 years a number of studies of recombination of this ion have been carried out, yet they did not lead to a unanimous value of recombination rate coefficient, α. We observed rate of de-ionisation of H_3^+ as low as α_{eff}~3×10^{-9} cm^3s^{-1} at hydrogen density decreased down to $5\times10^{10}cm^{-3}$. This rate increases with increasing hydrogen number density up to α_{eff}~2×10^{-7} cm^3s^{-1} at hydrogen density higher than $1\times10^{13}cm^{-3}$. This implies that the recombination in hydrogen plasmas is a three-body process enhanced by presence of neutral H_2 and that binary dissociative recombination of H_3^+ is very slow with $\alpha_{DR} < 3\times10^{-9}$ cm^3s^{-1}. This value is in agreement with theoretical predictions.

1. Introduction

Because of its importance the H_3^+ ion naturally attracted attention of scientists for ninety years from the time of its identification (1911) by Thomson. The kinetics of H_3^+ formation and its reactions with neutrals has been studied extensively and it is well understood. Equally important for the hydrogen containing plasmas is to understand the process of recombination of H_3^+ with electrons. For over fifty years therefore scientists have been attacking this problem. In recent years over 30 measurements of rate coefficient of H_3^+ recombination were carried out (for more details see refs. ([3]), ([4]) and references therein). Despite these efforts however the recombination of H_3^+ still remains the most controversial topic in the field of electron-ion recombination. Even the results of very recent measurements of the rate of recombination are dispersed over at least one order of magnitude, from 1×10^{-8} to 3×10^{-7} cm^3s^{-1}. High credibility has value $\alpha \sim 1.8\times10^{-7}$ cm^3s^{-1} obtained by Amano in his study using infrared absorption technique ([5]). In recent beam experiments $\alpha \sim$ 0.7–2×10^{-7} cm^3s^{-1} was typically obtained ([3]). In late nineties it was generally accepted that α is increasing with temperature as $T^{-0.5}$ and for near thermal electrons and ground state H_3^+ is $\alpha \sim 2\times10^{-7}$ cm^3s^{-1} ([6]). This value, usually claimed as the rate of dissociative recombination, was accepted in agreement with majority of experiments but in contradiction with theoretical predictions based on calculated unfavourable curve crossing between the ion ground state and the dissociating neutral state (see e.g. ([7]), ([8]), ([9])). Agreement with theory was obtained just for electron energies close to 10 eV ([7]). We will demonstrate that presence of neutral H_2 is enhancing the overall recombination process. To explain the mechanism of recombination of H_3^+ we designed and built new afterglow experiment – **Advanced Integrated Stationary Afterglow (AISA)**. In our initial measurements we indeed observed recombination with rate coefficient α varying between 0.15×10^{-7} cm^3s^{-1} and 2×10^{-7} cm^3s^{-1} in the range of H_2 number density $n(H_2)$ from ~10^{11} to 2×10^{12} cm^{-3}) ([10]). In present studies we further upgraded AISA apparatus and we extended measurements towards H_2 number densities, down to ~ 5×10^{10} cm^{-3}. We also made preliminary studies of recombination of D_3^+ ions.

2. Experiment and data analysis

The main part of the new experimental system, **AISA**, is the cylindrical stainless-steel UHV discharge chamber. The details of construction are given in **Figure 6**. AISA is equipped by mass spectrometer and by 18-μm in diameter Langmuir probe. Plasma is generated by pulses of microwave power (frequency 2.45 GHz, peak power ~1kW, pulse length 0.2-5 ms, repetition period 40-100 ms). Microwave power entersthe discharge chamber via a quartz window. In order to eliminate the losses of H_3^+ due to reactions with impurities it was necessary to use ultra pure gases in the discharge chamber; the unwanted impurities had to be kept below 0.1 ppm. Prior to the measurements the discharge chamber and all UHV vacuum lines were pumped and heated for several days. The

([2]) R.K. Janev, Proceedings of the 1999 Conference on Dissociative recombination, *Theory, Experiment and Applications IV*, editors M. Larsson, J.B.A. Mitchell, I. F. Schneider World Scientific, Singapore, 40 (1999), p. 40.

([3]) M. Larsson, Phil. Trans. R. Soc. Lond. A (2000) **358**, 2433.

([4]) R. Plašil, J. Glosík, P. Kudrna, J. Rusz, V. Poterya, M. Tichý, Rev. Scient. Instr., sent for publication (2001).

([5]) T. Amano, J. Chem., Phys., **92** (1990) 6492.

([6]) M. Larsson et al., Phys. Rev. Letters 79 (1997) 395.

([7]) A.E. Orel, I.F. Schneider, A. Suzor-Weiner, Phil. Trans. R. Soc. Lond. A (2000) **358**, 2445.

([8]) M.R. Flannery, in *Atomic and Molecular Physics*, editors I. Alvarez, C. Cisneros, T.J. Morgan, World Scientific Pub. Co., London, 1995, p. 329.

([9]) D.R. Bates, M.F. Guest and R.A. Kendall. Planet. Space. Sci., **41** (1993) 9.

([10]) J. Glosík, R. Plašil, V. Poterya, P. Kudrna, M. Tichý, Chem. Phys. Letter, **331** (2000) 209.

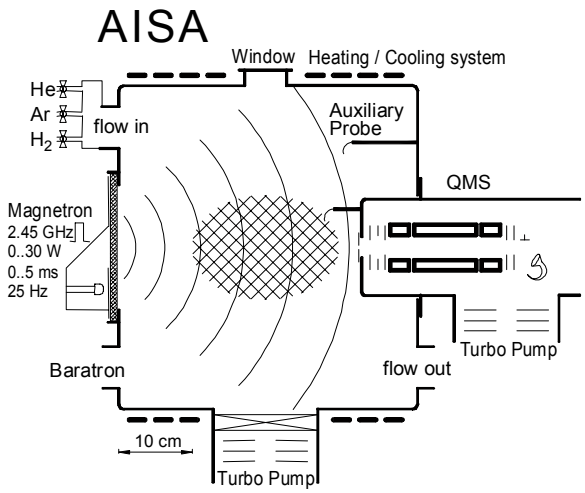

Figure 6 *Schematics of AISA system.*

ultimate background pressure in the discharge chamber was less than 5×10^{-9} Torr. The electron number density (n_e) and electron temperature (T_e) and their time evolutions were obtained from the probe measurements. In **Figure 7** is presented 3D plot of time evolution of probe characteristic. H_3^+ dominated plasma is formed in mixture of He-Ar-H_2 with over 99% of He. H_3^+ ions are formed in sequence of ion-molecule reactions, the actual sequence depends on the composition of the used gas mixture. Monte-Carlo calculations were used to compute the time evolution of the ionic composition for the used gas mixtures.

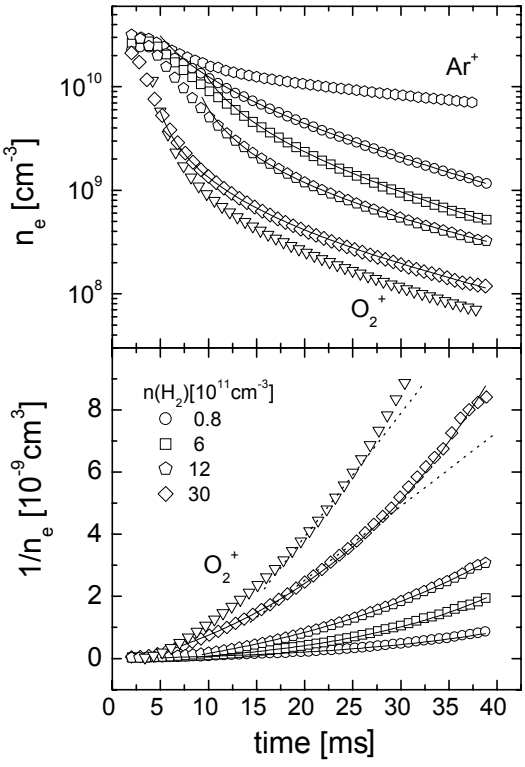

Figure 7 *Time evolutions of electron density measured by probe at different* H_2 *densities. Upper panel: Examples of decay curves,* $n_e(t)$*, in* H_3^+ *dominated afterglow plasma. Lower panel: Corresponding evolution of* $1/n_e(t)$*.*

In decaying quasineutral plasma with losses due to recombination characterised by α, diffusion characterised by ν_D (see e.g. [11]) and "reactive losses" characterised by ν_R the balance equation for electrons can be in first approximation written:

$$dn_e/dt = -\alpha\, n_+ n_e - \nu_D\, n_e - \nu_R\, n_e$$

The balance equation can be rewritten to the form (using n_e' for dn_e/dt):

$$\alpha + \nu_R/n_e = -(n_e'/n_e^2 + \nu_D/n_e) - F(t)$$

Where formation of H_3^+ at low t is accounted in small correction factor, $F(t)$. The terms on the right-hand side can be determined by measuring $n_e(t)$. If values $-(n_e'/n_e^2 + \nu_D n_e)$ are plotted versus $1/n_e$ the rate coefficient α can be determined.

3. Results

In an afterglow experiment the decay of electron (ion) number density is measured and the "de-ionisation" processes responsible for loss of electrons (ions) cannot be directly identified. We will use symbol α_{eff} for rate of observed effective recombination.

We studied the decay of plasma with four different dominant ions He_2^+, O_2^+, Ar^+, and H_3^+ in succession. Examples of obtained evolutions of n_e in H_3^+ dominated plasma at several partial pressures of H_2, the decay curves $n_e(t)$, are plotted in the upper panel of Figure 7. In the lower panel there are plotted reciprocal values $1/n_e(t)$. The slopes of linear parts in these second plots are used in standard analysis for calculation of α_{eff}. From the data given in Figure 7 it is apparent that there is a strong dependence of the rate of de-ionisation of H_3^+ on the hydrogen concentration, $n(H_2)$. This effect is further quantified in **Figure 8**, where we plot the quantity $(-n_e'/n_e^2 - \nu_D n_e)$ versus $1/n_e$

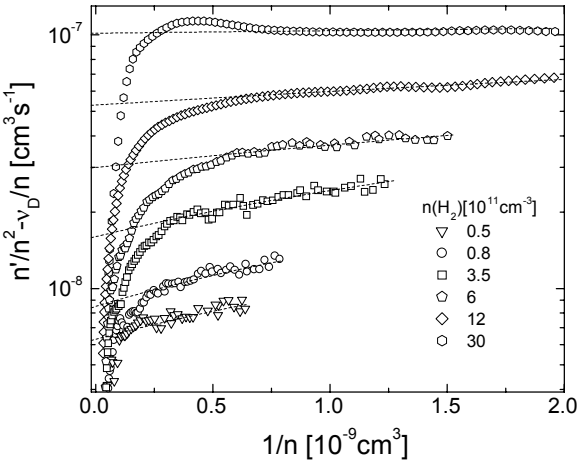

Figure 8 *Advanced analysis. Examples of* $(-n_e'/n_e 2 - \nu_D n_e)$ *versus* $1/n_e$ *plots for several* H_2 *number densities.*

([11]) E.W. McDaniel, J.B.A. Mitchell, M.E. Rudd, Atomic collisions, Heavy Particles Projectiles, A Wiley-Interscience, New York, 1993.

for several $n(H_2)$. Finally the obtained α_{eff} as a function of $n(H_2)$ are plotted in Figure 9.

4. Discussion

The α_{eff} plotted in **Figure 9** represents the overall rate coefficient of the processes in which loss of charged particles is proportional to the product $[H_3^+].n_e$. Because the binary dissociative recombination is just one of possible reaction channels that contribute to α_{eff} it implies, without any assumption on the character of the process(es) of de-ionisation, that the rate of binary dissociative recombination $\alpha_{DR} < 3\times10^{-9}$ cm^{3}s^{-1}. The coefficient α_{DR} is probably smaller, because even at the lowest H_2 concentration, at $n(H_2) = 5\times10^{10}$ cm^{-3}, the observed loss process still clearly exhibit a three body character.

The dependence of α_{eff} on $n(H_2)$ indicates that not only electron (e^-) and H_3^+ ion but also the H_2 molecule

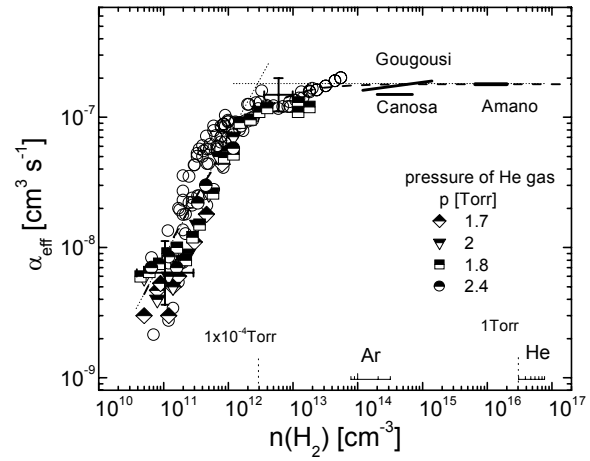

Figure 9 *Dependence of observed α_{eff} on hydrogen number density.*

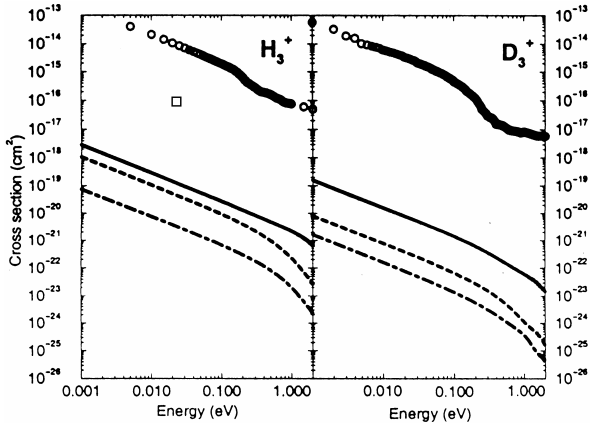

Figure 10 *Comparison of theoretical (lines)* [13] *and experimental (points)* [6] *recombination rates for* H_3^+ *and* D_3^+. *Lines represent computed direct cross sections,corresponding to* s^2A_1' *(dotted-dashed),* p^2A_1' *(dashed) and* p^2B_2' *(solid) symmetries of the "ion + electron" system. Our datum at thermal energy shown as* □.

participate in the observed de-ionisation process. We can assume that the indicated reaction proceeds in two stages: the initial step involves the capture of electron by H_3^+ and formation of an excited intermediate neutral molecule H_3^*, probably in vibrationally excited Rydberg state. This H_3^* can either dissociate back to the reactants or it can lose part of its energy in some process and hence the possibility of autoionisation. Such stabilisation process can be a collision with H_2. The suggested overall reaction scheme therefore is as follows:

$$H_3^+ + e^- \underset{k_{-1}}{\overset{k_1}{\rightleftarrows}} H_3^* \xrightarrow{k_2[H_2]} \textit{neutr. products}$$

Here k_1 is the binary rate coefficient of H_3^* formation, k_{-1} is the rate coefficient of unimolecular autoionisation corresponding to H_3^* lifetime, $k_{-1}=1/\tau_{-1}$. The binary rate coefficient, k_2, describes the possible de-excitation processes, here the collisions with H_2. By application of steady state approximation we can obtain for the overall effective recombination rate coefficient the following formula:

$$\alpha_{eff} = k_1\, k_2\, n(H_2)/(k_{-1} + k_2\, n(H_2)) \,.$$

□

The dashed line plotted in Figure 10 indicates the best fit of our data by this formula. From the fit we obtain the rate of formation of H_3^*, $k_1 = 1.8\times10^{-7}$ cm^{3}s^{-1} and $k_2/k_{-1} = 5\times10^{-13}$ cm^3. If we assume that the rate coefficient of the reaction of highly excited H_3^* with H_2 is given by the rate of interaction of a slow electron with H_2 and is of the order $k_2 \sim 5\text{x}10^{-7}$ cm^{3}s^{-1}, we obtain the autoionisation lifetime of H_3^* $\tau_{-1} = 1/k_{-1} \approx 10^{-6}$ s. This estimate is in agreement with observed rates of interaction of the electrons with Rydberg state molecules. Our assumption of the long lived H_3^* is supported by several spectroscopic observations of the high - n Rydberg states produced in discharges (see e.g. discussion by T. Amano and M.-C. Chan in ref. ([12]) and references therein).

Furthermore the assumption that the H_3^+ recombination proceeds via formation of long-lived H_3^* is also supported by the observation of field ionisation in some merged beam experiments.

5. Conclusions

We measured the rate coefficient of the overall effective recombination of H_3^+ with electrons (α_{eff}) in decaying plasma in He-Ar-H_2 mixture. We observed that α_{eff} depends on the H_2 number density, indicating that the recombination is a three-body process. The observations are consistent with proposed two-step process in which a long-lived highly excited H_3^* molecule is first formed and than it is stabilised against autoionisation by collision with a H_2 molecule.

The observed H_2 partial pressure dependence of the effective recombination rate constant helps us understand the previously puzzling discrepancies in

([12]) T. Amano, Man-Chor Chan, Phil. Trans. R. Soc. Lond. A **358** (2000), 2457.

the measured H_3^+ recombination rates. For many hydrogen containing discharge plasmas the effective recombination rate coefficient governing the loss rate of H_3^+ ions in the interaction with electrons can reach values up to $\alpha_{eff} \sim 2\times10^{-7}$ cm^3s^{-1}, in dependence on $n(H_2)$ and T.

Comparison of theoretical and experimental values of the recombination rates for H_3^+ and D_3^+ is given in ([13]), see Figure 5. Our datum (the assessed upper limit for the rate of binary dissociative recombination for H_3^+) reclines approximately two orders of magnitude below the up to now agreed experimental value ([6]). Our measurement hence seems to support the theoretical calculations and therefore also the calculated energy dependence of the recombination rate for H_3^+ with electron. Even if our measurement has been taken at thermal energies it suggests therefore the probable behaviour of the recombination rate for H_3^+ at the energies that are encountered in tokamak divertors (around 1 eV).

Acknowledgements

Thanks for financial support are due to GACR 202/00/1689, GACR 202/99/D061, GAUK 146/2000, GAUK 171/2000 B FYZ MFF and VZ 190 – 01/ 206054. The experiments were carried out with support of EU in frame of the ETR network (HPRN-CT-2000-000142) and support from EURATOM.

Publications

[1] J. Glosík, R. Plašil, V. Poterya, P. Kudrna, M. Tichý, The recombination of H_3^+ ions with electrons: *Dependence on partial pressure of H_2*, *Chem. Phys. Letter* **331** (2000) 209-214.

[2] P. Kudrna, R. Plašil, J. Glosík, M. Tichý, V. Poterya, J. Rusz**,** *Advanced integrated stationary afterglow apparatus for study of recombination in He-Ar-H_2 plasma*, *Czech. J. Phys.* **50/S3** (2000) 329-334.

[3] J. Glosík, R. Plašil, V. Poterya, P. Kudrna, M. Tichý, A. Pysanenko, *Experimental study of recombination of H_3^+ ions with electrons relevant for interstellar and planetary plasmas*, *J. Phys. B: Atomic, Mol. Opt. Phys.* **34** (2001) L485-L494.

[4] J. Glosík R. Plašil, V. Poterya, P. Kudrna, A. Pysanenko, M. Tichý, J. Rusz, *Stationary afterglow study of recombination of H_3^+ ions with electrons*, ECAMP VII, The Seventh Eur. Conf. on Atomic and Molecular Physics, Eur. Conf. Abstracts, Vol. 25 B, Berlin 2.-6. April 2001, A 10.32, p.70.

[5] J. Glosík, V. Poterya, M. Vicher, R. Plašil, P. Kudrna, A. Pysanenko, M. Tichý, *Kinetics of formation and destruction of H_3^+ ions in He-Ar-H_2 plasma influenced by recombination of H_3^+ ions*, Proc. 15th Int. Symp. on Plasma Chem. (15 ISPC), Orleans - France, 9-13 July 2001, Vol. III, p.789.

[6] M. Tichý, V. Poterya, R. Plašil, P. Kudrna, A. Pysanenko, J. Glosík, *Application of Langmuir probe for study of recombination of H_3^+ ions with electrons in He-Ar-H_2 stationary afterglow plasma*, Proc. XXV Int. Conf. on Phenomena in Ionized Gases, Nagoya (Japan), July, 17-22, 2001, Vol .3., pp.267-268.

([13]) I.F. Schneider, M. Larsson, A.E. Orel, A. Suzor-Weiner, Proceedings of the 1999 Conference on Dissociative recombination, *Theory, Experiment and Applications IV*, editors M. Larsson, J.B.A. Mitchell, I. F. Schneider World Scientific, Singapore, 40 (1999), p. 131.

III TECHNOLOGY

1 IFMIF Test Experiments

P. Bém, V. Burjan, J. Dobeš, M. Götz,
V. Kroha, R. Mach, J. Novák, E. Šimečková,
J. Štursa

Nuclear Physics Institute Řež

1. Introduction

Cost and reliability of future fusion devices strongly depend on the solution of the structure materials issue. Radiation damage from fusion neutrons of the first wall of fusion reactors determines the lifetime of the device. The project IFMIF (International Fusion Material Irradiation Facility) is aimed to provide a neutron source with an energy spectrum simulating that of fusion neutrons at sufficient intensity to test samples of structure materials.

The IFMIF design concept consists of future high power deuteron accelerator (40 MeV, beam power of 5 MW) and flowing liquid (jet) lithium target.

The neutron source reaction d(40 MeV)+Li produces a white spectrum with mean energy of 14 MeV and a high energy tail up to 50 MeV. Therefore, in the conceptual design phase of the project, the response of and radiation effects on IFMIF are to be investigated at relevant neutron energies.

At present stage of the art, high energy neutron sources based on protons and deuterons from cyclotrons interacting with thick targets of light nuclei provide intensities that cannot be generated by other methods. Other possible neutron generators, such as fast breeder reactors, spallation reactions on heavy ion - and high-energy proton accelerators, have the disadvantage of a dominant contribution of low energy neutrons.

The NPI Cyclotron-based Fast Neutron Facility (CFNF) employ the variable energy cyclotron U-120M. In the positive-mode of cyclotron operation, protons, deuterons and $^{3,4}He^{++}$-ions of energy up to 22, 18 and 50 MeV, respectively are at disposal for the NG1 target station (see **Fig. 1**). Higher-power beam (current up to 20 μA) of protons and deuterons (energy of 35 and 18 MeV, respectively) could be delivered on the NG2 target station in the negative-ion extraction mode. Fast-neutron spectrometers with relevant hardware and software are at disposal.

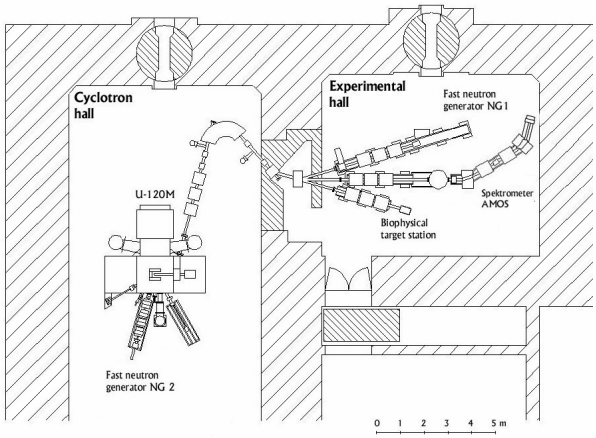

Figure 1 *The NPI Cyclotron-based Fast Neutron Facilities (CFNF). Target stations NG1 and NG2 are located on beam lines of particles accelerated in the positive- and negative-ion mode of cyclotron operation, respectively.*

After design the NG2 station and appropriate upgrading of basic target-station hardware will be performed, the NPI CFNF are suitable for solving selected tasks of the IFMIF neutronics. Relevant R&D program for the 2000-2 year period has been started at NPI in the framework of the Association EURATOM/IPP.CR. It is supported by the EFDA - and Underlying Technology funds and performed in close cooperation with IFMIF experts from FZK Karlsruhe, ENEA Frascati and CEA Cadarache.

2. EFDA Technology Programme

2.1. EFDA/IFMIF Task TTM 8

Activation foils and sub-miniature fission chambers: Experimental tests

Cooperation: B. Esposito, ENEA Frascati,
C. Blandin, CEA-Cadarache
J. Kopecky, JUKO Research

2.1.1. Description

The proposed program aims at the test of prototype on-line high-flux neutron monitors (sub-miniaturized fission chambers) for IFMIF (developed at CEA Cadarache and ENEA Frascati) on an IFMIF-like neutron field. Tests will be provided by the NPI CFNF. In parallel, integral tests on activation foils selected for IFMIF neutron dosimetry will be also performed.

To explore the ability of CFNF to simulate an IFMIF-like neutron field with source strength, relevant to perform tests of selected characteristics of proposed monitors, most suitable source reaction is to be selected. After this, the cyclotron target station will be upgraded accordingly. Finally, experimental validation of the dosimetry foil package (multifoil activation) selected for IFMIF and tests of fission chambers through the measurements in the IFMIF-like neutron field will be performed at NPI.

2.1.2. Milestones

- search for IFMIF-like neutron source reaction,
- design of high-power heavy-water neutron target station and NG2 target station,
- preliminary neutron spectrum measurements with activation foils and scintillators on cyclotron
- final tests on cyclotron of IFMIF neutron monitors (sub-miniaturized fission chambers and activation foils)

2.1.3. Results

The start of the work was based on results of previous experimental investigations of light-nuclei break-up reactions at medium incident energies, performed at the NPI cyclotron [1]. So as deuterons can be accelerated up to 18 MeV only on the NPI cyclotron, in order to simulate the IFMIF d(40 MeV)+Li neutron spectrum, another reactions have to be selected. Among them, the deuteron break-up in the p(35 MeV)+D reaction has also been considered (intensively cooled heavy-water flow is proposed for the target with respect to heat dissipation of kW beam power).

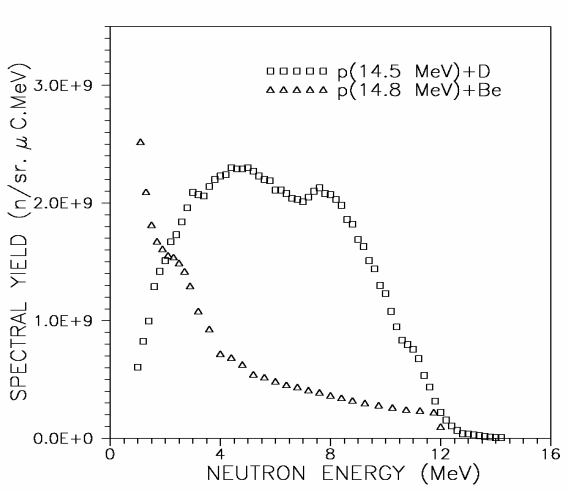

Figure 2 *The zero-degree spectral neutron yield for the* D(p,n)2p *measured at 14.5 MeV on the proton beam of the NPI cyclotron. Relevant data of* Be(p,xn) *reaction [EXFOR database] are given for comparison.*

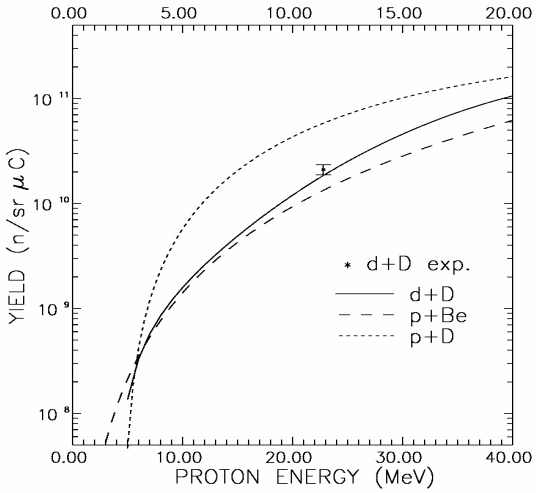

Figure 3 *Thick-target zero-degree neutron yield from* D *and* Be *targets as a function of incident particle energy.*

Measured and available data on the dominating reaction branch p+D shows Gaussian-like white neutron spectrum with the peak located at $E_n \sim 0.45E_p$ (see **Fig. 2**). A simple theoretical consideration applied to present experimental results and to available cross section data of the D(p,n)2p reaction permit to predict the energy dependence of the spectral yield (see **Fig. 3**) and to evaluate the source strength of 3×10^{12} n/sec.×sr for 35 MeV/20 μA proton beam, expected for the NG2 target station.

Due to lack of relevant data, the contribution of proton reaction on oxygen to the integral and spectral neutron yield could not be calculated correctly. Instead, the p+D_2O reaction was investigated experimentally (at 22 MeV proton energy, the maximum value available for the NG1 target station, where spectral measurements could be performed). Preliminary results show

some acceptable lowering of the integral neutron yield (factor of 0.3) and unimportant rise of low-energy part of spectra compared to the p+D reaction. Thus the p+D_2O reaction endures being selected as a most suitable simulation of the IFMIF source reaction with highest source strength available at the NPI cyclotron.

Design and manufacture of NG2 target station which includes the high-power heavy water target (800 W) and a special beam line from the negative-ion extractor device of cyclotron is under progress. The conceptual design of NG2 target station facility is given in **Fig. 4**. At present, the doublet/triplet variant of electromagnetic quadrupole for the loss-free transfer of accelerated beam to the target is investigated.

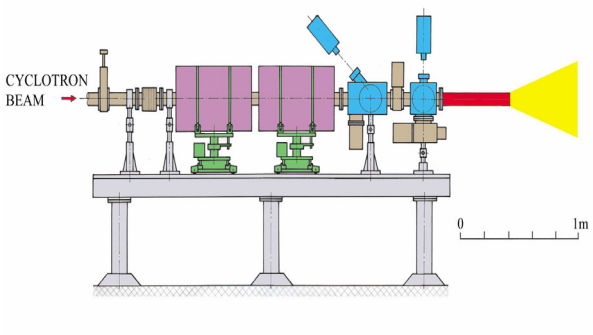

Figure 4 *The conceptual design of the NG2 target station incorporated with high-power heavy-water neutron source target on negative-ion beam line of the NPI cyclotron.*

2.2. EFDA/IFMIF Task TTM 13:

D-Li reaction source term, experimental verification of neutron yield

Cooperation: U. von Möllendorff
U. Fischer, FZK Karlsruhe

2.2.1. Description

The calculation of the neutron flux, the spectrum and the neutronic responses in the IFMIF Test Cell suffer from the lack of an accurate, validated cross section database of the Li(d,xn) source reaction. Reduction of the current flux uncertainty to a tolerable level is urgently required. Therefore, the need for relevant experimental differential yield data is evident.

Measured data will also been used for benchmark tests of the semi-empirical M^{c}DeLi model of the Li(d,xn) reaction. The research program is intended to provide accurate data concerning the neutron yield observables of the d+Li reaction at incident deuteron energies up to 18 MeV. Measurements are needed to validate the Li(d,xn) cross-section evaluation recently produced by FZ Karlsruhe/INPE Obninsk.

2.2.2. Milestones

- lithium-metallic technology development
- thick Li-target chamber for the NG1 target station, design and installation
- unwanted-neutrons contribution, determination
- measurement of the differential as well as the total (thick target) spectral yield of neutrons from the Li(d,xn) reaction at and below 18 MeV deuteron energy, in the angular range from 0^o to 150^o
- use of the differential yield results for comparison with and possibly improvement of the Li(d,xn) evaluated nuclear data files.
- use of the thick-target yield data to benchmark M^{c}DeLi model calculations.

2.2.3. Results

Planned measurements require to operate with backing-free foils and layers from metallic lithium in target chamber. To prepare lithium targets, the vacuum stand of 80 dm^3 volume with vacuum/argon mode of operation was completed and proved for routine running.

New Li-target chamber was designed and installed on beam line of the NG1 target station and tested. In the experiment, the entrance-foil-free thick lithium target (6 mm thickness – slightly above the range of 18 MeV deuterons, 50 mm of diameter) was irradiated by 17 MeV deuterons of 0.01 – 0.1 μA beam intensity. No destruction was observed on Li-layer surface after 48 hours of beam operation.

In the measurements of neutron yield from charged-particle reaction, unwanted neutrons could come from reactions of projectiles with the target- and the beam-guide hardware. In order to suppress such effect, the target and beam-guide aperture have been enlarged and also the slit-free beam guide of the NG1 target station was designed (see results of following TTM 14 Task). Nevertheless, the fluctuation of the beam-spot position out of the target window could be expected, due to fluctuated instability of electrostatic modules of the cyclotron.

To exclude such source of unwanted neutrons, new method has been developed employing an off-line analysis of data-acquisition sequence: In the present data acquisition system, pulses from neutron detectors are collected in an external buffer, which is transferred to the on-line computer whenever it filled (a “list mode”). Each transfer also includes information about the monitoring detectors and beam charge collected in the Faraday cup. In this way, each measurement is divided into several tens of data blocks, giving full information about its history.

The effect of the beam drift is recognized and corresponding part of measured data is excluded during an off-line analysis of registered events, for which the N/Q ratio is computed from neutron events

N and the beam charge Q (on the target) for every transferred buffer. As an example of this procedure, the dependence of the N/Q ratio on a buffer sequence is shown in **Fig. 5**. This ratio remains constant within a statistical error σ in most transferred buffers.

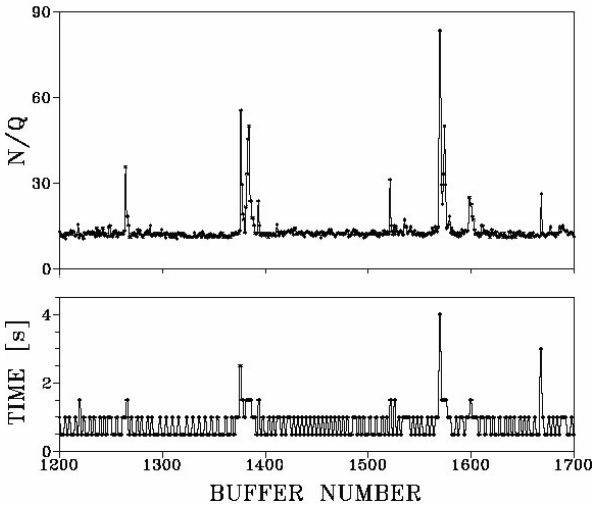

Figure 5 *The behavior of the N/Q ratio computed from registered neutron events N and beam charge Q (on the target) for every transferred buffer (a list). The time duration of individualtransfers is also shown. For further explanation, see text.*

However, in few isolated and randomly distributed cases this ratio suddenly grows exceeding the mean N/Q value by 3σ. Such events indicate the decrease of the charge on the target (because the preselected number of N is constant). Due to rather constant intensity of the incident beam, the time duration of buffer filling (see the lower part of Fig. 5) reveals steady value through all the selected part of the exposition, except some cases of the growth that well coincide with the fluctuations of the N/Q ratio. Such events could be unambiguously attributed to the random irradiation of the tantalum entrance slit of the target and excluded from further analysis.

2.3. EFDA/IFMIF Task TTM 14,

Neutron data above 20 MeV;
Neutron transport benchmark tests

(supported in part by Underlying Technology Programme)

Cooperation: U. von Möllendorff, FZK Karlsruhe

U. Fischer, FZK Karlsruhe

2.3.1. Description

The IFMIF neutron source reaction d(40 MeV) +Li produces a white spectrum with a high energy tail up to 50 MeV. Currently, under the INR Karlsruhe/INPE Obninsk evaluation work, characteristics such as the high energy flux ($E_n \geq 14$ MeV) in the Test Cell region of the IFMIF are calculated at Karlsruhe employing the MCNP transport code.

The existing neutron transport data files up to 50 MeV are mainly based on theory, with little backing by experimental cross section data. The only way to validate the data and tools for IFMIF neutron flux calculations is by benchmarking them against experiments with a neutron beam having a realistic (IFMIF-like) energy distribution.

Such benchmark tests will be performed at NG1 target station of the NPI CFNF. Among materials of interest, iron is of primary preference for such benchmarking. As a first step, the transport of neutrons through an iron slab will be measured in an open geometry employing a white neutron spectrum ranging from 2 MeV to 30 MeV. The analysis of available (EXFOR) database has shown that for a simulation of the IFMIF neutron spectrum on the NG1 target station facility, the ^{3}He-ion induced deuteron break-up (thick D_2O target) reaction is most suitable. An upgrade of the NG1 target station will be performed to reach appropriate flight path (the pulse pile-up consideration) for neutrons registered in the angular range of 0-150 degree, employing the open-geometry and the shadow-bare method of measurement.

2.3.2. Milestones

- thick D_20 target chamber and slit-free ^{3}He-beam guide of NG1 target station, design, installation and tests
- measurement of the spectral flux of fast neutrons penetrating the and emerging from the iron slab in an irradiation experiment performed in an open geometry with a white IFMIF-like primary neutron spectrum
- use of the experimental results to benchmark the evaluated nuclear data files produced within the IFMIF work by comparison with calculations

2.3.3. Results

An upgrade of optical system hardware of the NG1 beam-guide was performed. After calculation of emitance behavior of the beam, a triplet of quadrupole magnets was located on beam-guide to reach a loss-free transport of ^{3}He beam (2 μA, beam spot of 8 mm in diam) to the target. New installation of NG1 target station permit to enlarge a flight-path of neutrons emitted at zero degree (maximum neutron intensity) up to 5 m (see Fig. 1), which enable to perform data acquisition of proposed experiments at acceptable count-rate with correctly handled dead-time effect (pile-up consideration).

To test all these options of upgraded NG1 facility, the measurement of neutron spectral yield from $D_2O(^3He,xn)$ neutron source reaction has been undertaken. Detail description of the experimental method is given elsewhere [1,2]. Preliminary results of

data processing prove an expected strongly forward-directed neutron flux (the FWHM ~ 30 degree) as a result of selected reaction kinematics (heavier mass of incident particle over that of target nucleus).

Presence of ^{16}O in the target was found to have no substantial disturbing effect on overall characteristics of neutron flux originated from dominating ^{3}He+D process. At present, the data reduction and analysis is completed and spectral analysis is under progress (see UNTECH Task 1).

2.3.4. Future direction

In the next step, a collimated neutron beam will be employed for measuring the angle-dependent characteristics of neutron transport.

The results will be used to benchmark MCNP calculations performed at FZK Karlsruhe using the IFMIF evaluated neutron transport data files.

3. Underlying Technology Programme

3.1. UNT Task 1

Benchmark tests of IFMIF Neutronic Calculations

Cooperation: U. von Moellendorf, FZK Karlsruhe
U. Fischer, FZK Karlsruhe
S. Meigo, JAERI, Tokai

3.1.1. Description

The research program is intended to prove ^{3}He-ion induced deuteron break-up process (thick D_2O target) for simulating the IFMIF d+Li neutron spectrum and to define primary irradiation conditions for neutron irradiation and neutron benchmark experiments.

With this aim, the spectral and angular distribution of neutrons originating from this type of source reactions has to be measured employing fast neutron spectrometer. Response functions and detection efficiency of employed scintillation detectors (stilbene and NE213 of various dimensions) have been calibrated for neutron energies between 0.8 and 20 MeV using neutron reference fields of the PTB Braunschweig facilities.

However, so as the IFMIF neutron source reaction d(40 MeV)+Li and consequently all simulating reactions will produce a white spectrum with high energy tail up to 50 MeV, the detectors should operate also in this energy range. For the calculation of response function and efficiency of detectors for energies above 20 MeV, appropriate codes have to be implemented and tested.

3.1.2. Milestones

- cyclotron ^{3}He-beam line (collimator free mode of operation), NE-213 detector assembly,
  design and installation,
  $^{3}He(40MeV)+D_2O$ reaction, neutron yield measurement (complementary to the deliverable of EFDA/IFMIF task TTM 14)
- NE213, detection efficiency, response functions,
  code implementation and tests

3.1.3. Results

An upgraded target station and beam-guide of the NG1 facility was tested in the measurement of neutron-yield observables of the source reaction $D_2O(^{3}He,xn)$. The experimental arrangement and the neutron scintillation spectrometer have been described elsewhere [1,2]. In the experiment, the ^{3}He-beam current on the target has been kept below some tens of nA and monitored with an accuracy of 0.8%. Emitted neutrons were detected with NE 213 scintillator of dimension ϕ 4.5 x 4.5 cm^3, respectively. The angular distribution of the spectral neutron yield has been measured in an open geometry. To subtract neutron-room background, the conventional shadow-bar method has been employed. The fast-neutron spectrometer has operated with the two-dimensional n-γ discrimination hardware. Pulses from detectors were collected in an external buffer,. which was transferred to the on-line computer. In an off-line analysis of the pulse-shape timings vs. pulse-height spectra, a complete discrimination between neutrons and photons was achieved above recoil proton energy of 2.2 MeV. A list-mode operation was used to exclude unwanted neutrons from random irradiation of target hardware.

Below 20 MeV neutron energy (spectral yield at backward angles) the pulse-height spectra from detector were unfolded using the procedure DIFBAS with simulated response function NRESP7 (PTB Braunschweig code). To unfold spectra of higher neutron energy, the SCINFUL-R code (S. Meigo, JAERI, priv. com.) is now implemented for PC at NPI CFNF.

For an illustration of preliminary results, neutron induced light-output spectrum from NE-213 detector (gama ray discriminated) is compared with curve calculated by SCINFUL-R code at 27 MeV neutron energy (**Fig. 6**). Note, that this value corresponds to the upper cinematic limit for the D(3He,n p)^{3}He break process at about 40 MeV incident energy of ^{3}He.

Expected neutron energy range in the simulation of IFMIF-like spectrum is thus confirmed. Complete analysis (deconvolution procedure) of measured data is in progress.

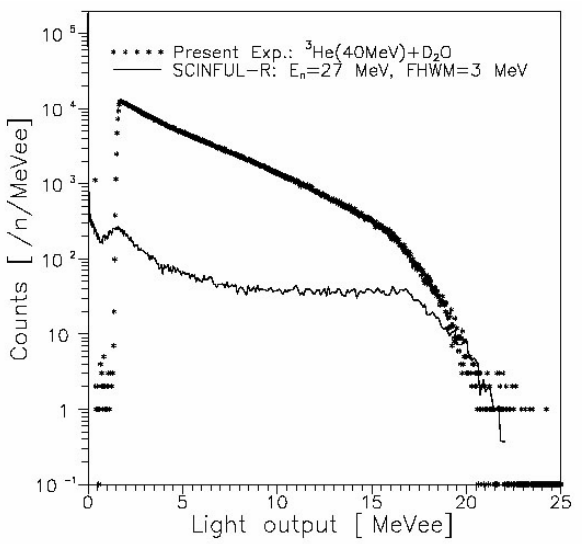

Figure 6 *Measured neutron pulse-height spectrum [NE 213 detector (zero-degree yield, D_2O target irradiated by 40 MeV ^{3}He-ions)]. Data are compared to the response function calculated for 27 MeV neutrons with SCINFUL-R code.*

References

[1] P. Bém, V. Burjan, F. Cvachovec, M. Gotz, V. Kroha, E. Yu. Nikolskii, E. Šimečková, J. Vincour: Fast neutrons from thick deuterium target irradiated by 15.8 and 14.1 MeV deuterons, *Nucl. Instr. Meth.* **A 425** (1999) 522.

[2] P. Bém, V. Burjan, F. Cvachovec, M. Gotz, M. Králík, V. Kroha, E. Lukášová, E. Šimeč-ková and J. Vincour: Fast neutrons from thick helium target irradiated by 17 MeV deuterons. *Nuclear Instruments and Methods in Physics Research. A - Accelerators Spectrometers Detectors and Associated Equipment*, **466** [3] 509-512 (2001).

[3] P. Bém, V.Burjan, J.Dobeš, B.Esposito, U.Fischer, M. Götz, M. Honusek, V. Kroha, R. Mach, U. von Mollendorff, J. Novák, E. Šimečková, J. Štursa, and J. Vincour: IFMIF neutronic calculations and neutron monitors: Experimental tests. in: *Bienial Report 1999-2000*, NPI AS CR Řež (2001).

2 Plasma Spraying of Boron Carbide

P. Chráska, J. Matějíček, K. Neufuss, J. Stöckel, J. Žáček

Institute of Plasma Physics, Prague

1. Introduction

For many plasma facing components of fusion research devices, special materials are sought for. Since "single" materials (such as steels, special alloys, etc.) are often at the limits of their properties, new type of materials must be developed. One of them are, for instance, composites. Using thermal spraying, composite materials consisting of a substrate and one or several deposited layers can be produced, whose properties augment the properties of the base substrate. Specifically, for certain plasma facing components, refractory materials with low Z are required. One of the candidate materials is boron carbide. IPP's unique water-stabilized plasma torch has several advantages:

- high enthalpy plasma, thus is able to spray high melting point materials,
- high throughput, which enables to spray large areas conveniently,
- operates in air, thus offers a possibility of on-site repairs.

The goal of this research is to select/manufacture possible candidate powder materials, used for subsequent plasma spraying, examine the resulting deposits for their structure, phase and chemical composition, determine their application-relevant properties and optimize the spraying procedures based on these results.

2. EFDA Technology Programme

EFDA Task: DV4/04 Plasma Spraying of Boron Carbide

Cooperation: J. Linke, FZJ Jülich

2.1. Description

Boron carbide is one of the candidate materials for plasma facing components of stellarator-type fusion reactors. Boron carbide has high melting point, low Z and is a good oxygen getter.On the other hand, it is rather difficult to melt by means of plasma spraying – due to its high melting point, high specific heat and melting enthalpy, as well as low density. The IPP's water-stabilized plasma torch exhibits high temperature and enthalpy of the plasma jet (compared to gas-stabilized plasma torches) and thus enables plasma spraying of high melting point materials. Since it has not been used before for spraying of boron carbide, new spraying procedures have to be developed. A complex characterization of the resulting deposits is used for subsequent process optimization.

2.2. Milestones

- selection of feedstock powder, process development
- plasma spraying and optimization
- deposit characterization and testing

2.3. Results

Numerous spraying runs were made. During these, several process parameters were chosen and – based on examination of the coatings – adjusted for improved particle melting, adhesion and reduced in-flight oxidation. These parameters included: powder feeding distance, spraying distance, plasma jet shrouding, carrier gas type and substrate preheating temperature and use of a bonding interlayer.

A complex deposit characterization was performed using the following techniques: SEM, XRD, porosimetry, oxygen content analysis, mechanical testing, dilatometry, microwave reflectometry. The deposits had porosities ranging from 5 to 40% and oxygen content from 2 to 12%; elemental boron was also observed. After the initial runs and tests, insufficient particle melting in the jet and oxidation of boron carbide were determined as problematic issues.

Figure 1 shows the deposit structure before and after spraying optimization. The un-optimized deposit exhibits loosely bonded, angular particles, indicating insufficient melting, and a multitude of fine particles (oxides). The optimized deposit exhibits improved melting and bonding of the particles, albeit with a considerable porosity. The improvement in particle bonding is further reflected in mechanical properties, presented in Table 1.

For deposits on stainless steel, a MgSiO4 interlayer was used for improvement of adhesion, as it has an intermediate CTE between B4C and stainless steel.

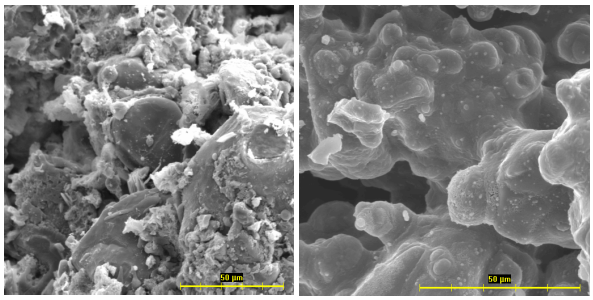

Figure 1 *Structure of B4C deposits before and after spraying optimization.*

Sample	Young's modulus	flexural strength
FD-SD-tube-shroud	(GPa)	(MPa)
26-300-tube-He	73	238
26-300-tube	56	122
28-300-tube	44	83

Table 1 *Mechanical properties of B4C deposits. FD = powder feeding distance, SD = spraying distance, tube = protective tube around the jet, shroud = gas shrouding of the jet. Typical values of Young's modulus for WSP-sprayed ceramics are 10-40 GPa.*

Several different deposits on stainless steel and molybdenum substrates, with or without the MgSiO4 interlayer, have been tested for thermal shock resistance at FZJ Jülich.

A summary of the electrical properties was presented on the International Conference on Fusion Reactor Materials (Baden Baden, 2001) [1]. The plasma spraying aspects will be presented on the International Thermal Spray Conference (Essen, 2002) [2]. A general overview of the material properties in relation to their processing and structure was presented on the Materials Week conference (Munich, 2001) [3].

The new findings presented by other researchers at the ICFRM led to a conclusion that vacuum plasma spraying is the optimum technology for both of the above applications; thus, the program on spraying by water-stabilized plasma was discontinued. A new research program on spraying tungsten-based plasma facing components for potential application in ITER and future devices is envisaged and a collaboration with Forschungszentrum Juelich in this field was initiated.

3. Underlying Technology Programme

UNT Task: Coatings from low-Z materials for fusion applications

Cooperation:

S. Nanobashvili, Georgian Academy of Sciences, Tbilisi

M. Blaumoser, J. Botija, CIEMAT, Madrid

V. Brožek, Institute of Chemical Technology, Prague

3.1. Description

In connection with the EFDA Technology Task, plasma sprayed coatings of B4C and other materials were developed for fusion-related applications.

Besides the main direction (plasma facing components), two applications were aimed at: coatings for CIEMAT's TJ-II waveguide (as an additional biological shielding) and coating for a Langmuir probe for CASTOR Tokamak (as an electrical shielding).

3.2. Milestones

- plasma spraying of low-Z coatings
- coatings characterization, mainly microwave reflectometry

3.3. Results

For the waveguide shielding coatings, three materials were used – B4C, Al2O3 and Si. The primary funcion of such coatings would be to absorb microwaves, thus, microwave reflectometry was used as a main characterization technique. Additional characterization was also performed (XRD, AAS). B4C and Al2O3 coatings were tested with and without additional treatment – oxide dissolution and colloidal graphite coating, respectively.

The untreated B4C coatings showed values of the power reflection coefficient Rp ranging from 0.15 to 0.82. The treated B4C, Si and untreated Al2O3 coatings had Rp around 0.7. Excellent absorption was achieved with the graphite-coated Al2O3, having Rp = 0.03. The tests were performed at the most harsh condition – normal incidence; in practice, with off-normal incidence, the absorption would be even better.

The Langmuir probe for CASTOR Tokamak was successfully coated with B4C and tested in operation. Here, the B4C coating presents optimum properties for absorption of electromagnetic radiation – between a dielectric (total transmission) and a conductor (total reflection).

Publications

[1] S.Nanobashvili, J. Matějíček, F. Žáček, J. Stőckel, P. Chráska, V.Brožek: Plasma Sprayed Coatings for RF Wave Absorption, *ICFRM Baden Baden* 2001, *J. Nucl. Mater.* **307**: 1334-1338 Part B, Dec. 2002.

[2] J.Matějíček, K.Neufuss, P.Chráska, S. Nanobashvili, V.Brožek, J. Linke: WSP-Sprayed Boron Carbide Coatings for Fusion Applications; in preparation for *Intl. Thermal Spray Conf., Essen*, 2002.

[3] J. Matejíček, S.Nanobashvili, P.Ctibor, K.Neufuss, V.Brožek, P.Chráska: Properties of Boron Carbide Coatings and Free-Standing Parts Prepared by WSP®, *Materials Week & Exhibition MATERIALICA*, October 1-4, 2001 Munich, CD-K5-914.

3 SiC/SiC Composites

Principal Investigator: V. Bálek

Nuclear Research Institute Řež

EFDA Technology Programme

EFDA Task: TTMA-001/D3
SiC/SiC composites – Thermophysical properties: diffusion, permeability

1. Investigation of inert gas diffusion and microstructure changes of SiC/SiC treated in various gas environments

Thermal behavior of SiC/SiC composites (commercial samples denoted N3-1, N4-1; NIPON Carbon) in two different gases (argon and air resp.) was investigated during heating from 20 to 1300 °C. Diffusion structure analysis (DSA) was used to characterize microstructure changes. From DSA the temperature intervals of the annealing of voids in the SiC/SiC composites were determined. The onset of the oxidation of SiC during heating in air under normal pressure was determined. The microstructure was characterized before and after heat treatment by means of SEM.

The microstructure changes of SiC/SiC composites, N3-1 and N4-1 materials produced by CERASEP® were tested under conditions of heating in argon and air, respectively. The behavior of samples produced by CERASEP® and NIPON Carbon was compared [1]. Moreover, additional materials as PIP-Hi Nicalon (UBE Industr. Japan), CVI-GA-Hi Nicalon as well as the fibers Nicalon CG and Tyranno SA and SiC fibers will be tested from the view point of thermal behavior under different gas environment. Helium ions will be implanted into the SiC/SiC composite materials mentioned above with the aim to characterize helium diffusion and possible microstructure changes caused by the implantation. The latter materials were not considered for testing in original proposal, therefore the due date for the delivery was postponed until 30. 10. 2002. For deposits on stainless steel, a MgSiO4 interlayer was used for improvement of adhesion, as it has an intermediate CTE between B4C and stainless steel.

2. Characterization of thermal desorption of inert gases from surfaces and near surface layers of SiC/SiC composites

Thermal desorption of radon from surfaces and the near surface layers of SiC/SiC composites (commercial samples denoted N3-1, N4-1; NIPON Carbon) was investigated. The mathematical model for the evaluation of the thermal desorption of inert gases was developed. In the next period desorption of radon from SiC N3-1 and N4-1 materials produced by CERASEP® will be studied. The helium ions will be implanted into the samples with the aim to characterize its desorption from the composite materials and from the individual components like fibres.

The above mentioned mathematical model will be used further for evaluation of the experimental results.

Publications

[1] V. Bálek, V. Zeleňák, T. Mitsuhashi, J. Šubrt, H. Haneda: Emanation thermal analysis of SiC based materials, submitted (appeared in *Journal of Thermal Analysis and Calorimetry* **67** [1] 83-89 (2002), 1418-2874.)

IV INERTIAL FUSION
KEEP-IN-TOUCH ACTIVITY

Keep-in-Touch Activities on Inertial Confinement

J. Ullschmied, V. Petržílka

Institute of Plasma Physics, Prague

1. Introduction

The reported keep-in-touch activity is aimed at experimental and theoretical studies on key aspects of target physics relevant to inertial fusion. It is substantiated

(1) by the encouraging experimental prospects opened at IPP AS CR by a successful launching of the terawatt iodine laser system PALS, and

(2) by the experience gained at IPP during its long lasting theoretical effort at studying physical processes in hot fusion plasmas.

The first year of the keep-in-touch activity project was devoted among others to the assessment of the future fusion-relevant experiments to be performed at the upgraded PALS facility, and to the formulation of some relevant theoretical tasks.

2. Status of the PALS facility

One of the European most powerful lasers, the terawatt iodine laser system ASTERIX IV, has been recently transferred to Prague from the Max-Planck-Institute für Quantenoptik (MPQ) in Garching, Germany. Under the a name - PALS (**P**rague **A**sterix **L**aser **S**ystem) - it is operated by the PALS Research Centre, a joint laser laboratory established by the Institute of Plasma Physics (IPP) and the Institute of Physics (IP) of the Academy of Sciences of the Czech Republic. The Centre is aimed at performing the research of high-power lasers and the laser-produced plasmas with applications in both the science and the technology. Its research programme covers a broad range of experimental activities, from the development of X-ray sources including X-ray lasers and of the sources of highly stripped ions, up to the experiments pertinent to the physics of shock waves nad ultra-high pressure, and to inertial confinement fusion.

The PALS system, as it is now implemented in Prague [1] (see **Fig. 1**), is a single beam iodine photodissociation laser system, based on a master oscillator - power amplifier (MOPA) configuration. It is capable of supplying up to 1 kJ of energy at the fundamental wavelength 1.315 μm, in pulses of ~ 400 ps duration.

Figure 1 *View of the PALS laser hall, April 2000.*

The primary pulse is generated in an opto-acoustical mode-locked oscillator equipped with a high-extinction ratio pulse selection system (contrast ratio ~10^9). This pulse is seeded into a chain of one preamplifier and five power amplifiers separated by spatial filters which remove the high spatial components from the angular beam spectrum and simultaneously act as image relay pairs ensuring optimum coupling between adjacent amplifiers.

The beam at the output of the last amplifier is 29 cm in diameter. According to the need of a given experiment it may be frequency doubled to 658 nm or tripled to 438 nm, by using DKDP crystals, prior to its final focusing in the target chamber. The main aspheric

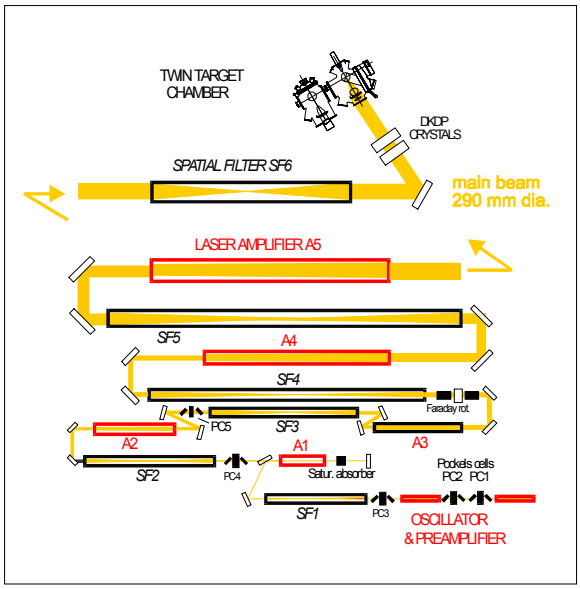

Fig. 2 *Schematic of the PALS main beam line.*

focusing lens ($f_{1\omega}$ = 593 mm, $f_{2\omega}$ = 580 mm, $f_{3\omega}$ = 564 mm) was designed to produce a focal spot of the diameter of ~50 μm only (about eight times the diffraction limit at 1ω). A simplified layout scheme of the PALS laser system is shown in **Fig. 2**.

The laser is capable to fire a full-energy shot each 20 minutes, delivering on the target up to $3 \cdot 10^{16}$ Wcm^{-2} of the focused beam power.

The PALS reached its standard parameters at the fundamental wavelength in spring 2000 and was officially launched on June 8, 2000. Typical energies at the outputs of the laser amplifiers I–V are shown in the following Table:

Amplifier	I	II	III	IV	V
Output energy [J]	1	2	30	100	500

First target experiments on the PALS facility started in September 2000. The PALS target chamber of an original twin conception was designed in co-operation with French laser laboratories (*Laboratoire de Spectroscopie Atomique et Ionique, Université Paris-Sud* and *Laboratoire pour l'Utilisation des Lasers Intenses*). The chamber makes it possible to perform a broad range of experiments, the interaction experiments with X-ray lasers beams in particular. It consists of two parts (see **Fig. 3**): of a main spherical chamber (~1 m in diameter), and of an auxiliary cylindrical chamber (∅ 65 cm x 1 m). While in the main chamber a main laser beam focusing assembly and primary target mounts are located, the auxiliary chamber may be used for various secondary targets e.g. for X-ray beams. Both the chamber parts may be used also independently for different experiments.

The main chamber has a large pneumatically controlled gate to facilitate access to the target optical bench. A double bellow compensating system ensures

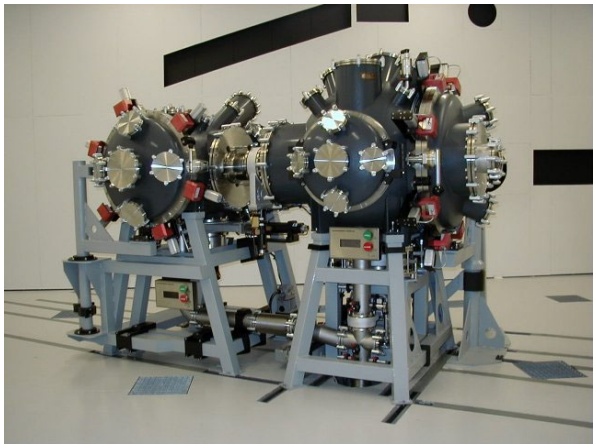

Fig. 3 *PALS twin target chambers.*

mechanical decoupling of the chamber bodies and the internal optical benches, preventing them from deformation during the evacuation cycles.

This arrangement assures a high mechanical stability of the target mounts, the target stages and all the internal optics in both the chambers. Digitally controlled positioning systems of the target mount (five degrees of freedom) and of the focusing optics assembly makes it possible to adjust the target position with a micrometric precision.

3. Current experiments at PALS

The first milestone was to produce laser plasma by using a point-focused laser beam. It was reached in September 2000.

Already the first series of experiments with a point focusation proved excellent focusability of the laser beam [2]. The power density in a tightly focused full-energy beam exceeds 10^{16} W/cm^2. Various metallic plates (Al, Ti, Mo, Ag, Ta, Au) were used as targets. As a practical illustration of the focal spot size, several scanning electron microscope (CamScan 4 DV) pictures of the craters excavated by a tightly focused beam in Al and Mo targets are presented below (see **Fig. 4**).

The first physical experiments exploiting the plasma produced by a point-focussed beam started in the second half of 2000. They were aimed among others at the

- development of soft X-ray sources for lithography and contact microscopy of microbiological objects *in vivo*,
- development of advanced X-ray diagnostic methods of laser-produced plasmas (X-ray spectroscopy, detection and dosimetry),
- development and optimisation of laser ion sources for ion implantation.

Simultaneously, a linear focus arrangement for experiments with generation of coherent X-radiation has been prepared (Milestone 2); the X-ray laser experiments took place in the period May–June 2001.

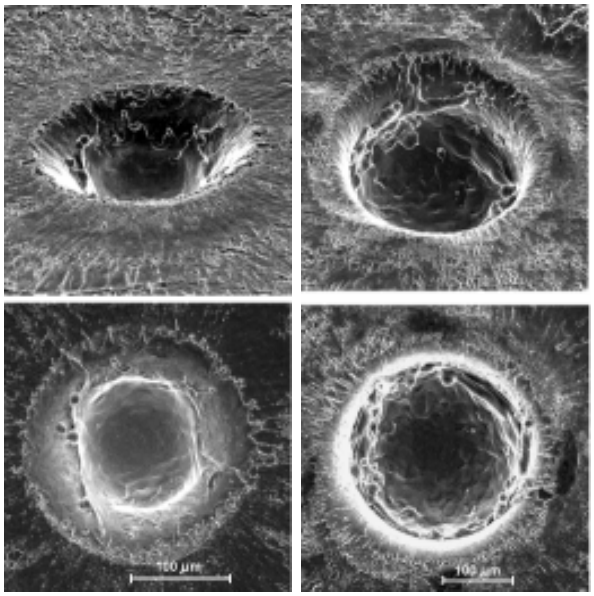

Fig. 4 *Craters produced by the reduced-energy PALS beam in* Mo *(left) and* Al *(right) targets. SEM pictures by B. Kolman, Material Engineering Dpt., Association Euratom/IPP.CR, Prague.*

4. Theory

A theoretical study of the enhancement of Electron Acceleration in Laser Wakefield Accelerators [4–7] was performed in collaboration with L. Krlín (Association Euratom/IPP.CR, Prague) and J.A. Tataronis (University of Wisconsin, Madison, USA).

By numerical modelling of ensemble of relativistic electrons in longitudinal plasma waves arising behind a transverse laser pulse (laser wake-field accelerator - LWA), it was demonstrated that electron trapping and acceleration in LWA is strongly enhanced in presence of another additional transverse laser beam, which propagates perpendicularly to the direction of the plasma wave propagation. A significant influence of phase randomisation of the additional laser beam on electron acceleration has been also found. Random phase changes may arise when the additional beam propagates through turbulent plasma, or when a randomising element is placed into the path of the beam (e.g. a random phase plate – RPP). Even thermal plasma particles may be then trapped and accelerated in LWA accelerators. Application of an additional perpendicularly propagating transverse laser beam thus leads to a significant improvement of efficiency of electron acceleration in LWA accelerators, and also to a significant improvement of subsequent fast ion production resulting from the charge separation field.

By theoretical modelling it has been also shown that even small ripple of the envelope of the accelerating plasma wave results in trapping of electrons much slower than is the wave phase velocity, and again even thermal plasma electrons may be trapped and accelerated. This effect is a result of a cascade Landau trapping in the wave, in which there is spontaneously created a whole spectrum of phase velocities as a result of rippling. Such a rippling may result from the nonlinear processes accompanying the propagation of intense plasma waves. It is also observed at numerical modelling of the plasma wave propagation in LWA.

5. Future plans

The PALS terawatt laser facility will be upgraded by new beam delivery options, which will make it possible to illuminate laser targets by various sequences of laser pulses. A double pulse regime interaction with a defined time delay between the pulses, the amplitude ratio and also the colour (1ω, 2ω, 3ω) of the illuminating laser light will be applied for plasma generation. The experimental results will be interpreted by a comparison with detailed 2D hydrodynamic calculations. The experimental work undertaken in the context of a keep-in-touch activity will be aimed at elucidating the role of heat transport in the smoothing mechanism inside the dense plasma regions beyond the critical surface.

Our long-term goal is to upgrade the PALS system towards a generation and subsequent target experiments with ultra short pulses in the femtosecond region, by using the method of OPCPA (optical parametric chirped pulse amplification). This upgrade will broaden the field of applications of the PALS system, up to real fusion-relevant experiments.

The theoretical part of the work will consist in the studies of fast electrons and ions production by intense electric and magnetic fields of laser beams, and in modelling of random field effects in laser-produced plasmas. We plan also to study the consequences of fast particles generation for other processes in plasmas, like for strong electric and magnetic field generation, for plasma channelling, and for X-rays and gamma-rays production in laser plasmas. In many cases, the fast particle generation has common features in laser plasmas and in plasmas heated by waves in the high-frequency range. Consequently, substantial effort will be given to works closely connected to our previous studies of the non-linear generation of fast particles by high-frequency and random fields in tokamaks and high-frequency plasma sources.

References

[1] K. Rohlena, B. Rus, L. Juha, J. Skála, B. Králiková, K. Jungwirth, J. Ullschmied, K.J. Witte, H. Baumhacker**:** *Prague Asterix Laser System (PALS) and its Upgrades***,** Proc. XIIIth International Symposium on Gas Flow and Chemical Lasers, Florencie 18. – 22.9.2000, accepted for publication at SPIE.

[2] K. Jungwirth, A. Cejnarova, L. Juha, B. Kralikova, J. Krasa, E. Krousky, P. Krupickova, L. Laska, K. Masek, T. Mocek, M. Pfeifer, A. Präg, O. Renner, K. Rohlena, B. Rus, J. Skala, P.Straka, J. Ullschmied: *The Prague Asterix Laser System PALS,* invited paper**,** 42nd Annual Meeting of the APS Division of Plasma Physics and 10th International Congress on Plasma Physics, 23.–27.10. 2000, Québec City, accepted for publication in Physics of Plasmas.

[3] V. Petržílka, J.A. Tataronis and L. Krlín: *Random Field Effects on Electron Acceleration in Crossed Laser Beams*, 19th Symposium on Plasma Physics and Technology, Prague, June 6–9, 2000, published in Czech. J. Phys., Vol. 50 (2000), Suppl. 3, p.202-206.

[4] V. Petržílka, J.A. Tataronis and L. Krlín: *Enhancement of Electron Acceleration in Laser Wakefields*, 26th European Conference on Laser Interaction with Matter (ECLIM 2000), Prague, June 12–16, 2000, Book of Abstracts, p. 201.

[5] V. Petržílka and J.A. Tataronis: *Synergetic Effects of Transverse, Longitudinal and Random Electric Fields on Electron Acceleration in Laser Plasmas*, ULIA-2 (Ultraintense Laser Interactions and Applications) Euroconference, Pisa, Italy, September 29 – October 3, 2000, Book of Abstracts p. 44.

[6] J.A. Tataronis, V. Petržílka and L. Krlín: *Two Dimensional Electron Acceleration in Laser Wakefields*, Plasma Physics Conference of the APS, Quebec, Canada, October 23-27, 2000, paper UP1.056, abstract published in Bull. Am. Phys. Soc. 45 (2000) 310.

[7] V. Petržílka, L. Krlín and J.A. Tataronis: "Enhancement of Electron Acceleration in Plasma Beat-Wave Accelerators by an Additional Laser Beam" (5th Workshop on fast ignition of fusion targets), 28th EPS Conference on Controlled Fusion and Plasma Physics, Funchal, Portugal, 18-22 June 2001 (European Conference Abstracts Vol. 25B).

The PALS web site: http://www.pals.cas.cz/

V PUBLICATIONS

1 Relevant Publications 2000

SPPT 2000

19th Symposium on Plasma Physics and Technology, Prague 6 – 9 June, 2000.
Czechoslovak Journal of Physics **50** [S3] (2000):

Brotánková J., Jakubka K., Kryška L., Stöckel J., Žáček F.: Measurement of energy confinement in CASTOR tokamak regimes with edge plasma polarization, pp. 75-80.

Brotánková J., Weinzettl V.: Hα–line measurement and Te profile estimation, pp. 71-74.

Dyabilin K., Hron M., Stöckel J., Žáček F.: Measurement of poloidal flows on the CASTOR tokamak, pp. 57-60.

Ďuran I., Stöckel J., Hron M., Jakubka K., Kryška L.: Self-organized criticality paradigm, pp. 42-46.

Pavlo P., Krlín L.: Nonlinear effects in lower hybrid heating and current drive, pp. 25-32.

Plíšek P., Nanobashvili S., Žáček F.: Reflectometric measurements of radial density fluctuations profile in tokamak CASTOR, pp. 61-66.

Preinhaelter J., Žáček F., Irzak M.A., Vahala L., Vahala G.: ECRH on CASTOR, pp. 51-56.

Vahala L., Vahala G., Carter J., Pavlo P.: Evolution of a neutral-ion 2fluid system using thermal lattice Boltzmann model, pp. 47-50.

Van Oost G., Tendler M., Stöckel J.: Role of electric field plasma confinement and exhaust, pp. 11-24.

Weinzettl V., Badalec J., Piffl V.: Impurity measurement and modelling in tokamak plasma, pp. 67-70.

EPS 2000

27th European Physical Society Conference on Controlled Fusion and Plasma Physics, Budapest, 12-16 June 2000.
27 EPS CCFP Contributed papers. (Ed. Szegö, K.; Todd, T.N.; Zoletnik, S.). Europhysics Conference Abstracts **24B**, Mulhouse, Eur. Phys. Society 2000:

Dyabilin K., Hron M., Stöckel J., Žáček F.: Ion flows measurements using a rotating Mach probe on the CASTOR tokamak, p. 1653.

Ďuran I., Stöckel J., Horáček J., Jakubka K., Kryška L., Hron M.: Validity of Self-Organized Criticality model for the CASTOR tokamak edge plasmas, p. 1693.

Krlín L., Kuhn S., Stöckel J., Svoboda V., Tendler M., Tskhakaya D., Zápotocký M.: Radial Electric Field Generation During Anomalous ExB Ion Diffusion., p. 45.

Pánek R., Krlín L., Pavlo P., Klíma R., Petržílka V.: The Role of Nonlinear Effects in LH Wave-Plasma Interaction. p. 1208.

Preinhaelter J., Irzak M.A., Pavlo P., Vahala L., Vahala G.: Excitation of electron Bernstein Waves in MAST, 1204

Stöckel J., Hron M., Ďuran I., Dyabilin K., Horáček J., Jakubka K., Kryška L., Martines E., Nanobashvilil S., Van Oost G., Tendler M., Žáček F.: Plasma polarization of the separatrix on the CASTOR tokamak, p. 1032.

Tskhakaya D., Kuhn S., Petržílka V.: Simulation of Particle Acceleration in Front of Lower Hybrid Grill. In: *Book of Abstracts,* p. 107.

Vahala L., Vahala G., Pavlo P.: Multi-Species Equilibration using Thermal Lattice Boltzmann Simulations, p. 536.

Žáček F., Petržílka V., Jakubka K., Stöckel J., Tskhakaya D., Kuhn S.: Radial variations of the floating potential in front the lower hybrid grill of the CASTOR tokamak, p. 1028.

APS 2000 & 10th ICPP

42nd Annual Meeting of the APS Division of Plasma Physics and 10th International Congress on Plasma Physics, Québec City, 23-27 October 2000

Physics of Plasmas. Special Issue **8** [5] (2001):

Gunn J.P., Boucher C., Devynck P., Ďuran I., Dyabilin K., Horáček J., Hron M., Stöckel J., Van Oost, G., Van Goubergen H., Žáček F.: Edge flow measurements with Gundestrup probes, pp. 1995-2001 .

Sauter O., Angioni C., Coda S., Gomez P., Goodman T.P., Henderson M.A., Hofmann F., Hogge J.P., Moret J.M., Nikkola P., Pietrzyk Z.A., Weisen H., Alberti S., Appert K., Bakos J., Behn R., Blanchard P., Bosshard P., Chavan R., Condrea I., Degeling A., Duval B.P., Fasel D., Favez J.-Y., Favre A., Furno I., Kayruthdinov R.R., Lavanchy P., Lister J.B., Llobet X., Lukash V.E., Gorgerat P., Isoz P.-F., Joye B., Magnin J.-C., Manini A., Marlétaz B., Marmillod P., Martin Y.R., Martynov A., Mayor J.-M., Minardi E., Mlynar J., Paris P.J., Perez A., Peysson Y.R., Piffl V., Pitts R.A., Pochelon A., Reimerdes H., Rommers J.H., Scavino E., Sushkov A., Tonetti G., Tran M.Q., Zabolotsky A.: Steady-state fully non-inductive operation with electron cyclotron current drive and current profile control in the Tokamak á Configuration Variable (TCV), pp. 2199-2207.

Bulletin of the Amer. Phys. Society **45** [7] (2000):

Pavlo P., Vahala L., Vahala G.: Energy-Dependent Octagonal Lattice Boltzmann Modeling for Compressible Flows, p. 73.

Pitts R.A., Horáček J., Loarte A.: On the Measurement of Electron Temperature by Single Langmuir Probes in High Recycling Divertors, p. 314.

Preinhaelter J., Irzak M.A., Vahala G., Vahala L.: ECE and ECRH from O-X-EBW Mode Conversion in Spherical Plasmas. *Ibid.*, p. 254.

Vahala G., Pavlo P., Vahala L.: Mesoscopic Repres-entations of Nonlinear Macroscopic System, p.73.

2000 International Congress on Plasma Physics, Proceedings.

Stockel J., Van Oost G., Gunn J., Dyabilin K., Nanobashvili S.: Control of edge electric field and flows in the CASTOR tokamak, Proc. 10th ICPP,, Quebec City, Canada, Vol. III, p. 772.

Krlín L., Kuhn S., Stöckel J., Svoboda V., Tendler M., Tskhakaya D., Zápotocký M., Klíma R.: Radial electric field generation during anomalous ExB impurity diffusion, Vol. II, p. 716.

IAEA 2000

18th IAEA Fusion Energy Conference, Sorento, Italy, 4-10 October 2000.

In: *18th IAEA Fusion Energy Conference.* - (Ed. Kruger, C.). - Vienna, IAEA Vienna 2000.

Petržílka V., Žáček F., Kolman B., Kroupa F., Jakubka K., Stöckel J., Klíma R., Krlín L., Pavlo P., Gunn J., Goniche M., Fuchs V., Devynck P., Tskhakaya D., Kuhn S., Tataronis J.A., Lörinčík J.: On the Fast Electron Beam, Consequent Generation of Electrostatic Fields and Fast Ion Production in front LH Grills: Measurements and Theory, pp. 253-257.

Pitts R.A., Duval B.P., Loarte A., Moret J.-M., Horáček J: Detachment in Variable Divertor Geometry on TVC, p.1

OTHER CONFERENCES

Pitts R.A., Duval B.P., Loarte A., Moret J.-M., Boedo J.A., Coster D., Furno I., Horáček J., Kukushkin A.S., Reiter D., Rommers J.: Divertor Geometry Effects on Detachment in TCV. *14th International Conference on Plasma Surface Interactions in Controlled Fusion Devices*, Rozenheim, Germany, 22-26 May 2000.

Van Oost G., Stockel J., Hron M., Devynck P., Dyabilin K., Gunn J., Horacek J., Martines E., Tendler M.: Potential Structures and Flow Measurements with Separatrix Biasing in the CASTOR tokamak. *International Conference TOKI 2000*, December 2000.

OTHER JOURNALS

Krlín L., Stockel J., Svoboda V., Tendler M.: Stochastic (ExB) difffusion of ions in a spatially periodical potential field. *Physics Scripta* **T84**, (2001) 221-224.

Piffl V., Weisen H.: Ultra-soft X-ray spectroscopy using multilayer mirror. *Int.Conference on Open Magnetic Systems for Plasma Confinement,* Tsukuba, Japan, 3-6 July 2000. *Transactions of Fusion Technology. An International Journal of the American Nuclear Society* **39** [1] (2001) 155-158.

Preinhaelter J., Irzak M.A., Vahala L., Vahala G.: Electron cyclotron resonance heating in spherical plasmas: O-X-EBW mode conversion in MAST. *13th Topical Conference on High-Temperature Plasma Diagnostics,* Tuscon, Arizona, USA, 18-22 June 2000. *Review of Scientific Instruments* **72** [1] (2001) 391.

Vahala L., Wah D., Vahala G., Carter J., Pavlo P.: Thermal Lattice Boltzmann Simulation for Multispecies Fluid Equilibration. *Phys. Rev. E* **62** [1] (2000) 507-516.

Stöckel J., Dyabilin K., Ďuran I., Horáček J., Hron M., Jakubka K., Kryška L., Nanobashvili S., Nanobashvili I., Tendler M., Van Oost G., Žáček F.: Fluctuation Studies at Plasma Polarization on the CASTOR tokamak: *Journal of Technical Physics* **41** [2], Special Issue (2000) 49-56.

REPORTS

Dyabilin K., Ďuran I., Hron M., Horáček J., Klíma R., Pavlo P., Stöckel J., Žáček F.*: "Modelling of electrostatic turbulence at the edge of the CASTOR tokamak*". Res. Rep. IPPCZ-366, IPP Prague, Dec. 2000.

Preinhaelter J., Shevchenko V , Irzak M.A., Vahala L. and Vahala G.: "*ECRH in Spherical Plasmas: O-X-EBW. Mode Conversion in MAST*". Rep. UKAEA FUS 444, 2000, Culham Laboratory.

Preinhaelter J.: "*O-X-EBW mode conversion of 60GHz wave in MAST H-mode twin peak density profile*". MAST OPS NOTE No: 00.36

THESES

Horáček J.: "*Turbulent structures in tokamak plasma*". diploma thesis, Charles University, Prague, 2000.

Plíšek P.: "*Reflectometric measurements of plasma density fluctuations in tokamak CASTOR*". Diploma thesis, Czech Technical University, Prague, 2000.

2 Relevant Publications 2001

EPS 2001

28th European Physical Society Conference on Controlled Fusion and Plasma Physics, Funchal, Madeira, 18-22 June 2001.

Plasma Physics and Controlled Fusion **43** [12A] (2001)

Hofmann F., Behn R., Coda S., Goodman T.P., Henderson M., Lavanchy P., Marmillod P., Martin Y. Martynov A., Mlynar J., Moret J.-M., Pochelon A., Reimerdes H., Sauter O., Alberti S., Angioni C., Appert K., Bakos J., Blanchard P., Bosshard P., Chavan R., Condrea I., Degeling A., Duval B.P., Fasel D., Favez J.-Y., Favre A., Furno I., Gomez P., Gorgerat P., Hogge J.-P., Isoz P.-F., Joye B., Klimanov I., Lister J.B., Llobet X., Magnin J.-C., Manini A., Marletaz B., Mayor J.-M., Nikkola P., Paris P.J., Perez A., Pietrzyk Z.A., Piffl V., Pitts R.A., Scarabosio A., Scavino E., Sushkov A., Tonetti G., Tran M.Q., Weisen H., Zabolotsky A.: Stability and energy confinement of highly elongated plasmas in TVC., pp. 161-173.

In: *28th European Physical Society Conference on Controlled Fusion and Plasma Physics - Contributed Papers.* (Ed. Silva, C.; Varandas, C.; Campbell, D.). Europhysics Conference Abstracts. **25A**, Mulhouse, European Physical Society 2001:

Dyabilin K., Klíma R., Ďuran I., Horáček J., Hron M., Pavlo P., Stöckel J., Žáček F.: Modelling of Electrostatic Turbulence at the Edge of the CASTOR tokamak, pp. 1669-1672.

Ďuran I., Mank G., Finken K.H., Fuchs G., Flecken-Krämer A., Van Oost G.: Measurement of magnetic fluctuations using a multiple Hall probe on TEXTOR, pp. 1261-1264.

Fuchs V., Petržílka V., Goniche M., Gunn J.: Momentum and Heat Transfer From Lower Hybrid Antennas to the Tokamak Edge Plasma, pp. 317-320.

Hidalgo C., Goncalves B., Erents K., Silva C., Pedrosa M.A., Hron M., Matthews G.F., García-Cortés J., Balbín, R.: On the Radial Scale of Turbulent Transport in the JET Plasma Boundary Region, pp. 1657-1660.

Krlín L., Kuhn S., Lavička M., Pánek R., Stöckel J., Svoboda V., Tendler M., Tskhakaya D., Zápotocký M.: Anomalous ExB Ion Diffusion and Radial Electric Field Generation in a Fluctuating Electrostatic Potential, pp. 269-272.

MacNab A., Vahala G., Pavlo P., Vahala L., Soe M.: Lattice Boltzmann Model for Dissipative Incompressible MHD, pp. 853-856.

Martines E., Hron M., Stöckel J.: Coherent Structures in the Edge Region of the CASTOR Tokamak, pp. 1673-1676.

Pánek R., Krlín L., Pavlo P., Fuchs V., Klíma R., Petržílka V., Tskhakaya D., Kuhn S.: One-Dimensional Particle-In-Cell Simulation of Electron Acceleration in a Spatially Localized LH Wave, pp. 341-344.

Pavlo P., Vahala G., Vahala L.: Jet Flow in Thermal Lattice Boltzmann Simulations, pp. 849-852.

Petržílka V., Krlín L., Tataronis J.: Enhancement of Electron Accelaration in Plasma Beat Wave Accelerator by an Additional Laser Beam, pp. 53-56.

Petržílka V., Fuchs V., Klíma R., Krlín L., Pavlo P., Pánek R., Žáček F., Goniche M., Gunn J., Tskhakaya D.: A 3-D Two Fluid Model of the Plasma Vortex in Front of LM Grills, pp. 289-292.

Piffl V., Badalec J., Weinzettl V., Burdakov A.: Intensity radial profile study of CV (308eV) line at tokamak CASTOR, pp. 1233-1236.

Preinhaelter J., Stöckel J., Žáček F., Irzak M.A., Tregubova E., Vahala L., Vahala G.: Influence of the plasma surface density fluctuations on ECE in CASTOR, pp. 329-332.

Schrittweiser R., Adámek J., Balan P., Hron M., Ionita C., Jakubka K., Kryška L., Martines E., Pohoata V., Stöckel J., Tichý M., Van Oost G.: Plasma Potential Measurements with Emissive Probes in the CASTOR Tokamak, pp. 409-412.

Stöckel J., Gunn J., Van Oost G., Ďuran I., Hron M., Adámek J., Horáček J., Hrach R., Jakubka K., Kryška L., Vicher M., Žáček F.: Optimization of Gundestrup Probe for Ion Flow Measurements in Magnetized Plasmas, pp. 237-240.

Van Oost G., Stöckel J., Gunn J., Adámek J., Ďuran I., Horáček J., Hron M., Jakubka K., Kryška L., Žáček, F.: Direct measurements of ExB flows and its impact on edge turbulence in the CASTOR tokamak, pp. 1665-1668. -

Žáček F., Petržílka V., Jakubka K., Stöckel J., Gunn J., Goniche M., Devynck P., Podesta M., Nanobashvili S.: Probe measurements in front of the lower hybrid grill of the CASTOR tokamak, pp. 325-328.

REFPCE 2001

4th Workshop on the Role Electric Fields in Plasma Confinement and Exhaust, Funchal, Madeira, 24-25 June 2001.

Czechoslovak Journal of Physics, **51** [10] (2001):

Dyabilin K., Klíma R., Ďuran I., Horáček J., Hron M., Pavlo P., Stöckel J., Žáček F.: Modelling of the effect for the sheared poloidal flow on the electrostatic turbulence on the CASTOR tokamak, pp. 1107-1117.

Gunn J., Stöckel J., Adámek J., Ďuran I., Horáček J., Hron M., Jakubka K., Kryška L., Žáček F., Van Oost, G.: Direct measurements of ExB flow and its impact on edge turbulence in the CASTOR tokamak using an optimized Gundestrup probe, pp. 1001-1010.

Van Oost G., Gunn J.P., Melnikov A., Stöckel J., Tendler M.: The role of radial electric fields in tokamaks TEXTOR-94, CASTOR, and T-10, pp. 957-975.

Žáček F., Petržílka V., Jakubka K., Stöckel J., Gunn J., Goniche M., Devynck P., Podesta M., Nanobashvili S.: Plasma edge biasing on CASTOR tokamak using LHCD, pp. 1129-1138

APS 2001

43rd Annual Meeting of the Division of Plasma Physics of the American Physical Society, Long Beach, CA, 29 October – 2 November 2001.

Bulletin of the Amer. Physical Society **46** [8] (2001):

MacNab A., Vahala G., Pavlo P., Vahala L.: Lattice Boltzmann Model for Dissipative Incompressible MHD, p. 241.

Pavlo P., Vahala G., Vahala L.: Energy Dependent Streaming in Lattice Boltzmann Simulations, *ibid.*

Preinhaelter J., Stöckel J., Žáček F., Irzak M., Tregubova E., Vahala G., Vahala L.: Influence of the plasma surface density fluctuations on ECE in CASTOR, p. 307.

WDS'01

Week of Doctoral Students, Prague, 12-15 June 2001. Proceedings of contributed papers, Part II. (Ed. Šafránková, J.) Praha, Matfyzpress 2001.

Adámek J., Stöckel J., Schrittwieser R., Ionita C., Martines E., Tichý M., Van Oost G.: Plasma potential measurements with emissive probes in the CASTOR tokamak.

Brotánková J., Plíšek P., Žáček F., Badalec J.: Thomson scattering diagnostics on the CASTOR tokamak.

Ďuran I., Mank G., Finken K.H., Flecken-Krämer A., Van Oost G.: Magnetic turbulence measurements using array of Hall probes on TEXTOR-94 tokamak, pp. 298-301.

Hron M., Stöckel J., Adámek J., Ďuran I., Horáček J., Jakubka K., Kryška L., Žáček F., Gunn J., Van Oost G.: Direct measurements of ExB flows and its impact on edge turbulence in the CASTOR tokamak.

OTHER CONFERENCES AND JOURNALS

Baptista M.S., Caldas I.L., Heller M.V.A., Ferreira A.A., Bengston R.D., Stöckel J.: Recurrence in plasma edge turbulence. *Physics of Plasmas* **8** [10] (2001) 4455-4462.

Bém P., Burjan V., Cvachovec F., et al.: Fast neutrons from thick helium target irradiated by 17 MeV deuterons. ***Nuclear Instruments & Methods in Physics Research. Section A-Accelerators, Spectrometers, Detectors and Associated Equipment,*** 466 [3] (2001) 509-512.

Glosík J., Plašil R., Poterya V., Kudrna P., Tichý M., Pysanenko A.: Experimental study of recombination of H_3^+ ions with electrons relevant for interstellar and planetary plasmas, J. Phys.B: Atomic, Mol. Opt. Phys., 34 (2001) L485-L494.

Glosík J., Plašil R., Poterya V., Kudrna P., Pysanenko A., Tichý M., Rusz J.: Stationary afterglow study of recombination of H_3^+ ions with electrons**, *ECAMP VII, The Seventh European Conference on Atomic and Molecular Physics***, Euro. Conf. Abstracts, Volume 25 B, ISSN 0420/0195, Published by Eu. Phys. Soc., Ed. R. M. Pick, Berlin 2.-6. April 2001, A 10.32, pp.70.

Glosík J., Poterya V., Vicher M., Plašil R., Kudrna P., Pysanenko A., Tichý M.: Kinetics of formation and destruction of H_3^+ ions in He-Ar-H_2 plasma influenced by recombination of H_3^+ ions, *Proc. 15th Inter. Sym. on Plasma Chemistry (15 ISPC),* Orleans - France, 9-13 July 2001, Edited by A. Bouchoule, J.M. Pouvesle, A.L. Thomann, J.M. Bauchire and E. Robert, Volume III, pp.789-794.

Mank G., Duran I., Finken K.H., Van Oost G.: Measurement of magnetic fluctuations by means of a multiple Hall probe in TEXTOR-94, *Spring Meeting of the German Physical Society*, Berlin, Germany, 2-6 April 2001

Preinhaelter J., Irzak M.A., Tregubova E., Vahala G., Vahala L., Žáček F.: ECE on CASTOR. *14th Topical Conference on Radio Frequency*, Oxnard, USA, 7-9 May 2001. In: *Radio frequency power in plasmas.* (Ed. Mau, T.K.; de Grossie, J.). New York, Melville 2001, pp. 326-329.

Preinhaelter J., Irzak M.A., Vahala G., Vahala L.: Mode Conversion Processes for Electron Bernstein Wave Excitation in Spherical Tori. *28th IEEE International Conference on Plasma Science,* Las Vegas, US, 17-22 June 2001. In: *Pulsed Power Plasma Science 2001.* - Piscataway, IEEE Service Center 2001, pp. 537.

Tichý M., Poterya V., Plašil R., Kudrna P., Pysanenko A., Glosík J.: Application of Langmuir probe for study of recombination of H_3^+ ions with electrons in He-Ar-H_2 stationary afterglow plasma, ***Proceedings of the XXV International Conference on Phenomena in Ionized Gases***, Nagoya (Japan), July, 17-22, 2001, Toshio Goto, Editor, Vol .3., ISBN 4-9900915-1-5, p.267-268.

Van Oost G., Stockel J., Hron M., Devynck P., Dyabilin K., Gunn J., Horacek J., Martines E., Tendler M.: Potential Structures and Flow Measurements with Separatrix Biasing in the CASTOR tokamak. *Journal of Fusion Research SERIES* **4** (2001) 29-35.

Weisen H., Alberti S., Angioni C., Appert K., Bakos J., Behn R., Blanchard P., Bosshard P., Coda S., Condrea I., Degeling A., Duval B.P., Fasel D., Favez J.Y., Favre A., Furno I., Gomez P., Goodman T.P., Henderson M.A., Hofmann F., Kayruthdinov R.R., Lavanchy P., Lister J.B., Llobet X., Loarte A., Lukash V.E., Gorgerat P., Hogge J.P., Isoz P.F., Joye B., Magnin J.C., Manini A., Marlétaz B., Marmillod P., Martin Y., Martynov A., Mayor J.-M., Minardi E., Mlynar J., Moret J.M., Nikkola P., Paris P.J., Perez A., Peysson Y., Pietrzyk Z.A., Piffl V., Pitts R.A., Pochelon A., Reimerdes H., Rommers J.H., Sauter O., Scavino E., Sushkov A., Tonetti G., Tran M.Q., Zabolotsky A.: Overview of TVC results. *Nuclear Fusion*, **41** [10] (2001) 1459-1472.